

---

---

# Fibre Optic Sensor for Speed Measurement

Thesis submitted for the degree of

*Master of Science*

by

Ion Gogoasa, B.Sc.



Department of Applied Physics, Faculty of Science,

Victoria University of Technology

March 1996

---

---

---

FTS THESIS  
681.2 GOG  
30001005011772  
Gogoasa, Ion  
Fibre optic sensor for speed  
measurement

---

This thesis is dedicated to my son David and my wife Paula

---

## ABSTRACT

Determination of speed is an important requirement in a wide variety of technical and industrial applications. The measurement of speed has evolved from pure mechanical to magnetoelectric and radio frequency (RF) based devices. There is however a demand for low-cost sensors capable of operating in potentially hazardous environments in which optical fibre sensors are more suited. In this thesis the development of a non-intrusive speed measurement sensor, based on optical technology is described.

The optical fibre sensor described herein gives an almost instantaneous indication of the speed and is compared to a commercial speed sensor (Cateye, 1993) which relies on a magnet attached to a rotating surface yielding an averaged speed reading over several revolutions.

The optical speed sensor requires incoherent light, conveniently provided by two low cost 780 nm CD-type laser diodes. The light was directed through a pair of spatially displaced fibres illuminating the moving surface. Some of the back-scattered light from the moving surface was collected by a second pair of fibres leading to two photodiodes (where the light information was converted into an electrical signal). An analogue to digital converter in conjunction with a PC (386SX-33) was used to digitise the signals from the photodiodes. The numeric data was then used to compute the speed of the moving surface using a cross-correlation technique.

The optical fibre speed sensor was tested successfully on a large number of surfaces at speeds up to 30 km/h. It showed excellent agreement (better than 3%) with the commercial speed sensor. The absolute accuracy (about 9% at 30 km/h) is limited only by the quality of

---

the analogue to digital converters and indirectly by the data processing capability of the PC.

## **ACKNOWLEDGMENTS**

I wish to thank my supervisors, Dr. Michael Murphy and Dr. Jakub Szajman, for their counsel and support throughout this project. I would particularly like to thank Dr. Michael Murphy for initiating this project and his drive in ensuring its success. Many thanks to Dr. Stephen Collins for proof-reading the thesis and his helpful comments.

I am also grateful to Professor David Booth (Head of Department) for the opportunity to pursue this postgraduate degree in the Department of Applied Physics at the Victoria University of Technology and to Mark Kivenen for the manufacture of the transducer assemblies.

Finally an important thank-you to my family for their love and support during these studies.

---

---

# CONTENTS

## **Chapter 1      GENERAL INTRODUCTION**

1.1	Introduction to fibre optic sensors	8
1.2	Project aim	10
1.3	Summary of thesis	11

## **Chapter 2      REQUIREMENTS FOR FIBRE OPTIC SENSING SYSTEMS**

2.1	Introduction	12
2.2	System components	12
2.2.1	Light sources	12
2.2.2	Optical fibres	16
2.2.3	Optical detectors	19
2.3	Power loss and noise considerations	22
2.4	Conclusion	23

## **Chapter 3      SPEED MEASUREMENT TECHNIQUES**

3.1	Introduction	24
3.2	Non-optical speed measurement	24
3.3	Optical speed measurement	26
3.3.1	Laser Doppler velocimetry	27
3.3.2	Fibre Optic Doppler velocimetry	29
3.3.3	Distributed laser Doppler velocimetry	32
3.3.4	Laser speckle method	33
3.4	Conclusion	35

---

## **Chapter 4 THEORETICAL ANALYSIS**

4.1	Introduction	36
4.2	Time delay estimation	37
4.2.1	Power spectral density	39
4.2.2	Time delay estimators	41
4.3	Design of cross-correlation measurement systems	44
4.3.1	Model of measurement system	47
4.3.2	Spatial averaging effect of the cross-correlation sensor	51
4.4	Accuracy of cross-correlation based measurement system	53
4.5	Noise in the sensor electronics	57
4.5.1	Thermal noise	57
4.5.2	Shot noise	58
4.5.3	Signal-to-noise ratio	59
4.6	Conclusion	60

## **Chapter 5 APPARATUS AND ITS APPLICATIONS**

5.1	Introduction	61
5.2	Laser diode and power supply	63
5.3	Photodetectors	66
5.4	Sensor electronics	69
5.4.1	Transimpedance amplifier	69
5.4.2	The voltage amplifiers	70
5.5	Optical fibres and components	71
5.6	The transducer head	73
5.7	PCL-818, Laboratory Card	76
5.8	Software Drivers	77
5.9	Hameg oscilloscope	78
5.10	Cateye integrated velocimeter	79

---

## **Chapter 6      EXPERIMENTAL RESULTS**

6.1	Introduction	80
6.2	Initial trials	80
6.2.1	Discussion of results from the initial trials	84
6.3	Selection of surfaces for real time measurements	85
6.4	Real time speed measurements	87
6.5	Customisation of processing technique to improve sensor time response	94
6.6	Practical speed limits and uncertainties	98
6.7	Results	99
6.8	Conclusions	104

## **Chapter 7      CONCLUSIONS**

7.1	Final conclusion	105
7.2	Future work	106

<b>References</b>	107
-------------------	-----

<b>Apendices</b>	113
------------------	-----

Appendix 1	114
------------	-----

Appendix 2	116
------------	-----

Appendix 3	119
------------	-----

Appendix 4	123
------------	-----

Appendix 5	127
------------	-----

<b>Publications</b>	130
---------------------	-----

---

## Chapter 1. GENERAL INTRODUCTION

### 1.1 INTRODUCTION TO OPTICAL FIBRE SENSORS

An important branch of optical fibre technology is the area of sensors. Optical fibres have a number of advantages over electronic devices, for example, low power loss and cost, and they are impervious to many environmental effects such as electromagnetic interference and noise (Botez and Herskowitz, 1980). However, the environment can have an influence on the operating characteristics of optical fibres. For example, temperature, electric or magnetic fields and even fibre bending will affect optical fibre performance. We should therefore exercise caution to avoid or compensate for these effects. On the other hand, we can also take advantage of the sensitivity of the optical fibres to these environmental changes by building sensors to measure these effects.

Optical fibre sensors may be divided into two categories; the pure optical sensor, where the fibre itself is the sensing element, and the remote sensor, in which the fibres are used only to bring light to and from a separate sensing device. In the case of pure optical fibre sensors, the measurand interacts directly with the light travelling in the fibre. The resultant light can be either intensity-, phase- or polarisation-modulated within the fibre. However, the feed and return fibres may also impose modulation of the light passing within them, giving misleading information or error. A detection scheme that favours self compensation of these coincidental effects would be preferred. A remote sensor involves the use of a special sensing element (external to the fibre) that is sensitive to the physical phenomena one wishes to monitor. Subjected to the environmental change, such as temperature or pressure, the sensing element modulates the light going to and coming from the remote sensor

---

via the fibres. The detected light signal can be related to the respective changes of environment. The sensing element is a transducer and a change of energy form is involved.

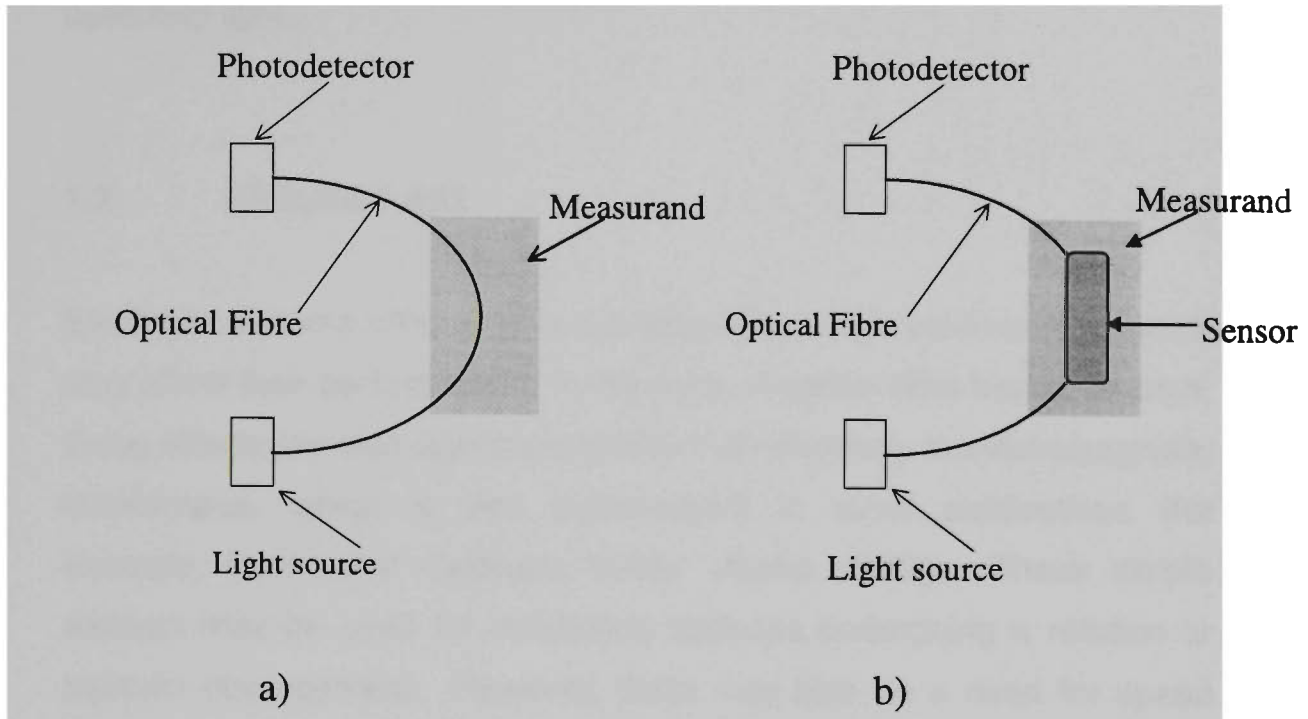


Figure 1. The basic types of optical fibre sensors:  
a) pure and b) remote sensor.

Intensity modulation is the most common method for fibre optic sensing because it is easy to implement. On the other hand, phase modulation is by far the most sensitive and accurate technique if used with an interferometric method. Polarisation changes may be also utilised to sense the environment. Other methods have been reported in the literature (Dakin and Culshaw, 1988) but are too numerous to mention and a detailed discussion is beyond the scope of this thesis.

Both singlemode and multimode fibres can be used as sensors. Multimode fibres are used for less demanding applications while

---

singlemode fibres are used when extreme sensitivity and accuracy is required. In the case of sensors where polarisation modulation is used, only singlemode fibre is recommended (Yeh, 1990).

The sensor that is the subject of this thesis is a remote, intensity-modulated type, and uses multimode optical fibres for transmitting and collecting light.

## **1.2 PROJECT AIM**

Electronic sensors often require consideration of the environment, which may affect their performance. In the case of optical fibre based sensors, these effects are less significant due to their immunity to electromagnetic interference, which is well documented in other publications (for example, Dakin and Culshaw, 1988; Krohn, 1988). These simple sensors may be used for monitoring surfaces undergoing a rotation or periodic displacement. However, there may also be a need for speed monitoring of a random surface such as a road or non-deterministic motion in a machine. By applying cross-correlation techniques on the digitised output signal of the sensor, the monitoring of such motion is possible by correlating the "randomness" of light reflected from a moving surface.

The aim of this project is to design, build and evaluate a fibre optic sensor for the non-contact measurement of speed for moving surfaces. The sensor development employed techniques which were first used in fluid flow monitoring (Section 3.3.1) and have been adopted in the work reported herein. To assist in the interpretation of the sensor signals, a dedicated system was developed.

---

### **1.3 SUMMARY OF THESIS**

The basic components of the fibre sensor and some of the factors affecting system performance are discussed in chapter 2. In chapter 3, a review of the existing methods and techniques for velocity measurement is given and their advantages and drawbacks are discussed.

The operating principles of the extrinsic sensor described in this work are discussed in chapter 4. Chapter 5 is dedicated to the optical, electronic and mechanical components of the system.

Chapter 6 details the experimental results along with the evolution of the system's components and the improvements in sensitivity and accuracy of the sensor gained by these developments. To complete this thesis a final conclusion and some proposals for future evolution of the sensor are presented in chapter 7.

---

## **Chapter 2      REQUIREMENTS FOR FIBRE OPTIC SENSING SYSTEMS**

### **2.1      INTRODUCTION**

Accuracy and reliability are essential requirements for all sensors. A good sensor must be sensitive, low noise, high efficiency, simple in design, competitively priced and have a fast time response. Not all requirements can be met in one design and usually compromises must be made. An optical fibre sensor is comprised of an intensity or phase modulator sensitive to environmental changes, and an optical fibre for carrying the light signal. A light source such as a light emitting diode (LED) or a laser diode (LD) with an appropriate photodetector completes the sensor.

### **2.2      SYSTEM COMPONENTS**

The basic components of any optical fibre sensing system are the light source, the optical fibre and the photodetector. These components and their operating conditions will be discussed later in this chapter.

#### **2.2.1      *Light sources***

The light source for an optical fibre sensing system should have a size and configuration compatible with the optical fibre used. A survey of available sources reveals that semiconductor light sources are the best candidates, not only for their size compatibility but for a number of other reasons. Semiconductor light sources are capable of giving relatively large power output, they are efficient, reliable and easy to modulate,

---

have low in-band noise, long life, and low cost (Yeh, 1993). General requirements of a good light source are discussed below.

**Power output.** High power output from a light source is usually desirable to overcome power losses in the sensor. However, care must be exercised in choosing the output power of a light source for fibre applications. A power density of  $1 \text{ MW/cm}^2$  is considered the limit for non-linear effects in silica and this translates to about 100 mW for a semiconductor light source.

**Coupling efficiency.** Light must be able to be coupled into the fibre efficiently in order to minimise the cost of the optical and mechanical components. The selected light source should have a radiation pattern compatible with the numerical aperture ( $NA$ ) of the fibre used (Section 2.2.2). This allows the use of lower power sources in a system, reducing the cost and enhancing the reliability.

**Source efficiency.** For a p-n injection-type semiconductor light source such as an LED or LD, the source efficiency is the product of carrier injection across the junction and radiative and external quantum efficiency. The selection of materials, processing and design consideration affect the overall source efficiency.

**Spectral emission and spectral width.** The emission characteristics of the light source are required to match the spectral properties of the optical fibre. Light-emitting diodes have a relatively wide spectral width, typically several tens of nanometers. For multimode optical fibres (MMFs), used in short links, LEDs are suitable. The light dispersion in silica for broad band spectral sources is unacceptable for long-haul systems, where only singlemode optical fibres (SMFs), combined with narrow line sources such as LDs, are used. Laser diodes with a narrow spectral width ( $\sim 0.2 \text{ nm}$ ) are now available (Yeh, 1993) and are used in a wide number of applications. Examples include infrared laser diodes at

---

wavelengths of 750 to 780 nm which are mass produced for use in compact disk players and laser diodes at 1300 and 1550 nm which are at the heart of today's communication systems.

Laser diodes and the other semiconductor light emitting devices, utilise the emission of light during recombination of electrons in the conduction band with holes in the valence band of the semiconductor (Optek Technology, 1990). Therefore the carrier recombination time dominates the frequency characteristics of these devices. In laser diodes the photons are mostly generated by stimulated emission, whereas LEDs operate by spontaneous emission. This fundamental difference causes laser diodes to emit very intense coherent light at only a few discrete wavelengths and LEDs to emit incoherent light over a relatively wide spectral range. Thus LEDs have a short coherence length (around 30  $\mu\text{m}$ ) and their signal rise time ranges from a few ns to 250 ns (leading to a maximum modulation frequency of about 100 MHz). Typical characteristic curves for LD and LED are presented in Figure 2.1.

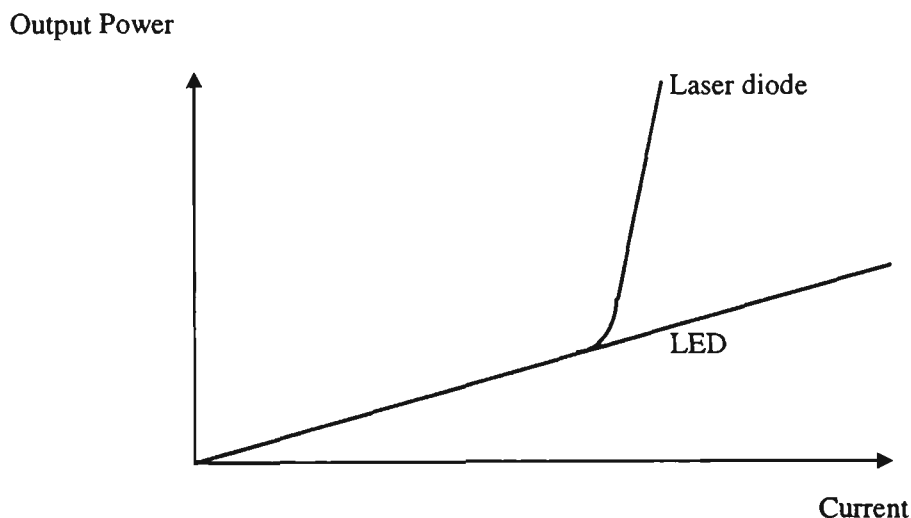


Figure 2.1. Optical power versus driving current for an LED and laser diode

---

On the other hand, LDs have a much narrower linewidth and, therefore, a greater coherence length (in principle the distance from the emitting source to the point in space where the phase of the wave can no longer be reasonably predicted), typically a few millimetres. Furthermore the short rise time of the order of 0.1 to 1 ns allows modulation as high as several gigahertz.

There are two types of laser diodes—singlemode and multimode. A laser diode allows propagation of specific distributions of optical power and wavelengths. These are referred to as ‘modes’ and consist of two basic types—transverse modes and longitudinal modes. Transverse modes refer to the optical power (or irradiance) across the axes of the output beam, whereas the longitudinal modes refer to the optical (or wavelength) spectrum. The optical power distribution across the emission area of the laser diode (Figure 2.2) has two components — one parallel and the other perpendicular to the active layer (Seastar Optics, 1993)

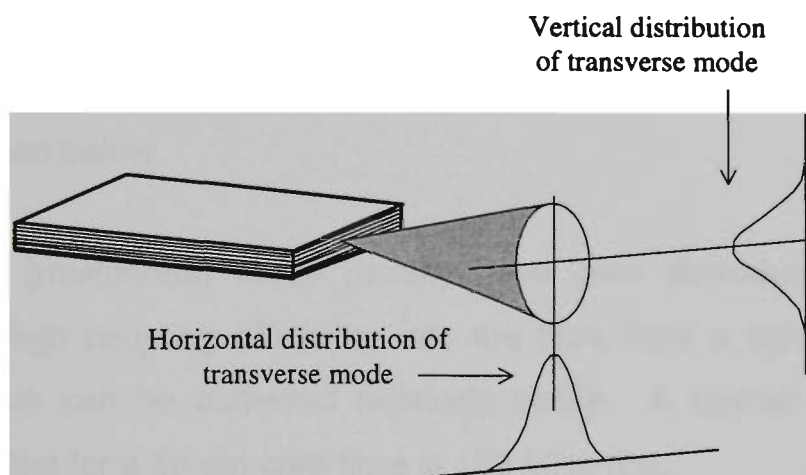


Figure 2.2. Horizontal and vertical distributions of optical power across the emission area of the laser diode.

---

In the work presented here, two low cost single mode CD player laser diodes were selected (Section 5.2) as the light sources for the speed sensor.

### 2.2.2 *Optical fibres*

Optical fibres are dielectric waveguides, and are designed to propagate light along their length. For easy fabrication and implementation, a silica preform is usually drawn into fibres of circular cross section. In general, optical fibres consist of a cylindrical core with a refractive index  $n_1$ , surrounded by a cladding with an index  $n_2$  (with  $n_1 > n_2$ ). If both  $n_1$  and  $n_2$  are uniform throughout their cross section, the fibre is known as *step index fibre* (SI). If  $n_1$  varies with the core radius, it is a *graded index fibre* (GI). Furthermore, for a given refractive index of core and cladding if the core diameter is small compared to the wavelength of the light used only the fundamental mode can propagate and the fibre is termed singlemode (SMF). Conversely, for larger core diameters the fibre will support higher transverse in addition to the fundamental ones. This leads to modal dispersion which limits the signal bandwidth of the fibre. Such a fibre is termed multimode (MMF). A brief summary of some commonly used fibres is given below.

Step-index (multimode) fibres usually have core diameters of 50 to 100  $\mu\text{m}$ . High coupling efficiency into the fibre from a light source or another fibre can be achieved relatively easily. A typical bandwidth-length product for a 50  $\mu\text{m}$  core fibre is 100 MHz-Km.

Graded index (multimode) fibres typically have core diameters of 50, 62.5 and 100  $\mu\text{m}$ , with a bandwidth-length product that can exceed 1 GHz-km for a 50  $\mu\text{m}$  core diameter (Seastar, 1993).

Most singlemode fibres have core diameters ranging from 3.5 to 10  $\mu\text{m}$ , depending on the wavelength to be used. At a specific wavelength they support only one guided mode and are capable of very high bandwidths. The cladding diameter is standardised to 125  $\mu\text{m}$ , although smaller cladding diameters are also available.

Polarisation-preserving fibres are based on the concept of a large difference in velocity between the two linearly polarised field components of a singlemode fibre. These fibres can hold the polarisation state of the launched light if the input polarisation is properly aligned with the preferred axes of the fibre.

The basic parameters for optical fibres are numerical aperture ( $NA$ ) and normalised frequency ( $V$ ). Numerical aperture is defined as the sine of the half angle (Figure 2.3) of the largest cone of rays that a fibre can accept for propagation through it (by a series of internal total reflections).

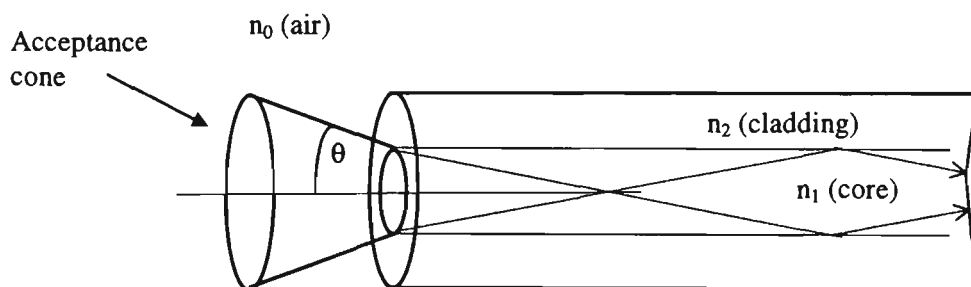


Figure 2.3. Acceptance cone for an optical fibre.

Rays outside this cone are not internally reflected along the fibre and are lost through the cladding. Mathematically, the  $NA$  of a fibre can be expressed as follows:

$$NA = n_0 \sin \theta = \sqrt{n_1^2 - n_2^2} \quad (2.1)$$

where:

$n_0$  (usually air), is the refractive index of medium outside of the fibre,

$\theta$  is the half angle of the cone,

$n_1$  is the refractive index of the core,

$n_2$  is the refractive index of the cladding.

Normalised frequency ( $V$ ) is defined as:

$$V = k a NA \quad (2.2)$$

where  $V$  = normalised frequency,

$k$  = wave number =  $2\pi/\lambda$ ,

$a$  = core radius.

If  $0 < V < 2.405$ , then the fibre will guide only one (i.e. the fundamental  $HE_{11}$ ) mode (Figure 2.4).

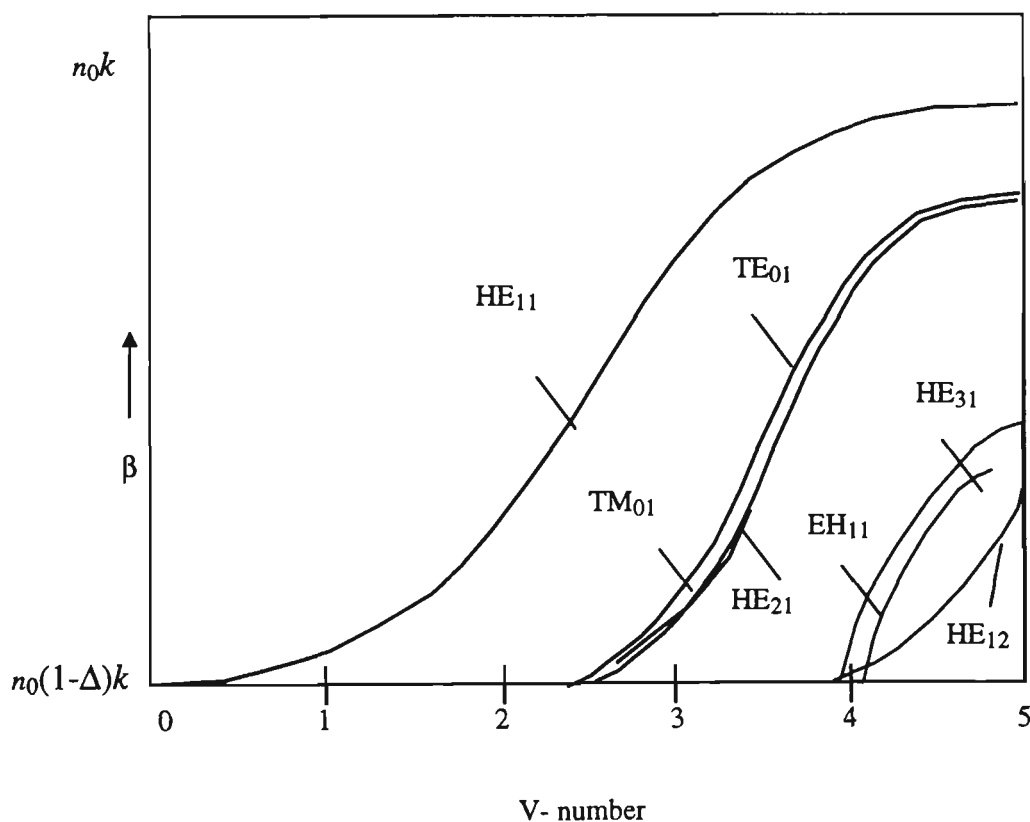


Figure 2.4. Determination of the number of guided modes as a function of  $V$  (after D. B. Keck, 1981).  $\beta$  is the propagation constant and  $\Delta = (n_1 - n_2)/n_1$ .

---

Both multimode and singlemode fibres can be used in sensing. Many of the less demanding applications will be served by MMF (the technology of which is well advanced). For some applications where extreme sensitivity is of paramount importance, however, it is likely that SMF technology will prevail. Singlemode fibres are more apt to be used in pure fibre sensors where the fibre itself is the sensor that measures the ambient conditions. In polarisation modulation schemes, SMF is an important component. By contrast, MMFs are mostly used to transmit and receive modulated light from a remote sensor.

In the work presented here two types of multimode optical fibre were used with core/cladding dimensions of 50/125  $\mu\text{m}$  and 100/140  $\mu\text{m}$  (Section 5.4).

### **2.2.3      *Optical detectors***

An optical detector is required to convert light to an electrical signal. The basic principle of operation of photodetectors relies on absorption and conversion of photons to an electrical current. The flow of charge carriers produces the electrical signals proportional to the light intensity. Although there are many types of light detectors, the eminently suitable detectors for the optical fibre system are those made from semiconductors. This is because only this type of detector can meet the size and cost compatibility requirement for optical fibres. A good detector must be sensitive, have high responsivity, have a short rise time, low in noise, high in efficiency, compatible in size with the fibre, simple in design, and low in cost. Not all requirements can be met in one design and according to the application a compromise has to be reached between various competing parameters. Some of the requirements for a good detector are discussed below (Wolf, 1979).

---

*Wavelength compatibility.* The peak efficiency of a photodetector should fall in the peak-wavelength region of the light sources used in the optical system.

*High speed.* The rise time of a photodetector should be short enough to accommodate the modulation frequency of the signal. Alternatively, they should have sufficient bandwidth to handle the incoming information. The electrical output of photodetectors should be linear with respect to the optical signal over a wide amplitude range.

*High sensitivity.* The photodetectors must be able to detect weak optical signals; that is, the quantum efficiency should be high enough to detect the smallest signal. The quantum efficiency ( $\eta_q$ ) of a photodetector is a measure of how effectively it generates electron-hole pairs in response to the incident photon energy. Some of the absorbed photon energy is converted to heat thereby reducing the total number of electron-hole pairs. The upper bound for  $\eta_q$  can be expressed as (Melchior, 1972):

$$\eta_q = (1-R)(1-e^{-\alpha d}) \quad (2.3)$$

where  $R$  is the surface reflectivity,  
 $\alpha$  is the absorption coefficient,  
 $d$  is the width of the absorption layer.

Figure 2.6 (c) shows the variation of the absorption coefficient as a function of wavelength for Si, Ge and GaAs semiconducting materials. In Figure 2.6 (b) various alloys, gas and Nd:YAG lasers used in different wavelength ranges are indicated. Common photodetectors used at various wavelengths are also shown in Figure 2.6 (a). The dotted vertical line represents the wavelength used by the optical fibre sensor presented in this thesis.

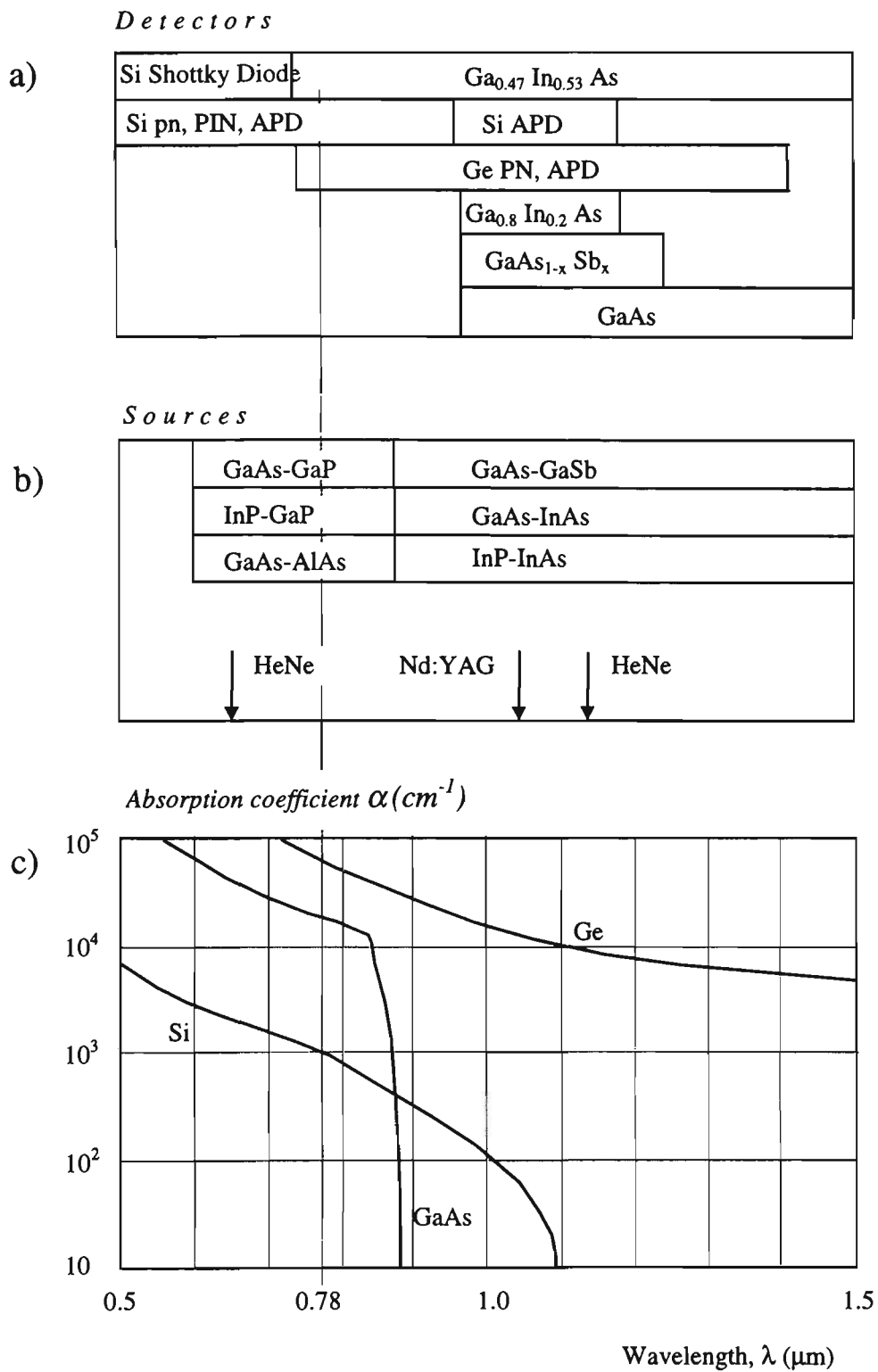


Figure 2.6. a) Light detectors. Here APD, pn and PIN stand for avalanche photodiode, pn-junction and PIN diode respectively.  
 b) Light sources.  
 c) Variation of the absorption coefficient as a function of wavelength for Si, Ge, and GaAs.

---

The most common semiconductor photodetectors are *pn* junction, PIN photodiode and avalanche photodiodes (APD). *pn* detectors are small, lightweight, require a low bias voltage and through careful design, have a short rise time. Typical *pn* diodes have rise times of the order of microseconds, and so are used for the detection of low frequencies only.

Although the bandwidths of PIN diodes and APDs are about 1 GHz, PIN diodes are preferred because they are cheaper, less sensitive to temperature changes and require a smaller bias voltage. Silicon, germanium and InGaAs PIN photodiodes are widely used and accommodate different operational wavelength ranges. Silicon diodes are ideal for shorter wavelengths (0.4 to 1.0  $\mu\text{m}$ ) whilst Ge and InGaAs are suitable for longer wavelengths ( $>1 \mu\text{m}$ ), although the latter introduce more noise than silicon devices. APDs have internal gain which makes them more appropriate for the detection of weak signals. An APD with a carefully optimised operating point, followed by a transimpedance amplifier can give a better SNR than a PIN diode followed by an appropriate transimpedance amplifier. Since the wavelength of the laser diode used in this work was 780 nm, a PIN silicon photodiode was an appropriate choice for a photodetector (Section 5.2).

### 2.3 POWER LOSS AND NOISE CONSIDERATIONS

As discussed earlier (Section 2.2.1), besides the size compatibility, a light source for optical fibres should have a radiation pattern compatible with the numerical aperture *NA* of the fibre (Figure 2.2). For example, a graded index fibre has a light-propagation distribution resembling a Gaussian shape and can be coupled efficiently to a light source having a similar intensity distribution. SMFs have a core diameter of only several micrometres and therefore the light source must have a matching emission area. The light acceptance cone angle of the fibre is small and

---

thus light from sources having a broad radiation pattern (large divergence) cannot be coupled efficiently into the fibre.

As the requirement for this project is to launch the highest possible power into the optical fibre at a low modulation frequency, MMF is therefore a better choice than SMF.

Besides the loss due to source-fibre mismatch, one of the most stringent requirements on an optical fibre sensing system is the reduction of noise. This is particularly important since the detector is normally the principal noise contributor. The subject of noise in the photodetector and electronic amplifier will be discussed in Section 4.5.

## **2.4 CONCLUSION**

This chapter has introduced the basic components of the optical sensor system and their relevance to the work presented in this thesis. Singlemode laser diodes at 780 nm are not only an inexpensive light source but also allow a simple and stable alignment (1 mW injected into the fibre, that is 30% of the available power). Two types of multimode optical fibres were used, 50/125  $\mu\text{m}$  and 100/140  $\mu\text{m}$ . Power levels of -10 dB and -5 dB were injected into the fibres respectively. To complete the system, silicon PIN photodiodes were selected because of their good responsivity at 780 nm (approaching the peak responsivity of 0.55 A/W which is close to the maximum theoretical responsivity of 0.64 A/W).

---

## **Chapter 3      REVIEW OF VELOCITY MEASUREMENT TECHNIQUES**

### **3.1      INTRODUCTION**

The measurement of velocity is an important requirement in many scientific and industrial applications. To date, devices mainly based on the principle of magnetic induction have been developed for velocity measurement.

Since the introduction of the laser a number of optical methods for flow velocity measurement have evolved, providing an opportunity for lower cost and simpler, nonintrusive measurements.

The aim of this chapter is to review some of the popular techniques for velocity measurement.

### **3.2      NON-OPTICAL VELOCITY MEASUREMENT**

The most common technique for velocity measurement is the so called inductive method. This method usually employs a transducer based on electrodynamic effects (Usher, 1985). There are two types of transducers - moving coil and moving magnet. The former is used mainly in instruments such as accelerometers and velocity meters, whereas the latter is available as off-the-shelf transducer for OEM (Original Equipment Manufacturer) applications.

*Moving coil transducer.* The most general arrangement comprises a cylindrical magnet in a ferromagnetic yoke with pole pieces. The coil is usually wound on a frame and attached to the object whose velocity is

---

required. When the object moves a time dependent *e.m.f.* is generated from which acceleration and velocity can be found. This method can only be used for short distances and the mass of the coil itself affects the measurement. Moreover, such a device measures a change in velocity, and so the moving object has to be at rest prior to making absolute measurements.

*Moving magnet transducer.* The simplest form of moving magnet transducer comprises a single coil with an internal magnet. In this case, the induced *e.m.f.* is proportional to the speed of the magnet (attached to the moving object). This has the disadvantage of a sensitivity which varies with the position of the magnet.

*Rotational velocity transducers.* The rotational equivalent of the moving coil velocity transducer is the tachometer. There are two main types of tachometers—direct current (*D.C.*) and alternating current (*A.C.*). The *D.C.* tachometer is essentially a *D.C.* generator with a permanent magnet. A coil rotates within the field of the magnet. Several poles are used to ensure a reasonably smooth output, with commutator rings required to produce a *D.C.* voltage proportional to velocity. The device is convenient and widely used in control systems where velocity feedback is needed. However, the device is unsatisfactory for precision measurements because of unavoidable ripple voltage (due to the finite number of poles) and electrical spikes generated by the commutator rings. The *A.C.* device is better in this respect as it consists of a rotating cylinder with two coils at right angles without commutator rings. One coil is excited at constant frequency and voltage whilst the second detects a voltage proportional to the rate of rotation of the cylinder from the effects of eddy currents (Mansfield, 1973).

*Piezo-electric method.* The basic physical effect used in these transducers is the generation of surface charge in response to mechanical deformation. The resulting voltage magnitude depends on

---

the direction of the applied force with respect to the axes of the crystal. These devices can be operated to give essentially a flat response to either displacement or velocity. However, it is important to note that the slow time response makes it unusable above a few tens of Hz (Mansfield, 1973).

*Digital methods.* As velocity is the rate of change of displacement with time, it is possible to calculate the velocity by counting the number of evenly spaced marks placed on the moving object over an interval of time. The marks can be read photo-electrically or can be protrusions which are detected by a capacitive or inductive proximity meter (Usher, 1985).

*Doppler effect.* The Doppler effect (Usher, 1985) is a very effective and accurate means of measuring velocity. If a narrow radio or ultrasonic beam is directed at an object, a proportion will be reflected back to the source. However, if the object is moving the frequency of the received signal differs from that of the transmitted signal, with the difference being a measure of the velocity of the moving object. The received frequency will be lower/higher than the transmitted frequency if the moving object is travelling away from/towards the source. The police radar “gun” is a well known example of this technique.

### **3.3 OPTICAL VELOCITY MEASUREMENT**

In recent years a range of optical methods have been developed for velocity measurement and those of relevance to the work presented here have been selected for review.

---

### 3.3.1 *Laser Doppler Velocimetry*

As discussed earlier (Section 3.2), the Doppler effect is used in conjunction with different sensors for velocity and displacement measurement. The introduction of the laser has made possible significant advances in the field of velocity measurement. Developments such as the laser Doppler technique provide high spatial and temporal resolution (Durst *et al.*, 1976). The early developments in laser Doppler velocimetry concentrated on optical systems for flow measurement and are well documented in the literature (Durst *et al.*, 1976; Beck, 1974; Dyot, 1978; Beck, 1984).

The most commonly used optical arrangements for laser Doppler velocimetry employ either the “*reference beam*” or “*dual beam*” (fringe) modes. A third arrangement, the “*two-scattered beam*” mode has not been used as extensively as the others (Durst *et al.*, 1976).

In the “*reference beam*” (or local oscillator heterodyning mode) the laser beam is split into an intense and a weak beam (reference). The reference beam is directed onto a photocathode of a photomultiplier where it beats with light scattered from the strong beam by particles moving with the flow. The frequency of the scattered light is altered by the Doppler effect and the interference with the reference beam provides a beat frequency which is proportional to the particle velocity. This arrangement was employed in the pioneering work of Yeh and Cummins, and has subsequently been used by many authors.

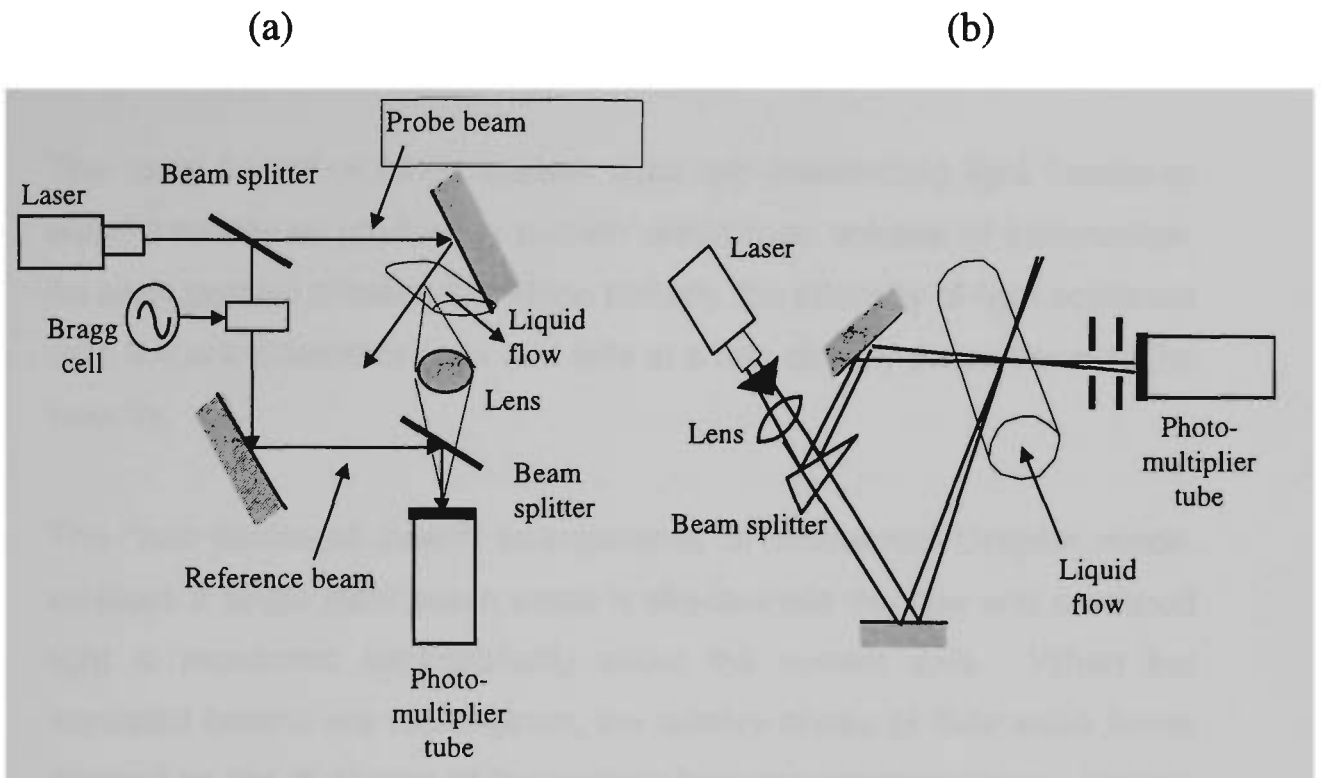


Figure 3.1 . The two basic arrangements for laser Doppler velocity measurement.  
 (a) Yeh and Cummins (1964).  
 (b) Goldstein and Kreid (1967).

In Figure 3.1. the optical configurations for early laser Doppler velocimetry are depicted. The first laser Doppler velocimeter was developed in 1964 by Yeh and Cummins (Figure 3.1 (a)). The reference beam was directed around the test region and combined with the light scattered from the probe beam at a second beam splitter. Such arrangements are difficult to align and operate since the position of the reference and signal beam are extremely critical. Goldstein and Kreid (1967) overcame this problem by means of the optical configuration shown in Figure 3.1 (b). In this case the reference and the scattering beams both pass through the flow and intersect at a common point. The reference beam passes directly through the flow and heterodynes with the light scattered along its path from the scattering beam. Alignment of

---

this system is relatively simple and is less sensitive to vibrations than those proposed by Yeh and Cummins.

The “*dual beam*” or fringe system uses two intersecting light beams of equal intensity to produce a pattern within their volume of intersection. As each particle crosses the fringe pattern, the intensity of light scattered onto the photodetector rises and falls at a rate directly proportional to the velocity.

The “*two scattered beam*” arrangement, or differential Doppler mode, employs a single laser beam which is directed into the flow and scattered light is monitored symmetrically about the system axis. When the scattered beams are recombined, the relative phase of their wave fronts depend on the distances of the particle from the aperture (lens). Hence, as the particle moves across the incident beam the scattered light beams interfere leading to a light intensity at the photocathode which fluctuates at the Doppler frequency. This system offers no clear advantage over the fringe mode other than its use in measuring simultaneously two velocity components by collecting pairs of scattered light beams in mutually perpendicular planes.

### **3.3.2     *Fibre optic Doppler velocimetry***

By combining the laser Doppler velocimeter technique with optical fibre technology, additional advantages are gained. Laser Doppler velocimetry is an optical technique usually employed to non-intrusively measure the velocity of a gas or liquid flow. For improved resolution, small particles are occasionally seeded into the flow (Krohn, 1988). By proper choice of seed particle size (small enough to ensure that the particle velocity follows the velocity of the fluid), the mean velocity magnitude, turbulence intensity and velocity vector can be measured. By suitable interpretation of the signals, particle loading and particle size

---

data can also be obtained. Dyott (1978), and Kyuma *et al.* (1981) have produced a small fibre velocity sensor, by using a single optical fibre. Their system amounted to a non-differential Doppler design which requires a prior knowledge of the velocity vector direction in order to accurately measure velocity magnitude. Ross *et al.* (1978) and Watkins and Hollaway (1978) have utilised such single fibre sensors in the construction of practical instruments. Danel (1975) and Sasaki *et al.* (1980), combined fibre optic transmission with some elements of ordinary laser Doppler anemometer equipment to perform differential measurements. Sasaki and Watanabe (1980) combined two single fibre devices to form what they called a dual single-beam sensor. Their sensor can measure velocity magnitude, using a rather complex signal processing scheme. Finally, Colella and Neti (1982), produced a true fibre optic sensor using multimode fibres. This sensor suffered from some fringe distortion problems but provided adequate measurement of velocity in a two phase flow.

To overcome the fringe distortion problem, Boiarski and Kingsley (1983) developed a differential Doppler velocimeter (Figure 3.2). Two singlemode polarisation maintaining fibres were used to direct the light onto the measurement volume. When particles, bubbles or surface irregularities move through the fringe region generated by the two laser beams, they scatter a proportion of the incident light back along the probe axis. A multimode fibre in conjunction with a microlens, is employed to collect this backscattered light and transmit it to the photodetector. The measured Doppler frequency, ( $f_D$ ) is then converted to velocity ( $\mathcal{V}$ ) using the simple equations:

$$\mathcal{V} = f_D \delta \quad (3.1)$$

$$\delta = \frac{\lambda}{2 \sin(\alpha/2)} \quad (3.2)$$

where  $\lambda$  is the wavelength of the laser beam,  $\delta$  is the fringe spacing and  $\alpha$  is the angle between the two beams (Boiarski and Kingsley, 1983). From Equation 3.1 it can be deduced that the resultant Doppler frequency can be viewed as the rate at which the scattering centres cross through the fringes. Furthermore, since the fringes are planar, only one particular velocity component is measured for a given input beam orientation. This component is the one that is perpendicular to fringes and in the plane of the two input beams.

The authors admit that while ordinary single mode fibres in conjunction with a polarising film can provide excellent fringe parallelism and contrast, the use of polarisation maintaining fibres is required for practical devices.

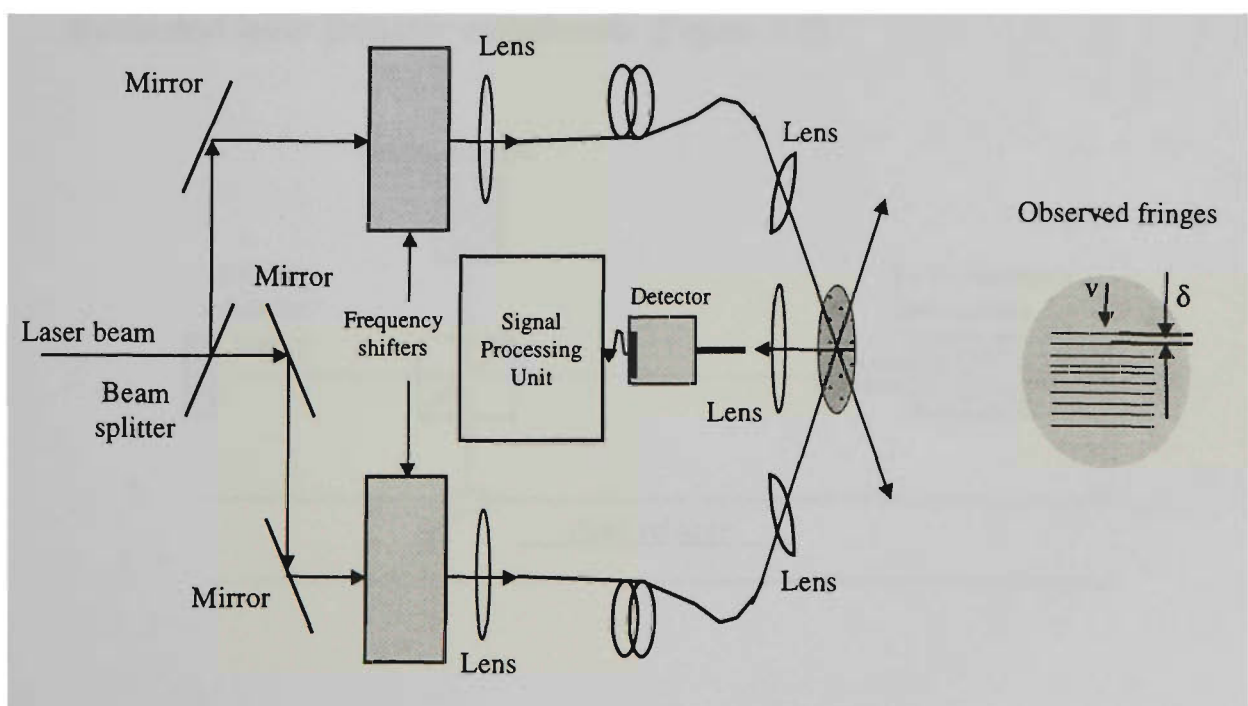


Figure 3.2. Schematic diagram of the optical arrangement of the differential Doppler velocimeter (Boiarski and Kingsley, 1983).

The accuracy of this device was determined by measuring the tangential velocity of a rotating surface. The measured velocity was within 3% of the calculated value based upon the rotational velocity of the driving motor and the distance of the measuring point from the centre of the disk.

### 3.3.3 *Distributed Laser Doppler Velocimetry*

In classic laser Doppler velocimetry, the location of the flow volume is determined by the orientation of the receiving or launching optics. Unfortunately, a method for the continuous interrogation of many different points in the flow stream required for a cross-sectional velocity profile, still represents an unsolved problem in many applications. In fact, the continuous interrogation requires a movement of the projection optics that causes a series of additional problems that degrade the performance of the laser Doppler velocimeter. To overcome this problem, Gusmeroli and Martinelli (1991) developed a monobeam distributed laser Doppler velocimeter (Figure 3.3).

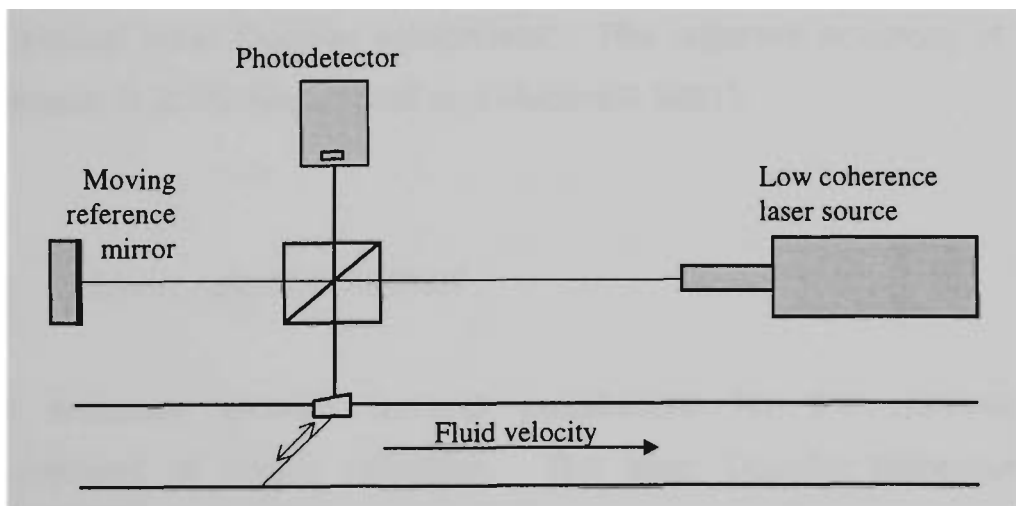


Figure 3.3. Design principle of the distributed laser Doppler velocimeter.

---

In the classical laser Doppler velocimeter (Figure 3.1) the light scattered by the fluid particles is localised and collected by the receiving optics and recombined with the local oscillator to produce the Doppler signal. The distributed laser Doppler velocimeter uses a collimated short coherence source combined with a Michelson interferometric configuration. Note that path compensation in the Mach-Zender configuration interferometer requires the use of long coherence sources (Krohn, 1988).

Among the many particles belonging to the flow volume intersected by the collimated sensing beam, only the particles at a distance comparable to the reference beam path contribute to the interference. In other words, the information on flow velocity comes only from the scattering volume whose optical distance from the beam splitter matches the optical distance of the reference mirror. The flow velocity vector  $\mathcal{V}$  is projected upon the sensing beam wave vector  $k$  to give the Doppler frequency shift. The advantage of interrogating many points along the flow is in producing the velocity distribution. The disadvantage of the distributed laser Doppler velocimeter is reduced signal-to-noise ratio requiring more sophisticated data analysis to preserve the accuracy of the classical laser Doppler velocimeter. The reported accuracy of this velocimeter is 2.5% (Gusmeroli and Martinelli 1991).

### **3.3.4      *Laser speckle method***

Laser methods provide several possibilities for the non-contact measurement of object velocities. The laser Doppler technique of crossed laser beams allows the measurement of the velocity component in the plane of the two laser beams and perpendicular to the bisector of their angle (Krohn, 1988). The crossed beams define the measurement volume. One of the problems with this method is that in many applications the distance between the measuring head and the object

cannot be held constant. To overcome this, Ruth (1987) has developed and investigated the optical fibre laser speckle velocimeter (Figure 3.4.).

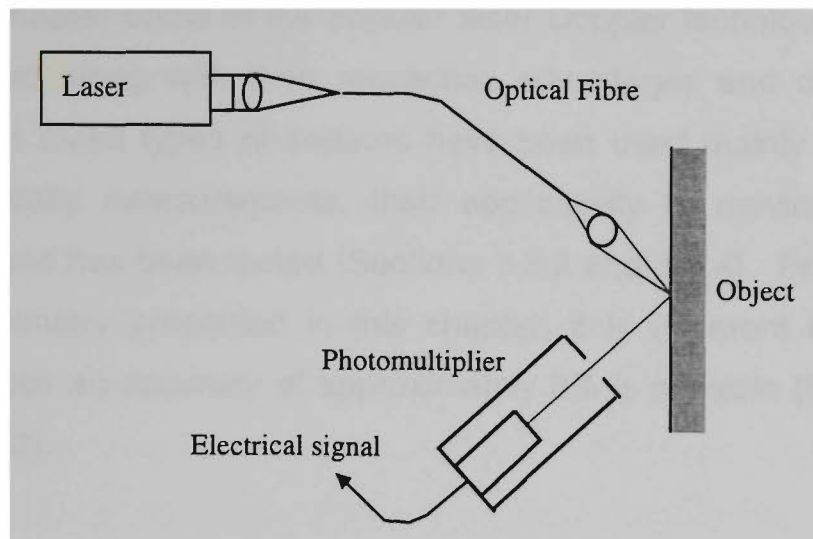


Figure 3.4. Experimental arrangement for velocity measurement by the speckle method.

Light directed onto a rough surface is scattered to produce a granular signal structure (speckles). The mean speckle width ( $\sigma$ ) at an observation point is given by  $\sigma = cl/D\lambda$ , where  $\lambda$  denotes the laser wavelength,  $l$  the distance between the observation point and the laser spot,  $D$  the diameter of the laser spot, and  $c$  a parameter which is dependent on the beam profile (Ruth, 1987). A laser spot with a Gaussian profile has a value of  $c = \sqrt{2\pi}$ . When the object is moving, the speckle pattern becomes time dependent, and a speckle velocity can be defined. The method for object velocity determination, used by Ruth, was speckle counting. That is, the intersections between the speckle intensity  $I(t)$  and a certain threshold are counted, and the counting rate is proportional to the speckle velocity. Difficulties arise from the noise, and the dependence of the counting rate on the threshold position.

---

### **3.4 CONCLUSION**

In this chapter some of the popular laser Doppler techniques have been presented along with their respective advantages and disadvantages. Although these types of sensors have been used mainly for liquid and gas velocity measurements, their applicability to moving surfaces is known and has been tested (Sections 3.3.2 and 3.3.4). From the review of velocimetry presented in this chapter, it is apparent that for these techniques an accuracy of approximately 3% is possible (Sections 3.3.2 and 3.3.3).

In the research work presented in this thesis it will be shown that the speed of moving surfaces can be measured with a relative accuracy better than 2% by using cross-correlation techniques in conjunction with optical fibre technology.

---

## Chapter 4      THEORETICAL ANALYSIS

### 4.1      INTRODUCTION

Correlation functions occupy a central position in the techniques available for the synthesis and analysis of linear and non-linear systems (Jordan, 1986). Their importance has been recognised for many years but it has only recently become possible to economically implement these functions with compact hardware (Jordan, 1986). The implementation of these functions has provided a wide range of interesting problems and considerable ingenuity has been expended to solve these problems as microelectronics technology has evolved to offer greater hardware complexity at low cost.

Correlation is used in a wide range of applications, especially in the measurement of flow rates or the velocity of fluids (Beck, 1984; Krohn, 1988; Bentley, 1992). The forms of velocity detection, described in the literature, include (Bentley, 1992):

- AC conductivity electrodes
- capacitance transducers
- radiation pyrometer with infrared detector
- ultrasonics.

The equipment based upon these sensors has been successfully adapted for industrial purposes, although their operation would be suspect in electromagnetically hostile environments. Use of optical fibres as both the sensor and signal guide would overcome this problem.

In this chapter attention is focussed on the theory of time delay estimators (Section 4.2), based on the treatment given by Bendat and Piersol (1980). Furthermore, some of the alternative forms of the cross-correlation function will be also presented (Section 4.2) and some of the advantages and disadvantages of their implementation discussed. Special attention will be given to the correlation algorithms and their applications to velocity measurement.

## 4.2 TIME DELAY ESTIMATION

Time delay estimation is an important issue in many signal processing areas. This includes direction of movement, range estimation in multisensor arrays, motion compensation in moving images, stereo vision and profiling in telesensing systems (Jacovitti and Scarano, 1993). Classical time delay estimation techniques consist of identifying the maximum value of the cross-correlation function between the reference and delayed signal (Jordan, 1986).

Specifically if two continuous random processes  $\{x(t)\}$  and  $\{y(t)\}$  are assumed to be stationary (long-term statistical quantities do not change with time) and can be represented by individual time histories  $x(t)$  and  $y(t)$ , then to assess the degree of linear dependence between  $x(t)$  and  $y(t)$  a covariance function  $C_{xy}(\tau)$  is used. The covariance function between  $x(t)$  and  $y(t)$  for any time delay  $\tau$  (Bendat and Piersol, 1980) is given by:

$$\begin{aligned} C_{xy}(\tau) &= \lim_{T \rightarrow \infty} \frac{1}{T} \int_0^T \{x(t) - \mu_x\} \{y(t + \tau) - \mu_y\} dt \\ &= R_{xy}(\tau) - \mu_x \mu_y \end{aligned} \quad (4.1)$$

where  $T$  = integration time,

---

$\tau$  = time delay,

$\mu_x$  = the mean of  $x(t)$ ,

$\mu_y$  = the mean of  $y(t)$ ,

and 
$$R_{xy} = \lim_{T \rightarrow \infty} \frac{1}{T} \int_0^T x(t)y(t+\tau) dt. \quad (4.2)$$

For the general case where  $x(t)$  and  $y(t)$  represent different data,  $R_{xy}(\tau)$  in equation (4.2) is called the cross-correlation function between  $x(t)$  and  $y(t)$ . For the special case where  $x(t)=y(t)$ ,

$$C_{xx}(\tau) = \lim_{T \rightarrow \infty} \frac{1}{T} \int_0^T \{x(t) - \mu_x\} \{x(t+\tau) - \mu_x\} dt = R_{xx}(\tau) - \mu_x^2 \quad (4.3)$$

where 
$$R_{xx}(\tau) = \lim_{T \rightarrow \infty} \frac{1}{T} \int_0^T x(t)x(t+\tau) dt, \quad (4.4)$$

is called the autocorrelation function of  $x(t)$ . It should be mentioned that some texts use the term correlation function to refer to the quantity defined here as the covariance function in equation 4.1. Since the two functions are interrelated by  $R_{xy}(\tau) = C_{xy}(\tau) + \mu_x \mu_y$ , it follows that  $R_{xy}(\tau) = C_{xy}(\tau)$  only if the mean of both functions is zero. Correlation functions are normalised as follows:

Autocorrelation: 
$$-1 \leq \frac{R_{xx}(\tau)}{R_{xx}(0)} \leq 1 \quad (4.5)$$

Cross-correlation: 
$$-1 \leq \frac{R_{xy}(\tau)}{\sqrt{R_{xx}(0)R_{yy}(0)}} \leq 1 \quad (4.6)$$

---

where  $R_{xx}(0)$  and  $R_{yy}(0)$  are the mean square values of the signals  $x(t)$  and  $y(t)$  respectively. Note that these two additional mean square value measurements are required to implement the normalised function.

#### 4.2.1 Power spectral density

The power spectral density  $\varphi(\omega)$  of a signal is defined (Bentley, 1992) as:

$$\varphi(\omega) = \frac{dW}{d\omega} \quad (4.7)$$

where  $W$  = signal power (W)

$\omega$  = signal frequency (Hz).

Thus the total power generated in the frequency range  $\omega_1$  and  $\omega_2$  is given by,

$$W = \int_{\omega_1}^{\omega_2} \varphi(\omega) d\omega . \quad (4.8)$$

Internal noise sources in electrical circuits can often be regarded as white noise (Bentley, 1992) which has uniform power spectral density over an infinite range of frequencies. Hence, the noise power is given by

$$\varphi(\omega) = A \quad \text{for} \quad 0 \leq \omega \leq \infty. \quad (4.9)$$

Another useful representation for both noise and measurement signals is the power spectral density which is constant up to a cut-off frequency  $\omega_c$  and zero for higher frequencies (band limited noise):

$$\begin{aligned}\varphi(\omega_c) &= A & 0 \leq \omega \leq \omega_c \\ \varphi(\omega_c) &= 0 & \omega > \omega_c\end{aligned}\tag{4.10}$$

The power spectrum can be obtained from the autocorrelation function by Fourier analysis. Conversely, the autocorrelation function can be obtained from the power spectrum by adding the harmonics together. For random signals, the autocorrelation function and power spectral density are related by the Fourier transform or Wiener-Khinchin relations, namely:

$$R_{xx}(\tau) = \int_0^{\infty} \varphi(\omega) \cos \omega \tau \, d\omega \tag{4.11}$$

$$\varphi(\omega) = \frac{2}{\pi} \int_0^{\infty} R_{xx}(\tau) \cos \omega \tau \, d\tau \tag{4.12}$$

The form of both functions for band limited white noise is shown in Figure 4.1 where it can be seen that  $R_{xx}(\tau)$  has its first zero crossing at  $\tau = \pm \frac{\pi}{\omega_c}$ , and a central peak width of  $\frac{2\pi}{\omega_c}$ . Consequently, a rapidly varying random signal has a high value of  $\omega_c$  (a broad power spectrum) but a narrow autocorrelation function that falls off sharply as  $\tau$  is increased. A slowly varying random signal, however, has a low value of  $\omega_c$  (narrow power spectrum) but a broad autocorrelation function that falls slowly as  $\tau$  is increased.

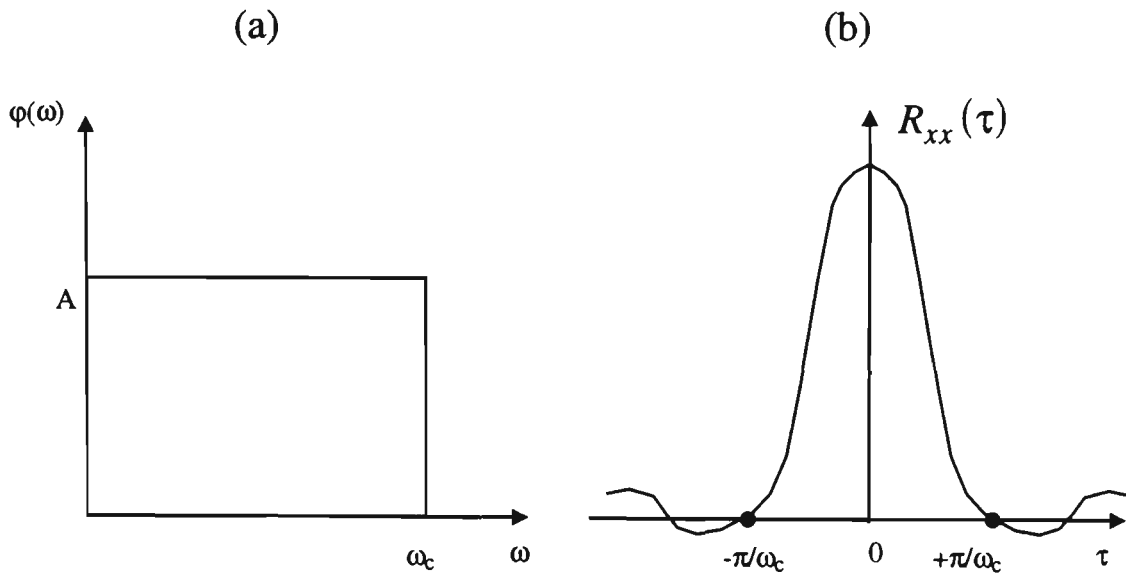


Figure 4.1. Relationship between power spectrum and autocorrelation function for band limited white noise.

(a) power spectrum.

(b) Autocorrelation function.

In the case of surface speed measurement involved in this work, the signal generated is not degraded by spurious noise (as usually occurs in fluid flow measurement), and so the cross-correlation function simplifies to the autocorrelation function time-shifted from the origin.

#### 4.2.2 Time delay estimators

Since cross-correlation is computationally intensive, it may be preferable in some applications requiring real time processing to replace cross-correlation by relay correlation or hybrid sign correlation (HS), polarity coincidence correlation (Cussani, 1989) or averaged magnitude difference function (AMDF, Sullivan, 1989). To avoid any confusion, the classical cross-correlation is called direct correlation (DC) and this formalism is used for the rest of this section.

In the DC method an estimate of the cross-correlation function between the received signals  $x(kt)$  and  $y(kt + \tau)$  is computed from the available data records as :

$$R_{DC}(\tau) = \frac{1}{N} \sum_{k=1}^N x(kt)y(kt + \tau) \quad (4.13)$$

where  $t$  is the sampling interval,  $k$  is a positive integer,  $N$  is the number of sample points and  $x(kt)$  and  $y(kt + \tau)$  the digitally converted values of the (continuous) analogue signals  $x(t)$  and  $y(t + \tau)$  respectively. The estimator for direct correlation is given by

$$\tilde{D}_{DC} = \arg(\max R_{DC}(\tau)). \quad (4.14)$$

Hybrid sign ( $R_{HS}$ ) and polarity coincidence ( $R_{PC}$ ) techniques replace (4.13) by the following:

$$R_{HS}(\tau) = \frac{1}{N} \sum_{k=1}^N x(kt) [\text{sign } y(kt + \tau)] \quad (4.15)$$

$$R_{PC}(\tau) = \frac{1}{N} \sum_{k=1}^N [\text{sign } x(kt)] [\text{sign } y(kt + \tau)], \quad (4.16)$$

where

$$\text{sign } x(kt) = \begin{cases} +1 & x(kt) > 0 \\ -1 & x(kt) < 0 \end{cases} \quad (4.17)$$

and

$$\text{sign } y(kt + \tau) = \begin{cases} +1 & y(kt + \tau) > 0 \\ -1 & y(kt + \tau) < 0 \end{cases} \quad (4.18)$$

These conditions impose a series of restrictions on the precision of the correlation function itself. The minimal number of multiplication operations assures that the estimators defined by (4.15), and (4.16) can be computed quickly. On the other hand, a certain loss in accuracy must be accepted or, alternatively, precision is preserved at the cost of an enlarged observation period. Therefore, direct correlation was chosen

for time delay estimation in the applications described in this thesis. By analysing the variance of above mentioned estimators with respect to the signal-to-noise ratio (which is plotted in Figure 4.2) it can be seen that the DC estimator outperforms the HS and PC for all values of signal-to-noise ratio (Cussani, 1989).

The continuous time delay estimation requires in principle the computation of the above defined statistics for an infinite number of values of  $k$ . In practice, this number is limited by the knowledge of the delay range and by the desired resolution. Since this resolution is often much finer than the sampling interval  $t$ , it is necessary to interpolate the signal or the statistics.

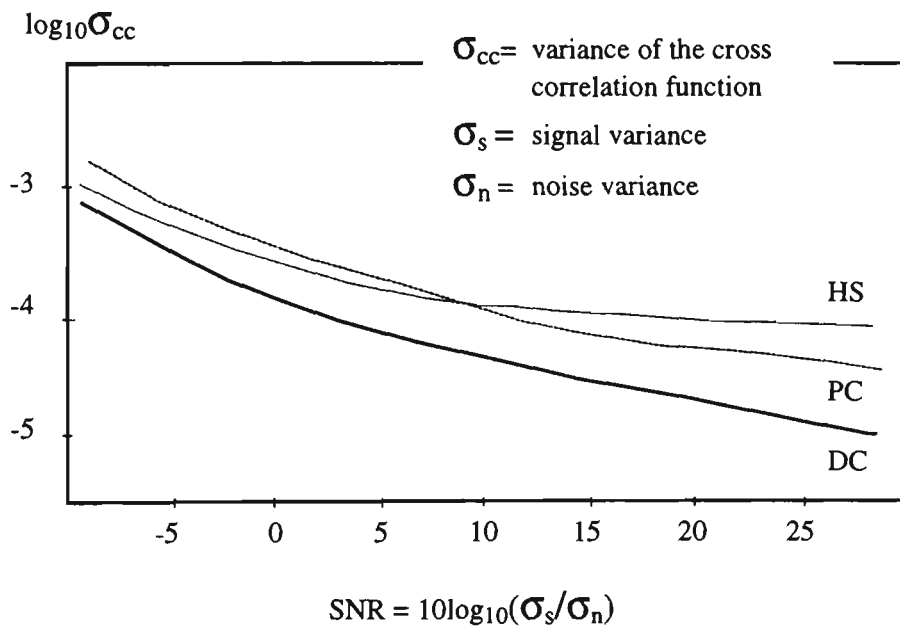


Figure 4.2 Variance of DC, HS and PC time delay estimators as a function of SNR for white signal and noise, after the theoretical model developed by Cussani, 1989.

In this work, the signals are band limited with  $t \leq \frac{1}{2f}$  (Section 4.3.2), so they can be ideally interpolated (see Figure 4.1) with the sinc function. In practice interpolation is performed using FFT techniques by employing either zero padding, or a linear phase shift into a time lock loop (Jordan, 1986). However, from a computational point of view it is more convenient to interpolate the statistics. As direct correlation is band limited inside  $f$  and presents a symmetric peak around  $\tau$ , it follows that it can be approximated with a convex parabola in the neighbourhood of its maximum (Jacovitti and Scarano, 1993):

$$R_{DC}(\tau) = a\tau^2 + b\tau + c \quad (4.19)$$

Here  $a$ ,  $b$  and  $c$  are parameters derived from the best fit to the measured correlation. Using this very simple approximation the continuous time delay estimate can be found by locating the apex of the parabola

$$\tilde{D}_{DC} = -\frac{b}{2a}, \quad (4.20)$$

using the maximum cross-correlation lag and two adjacent values. It follows that a subsample estimate can then be obtained (Jacovitti and Scarano, 1993) from (4.20) in the form

$$\tilde{D}_{DC} = -\frac{t}{2} \frac{R_{DC}(i_{m+1}t) - R_{DC}(i_{m-1}t)}{R_{DC}(i_{m+1}t) - 2R_{DC}(i_m t) + R_{DC}(i_{m-1}t)} + i_m t, \quad (4.21)$$

where  $i_m$  represents the index of the maximum value of the discrete cross-correlation function.

---

### 4.3 DESIGN OF CROSS-CORRELATION MEASUREMENT SYSTEMS

When the correlation functions were first recognised as an important tool in signal processing, the cost of implementation was large. The first practical correlators used magnetic tape recorders with specially designed additional sensing heads that could be precisely moved to establish a time delay relative to the fixed head. Data was gathered sequentially and consequently very long measurement times were required. Electrical delay circuits constructed from filter sections connected in series have also been implemented. Although they eliminated the need for the mechanical components, they were still expensive to produce. Other circuit techniques have been used to replace the complex analogue delay circuits. For example, a calculation procedure (Jordan, 1986) approximates the correlation function by polynomial, orthogonal functions which do not require any pure delay elements except a bank of simple filters. However this technique suffered from a considerable dependence on the filter coefficients and resulted in large uncertainties. As microelectronics technology developed the implementation of variable time delay became less of a problem.

Motion generated noise or pseudorandom patterns monitored at two points has been widely used for flow measurement applications. The correlation flowmeter shown in Figure 4.3 represents a typical application of this principle. In this case, turbulent flow noise is detected at two points along the flow stream (usually by monitoring the frequency modulation of the ultrasonic beams), and flow velocity is obtained from the spacing of the beams and the measured time delay. Numerous correlation flow measurement methods have been developed using this method (Beck, 1984).

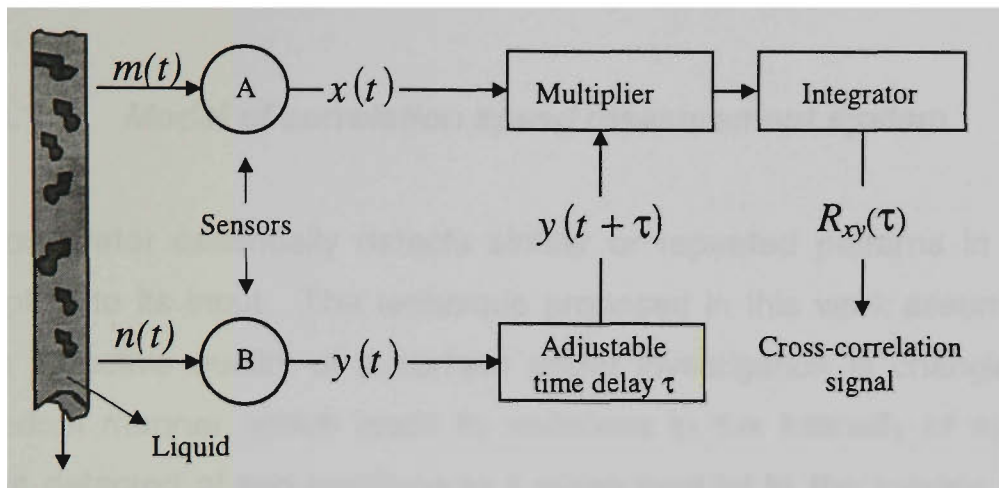


Figure 4.3. Schematic diagram of cross-correlation flowmeter.  
 –  $m(t)$  is the flow modulated signal.  
 –  $n(t)$  the delayed signal from another point.

The choice of sensors is frequently based upon their reliability and cost. The gain stability of the sensors is not important, because the cross correlator simply measures the time delay of signals between the sensors, and this time delay is not dependent on the actual gain. Some transducers have simple structures, such as conductivity probes and fringing capacitors which require only a modest amount of circuitry to derive the flow (noise) signal. A more complex transducer system has been developed for non-contact ultrasonic flow noise monitors, where a beam was transmitted and received by the transducers mounted on the outside of the containing pipe. A careful design was required to ensure that symmetrical, reproducible correlation functions were obtained (Beck and Ong, 1975). In contrast, piezoelectric transducers have to be in contact with the fluid and since the velocity of sound is much greater than the velocity of the fluid, considerable errors are introduced.

Even though it is recognised widely that optical transducers are potentially superior to those reviewed above, their application to industry

---

is limited because of the problem of soiling of optical surfaces (Beck, 1984).

#### **4.3.1 *Model of correlation speed measurement system***

A correlator essentially detects similar or repeated patterns in signals applied to its input. The technique proposed in this work assumes that the reflective quality of a surface under investigation is changing in a random manner, which leads to variations in the intensity of scattered light detected at two positions in a plane parallel to the moving surface (Section 5.1). Thus, the corresponding detector outputs  $x(t)$  and  $y(t)$  will also be random signals. In Figures 4.4 and 4.5 two random signals and their cross-correlation function are depicted.

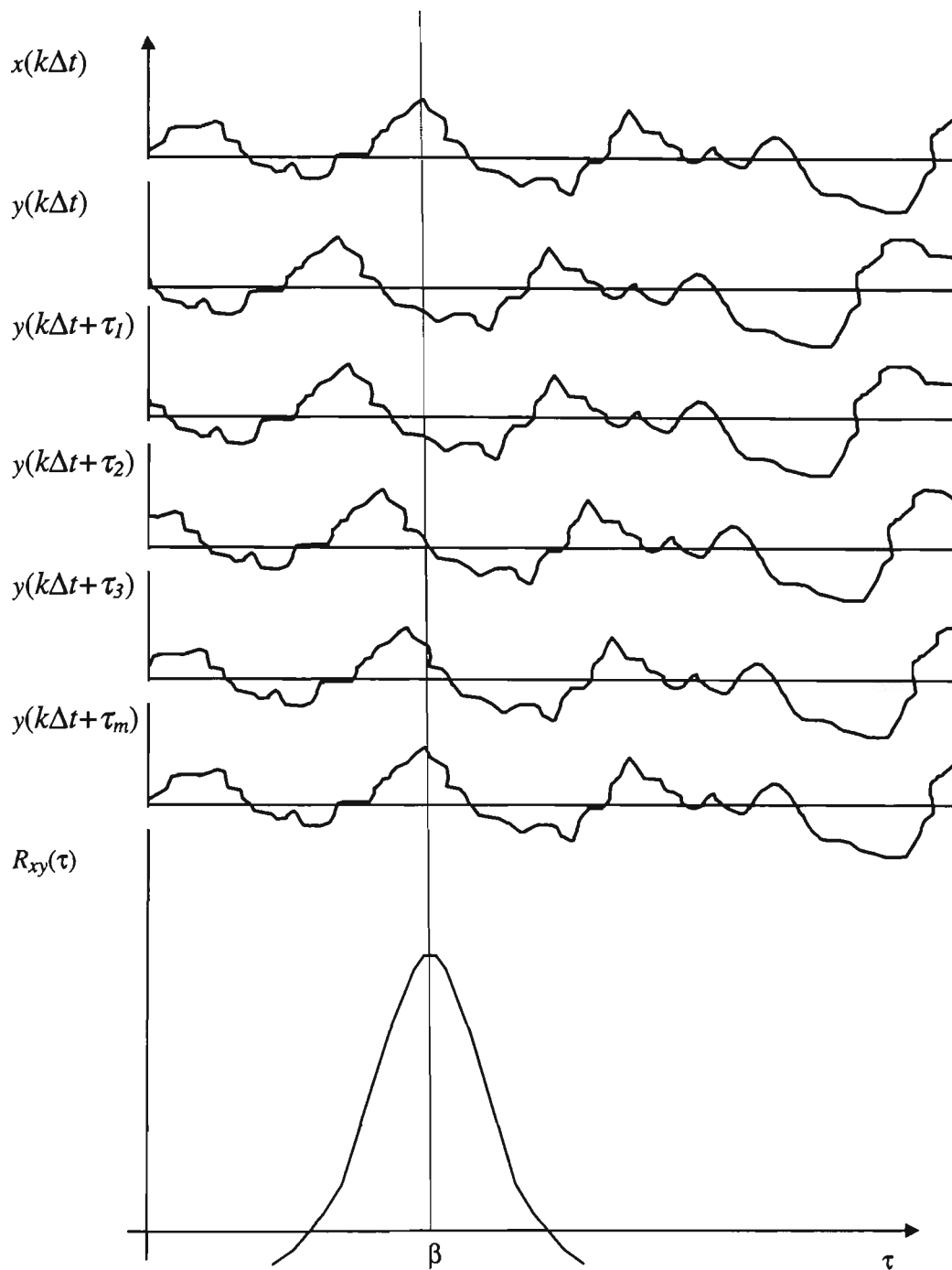


Figure 4.4. Cross-correlation function derived from simulated data. Signal  $y(k\Delta t)$  is time shifted with respect to  $x(k\Delta t)$ .

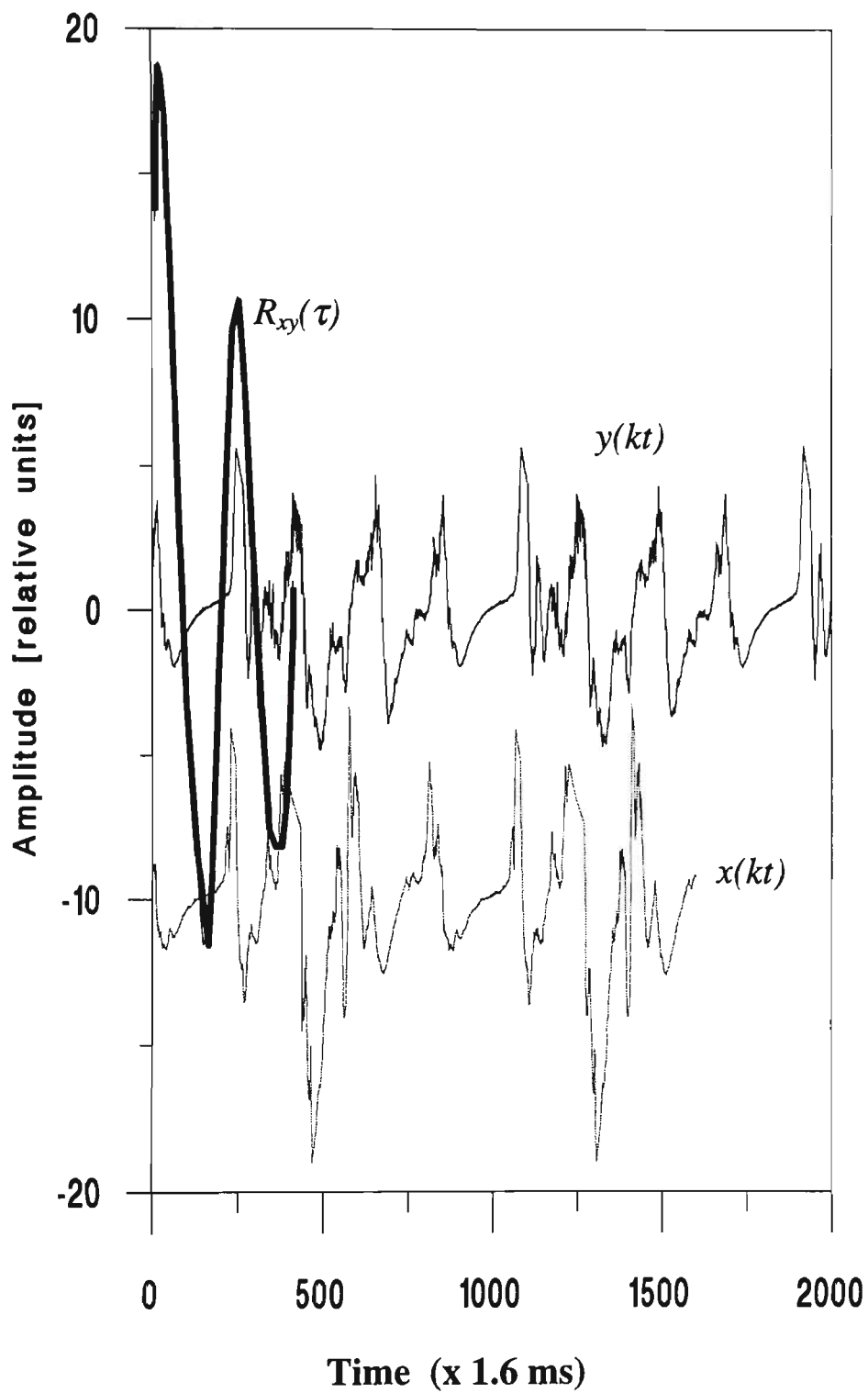


Figure 4.5 Two random signals and the cross-correlation function (experimental data collected during the initial trials).

It can be seen from Figure 4.4 that the cross-correlation function has a maximum when the transit time  $\tau$  equals the time delay  $\beta$ . Given  $\Delta t$  (the time between two iterations) and  $k$  (the index of iteration), the cross-correlation function ( $R_{xy}(\tau)$ ) is defined in terms of the mean value of the product  $x(k\Delta t)y(k\Delta t + \tau)$ , (Bentley, 1992), where  $x(k\Delta t)$  is the digitised undelayed version of the “upstream” and  $y(k\Delta t + \tau)$  is the digitised delayed “downstream” signal. That is

$$R_{xy}(\tau) = \frac{1}{N} \sum_{k=1}^N x(k\Delta t) y(k\Delta t + \tau) \quad (4.22)$$

where  $N$  is defined as the total number of iterations ( $N\Delta t = T$  is the total time span over which the summation is carried out).

It can be seen from Figures 4.4 and 4.5 that  $y(k\Delta t + \tau)$  is essentially the same as  $x(k\Delta t)$  when  $\tau = \beta$  (the mean transit time of a point on the moving surface between the two sampling points). Thus, in practice, speed can be measured by counting the number of delay steps  $k_m$  required to locate the maximum in the cross-correlation function, namely

$$k_m \Delta t = \beta \quad (4.23)$$

Since  $\tau = \frac{L}{v}$ , where  $L$  is the known distance between two points, then speed  $v$  may be found from

$$v = \frac{L}{k_m \Delta t} = \frac{Lf}{k_m} \quad (4.24)$$

where  $f = \frac{1}{\Delta t}$  is the frequency of sampling.

### 4.3.2 Spatial averaging effect of the cross-correlation

Referring to Figure 4.3, the spatial averaging effect can be defined as the function relating the qualities of the moving fluid at a point, to the output signals  $m(t)$  and  $n(t)$  from the sensor. Figure 4.6 can be used to demonstrate this averaging effect on surface speed measurement (Beck, 1984). The introduction of an angle  $\alpha$  allows for the different paths of the transmitted and received light. Assume a contamination area on the surface (which changes the reflected light intensity) passes at speed  $v$  through a light beam of diameter  $\gamma$ . The incident light intensity  $I_1$  is attenuated because of surface absorption, and results in a reduced intensity  $I_2$  reaching the detector. Thus the emergent light  $I_2$  corresponds to signals  $m(t)$  and  $n(t)$  shown in Figure 4.3.

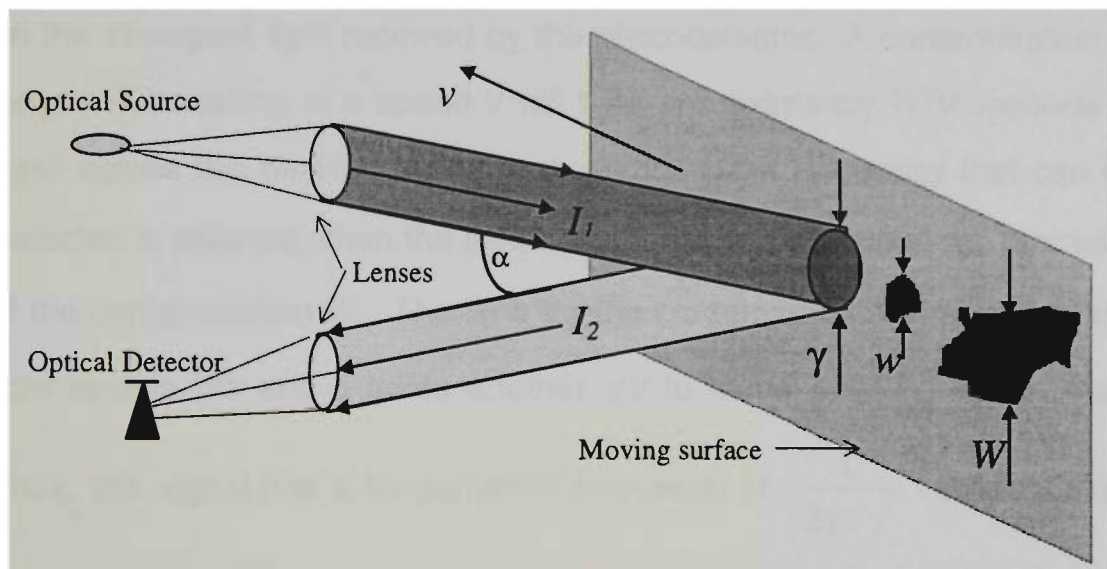


Figure 4.6. Spatial averaging effect on the scattered light.

Considering a contaminated area of diameter  $w$  which is smaller than the beam diameter  $\gamma$ , the emergent light intensity is then given approximately by :

$$I_2 = I_1 (1 - (w/\gamma)^2 r) \quad (4.25)$$

where  $r$  is the attenuation coefficient of the contaminated area. Conversely, any contaminated area which is larger than the beam diameter ( $W > \gamma$ ) will, for a period of time, reduce the intensity of the scattered beam according to

$$I_2 = I_1 (1 - r). \quad (4.26)$$

Examination of equations (4.25) and (4.26) suggests that contaminated areas with  $W > \gamma$  have a pronounced effect on the detected signal whereas smaller contaminations with  $w \ll \gamma$  have relatively little effect on the emergent light received by the photodetector. A contamination of length  $W$  travelling at a speed  $v$  will take approximately  $W/v$  seconds to pass across the beam. The highest unattenuated frequency that can be detected is attained when the light spot diameter  $\gamma$  equals to the diameter of the contamination  $W$ . The time for the contamination to move into the light spot is  $\gamma/v$  and it takes another  $\gamma/v$  to move out of the light spot.

Thus, this signal has a fundamental frequency of  $\frac{1}{2\gamma/v}$ . Summarising

the above result, the cut-off frequency (3 dB reduction) due to surface averaging is (Beck 1984) :

$$f \cong \frac{1}{2\gamma/v} = \frac{v}{2\gamma}. \quad (4.27)$$

---

This means that at a speed of say 6 m/s, and a sensor beam diameter of 2 mm, the cut-off frequency is

$$f = \frac{6}{2 \times 2 \times 10^{-3}} = 1500 \text{ Hz.}$$

These are in fact the typical experimental conditions for the work described in this thesis and they are verified by the spectrum of the received signals obtained using a Fast Fourier Transform (FFT). The experimental results for different surfaces (details given in Section 6.3) show a cut-off frequency of about 300 Hz at 1.6 m/s, which represents an acceptable agreement with the above considerations.

The sensor electronics can easily be designed to have a wider bandwidth than the spatially averaged bandwidth derived above. In this case, considering the cut-off frequency of the digitising card used (PCL-818 cut-off frequency is 100 kHz), the bandwidth of the sensor electronics has been designed to be 50 kHz. This allows the sensor to detect the high frequency signals required for good resolution and low *SNR* of the cross-correlation function.

#### **4.4 ACCURACY OF CROSS-CORRELATION BASED MEASUREMENT SYSTEMS**

The cross correlator is a digital device, with its timing controlled by a crystal clock. Given sufficient computing power, there is no significant fundamental uncertainty in the cross-correlation measurement of time delay. There could be errors due to quantisation of the time delay measurements by the digital device (i.e. sampling rate) but these errors can be overcome by suitable design of the digital system (Jordan and Kelly, 1976).

The requirement for the signals to be stationary (zero mean over a infinite integration period) means that this method must be treated with caution to avoid an erroneous interpretation of the cross-correlation. A most commonly observed variability occurs when the time delay relating the two signals changes during the correlation integration period. If these two signals are correlated and the time delay variation is slow, compared to the integration period, it can easily be seen that the calculated correlation function will track the changes. As the rate of change of time delay increases, the correlation function reduces in amplitude and becomes broader. If this change is too fast relative to the acquisition time, no correlation peak will be observed. Therefore, in the work presented in this thesis, the integration time was set between 0.5 s and 1 s. This period was considered to be short enough for the signals to stay stationary (for a surface moving with a constant speed) so the measurement could be done in real time and also sufficiently long to obtain a significant cross-correlation function.

Statistical errors are introduced by the use of short integration times and these errors are often referred to as variance errors (Jordan, 1986). For a particular integration period, if successive estimates are compared, a range of results centred on the expected value will be obtained. The normalised mean square error  $\varepsilon^2$  is defined by (Bendat and Piersol 1967; Papoulis, 1967):

$$\varepsilon^2 = \frac{\text{var}(R_{xy}(\tau))}{R_{xy}^2(\tau)} \quad (4.28)$$

where

$$\text{var}[R_{xy}(\tau)] \approx \frac{1}{T} \int_{-\infty}^{+\infty} [R_{xx}(t)R_{yy}(t) + R_{xy}(t+\tau)R_{yx}(t-\tau)] dt, \quad (4.29)$$

with the assumption that the fluctuations of the cross-correlation estimate can be represented by a Gaussian random process for large period  $T$ .

The output signal-to-noise ratio (*SNR*) is often used to describe the performance of a correlator. *SNR* is defined as the ratio of the expected correlator output to the standard deviation of the output fluctuations about its mean value. That is:

$$SNR = \frac{R_{xy}(\tau)}{\sqrt{\text{var}[R_{xy}(\tau)]}} = \frac{1}{\varepsilon} \quad (4.30)$$

Evaluating equation (4.28) by substituting for cross-correlation (equation 4.2) and autocorrelation (equation 4.4) functions, gives a relation for the normalised mean square error of the form:

$$\varepsilon^2(\tau) = \frac{K}{BT} \left[ 1 + \frac{1}{\rho^2(\tau)} \right]. \quad (4.31)$$

where  $\rho(\tau) = \frac{R_{xy}(\tau)}{R_{xx}(\tau)}$  is the cross-correlation significance,  $K$  is a constant dependent on the form of the correlation function or the power spectrum and  $B$  is the signal half-power bandwidth (Jordan, 1986). Since in this work the correlation significance was found experimentally to be approximately equal to unity it follows that

$$\varepsilon \approx \sqrt{\frac{2K}{BT}} \quad (4.32)$$

Thus the *SNR* becomes

$$SNR = \sqrt{\frac{BT}{2K}}. \quad (4.33)$$

As the constant  $K$  is typically 0.2,  $B = 1500$  Hz and  $T = 1$  s, the *SNR* for our cross-correlation system (analogue signals) is found to be

$$SNR = \sqrt{\frac{1500}{2 \times 0.2}} \approx 61,$$

---

or in dB this translates to

$$SNR_{dB} = 10 \log_{10} SNR = 18 \text{ dB}. \quad (4.34)$$

By consulting Figure 4.2, we conclude that this value of the  $SNR$  corresponds to a very small variance of the cross-correlation function. This value sets the upper limit for the global  $SNR$  of the system. Note that the  $SNR$  was computed at a half-power bandwidth that corresponds to a speed of 6 m/s (equation 4.27). With increasing speed the  $SNR$  improves. For example, if the speed increased five times (i.e., 30 m/s) the  $SNR$  will become

$$SNR \approx \sqrt{\frac{7500}{2 \times 0.2}} \approx 136,$$

which in dB is

$$SNR_{dB} = 10 \log_{10} SNR = 21 \text{ dB}.$$

In practice, such a large value of the  $SNR$  has little influence on the time delay estimation.

The implementation of cross-correlation with digitised signals adds quantisation noise to the signals leading to a degradation of  $SNR$ . Bowers and Klingler (1974) have defined a degradation factor  $D$  that can be used to describe the effect of quantisation, namely

$$D = \frac{SNR \text{ of analogue correlator}}{SNR \text{ of digital correlator}}. \quad (4.35)$$

$D$  is a function of quantisation levels, magnitude of the quantisation steps, and sample rate. For polarity correlation (i.e. using two levels of quantisation), Bowers and Klingler found that sampling at the Nyquist rate (twice the frequency of the sampled signal), the  $SNR$  degrades by a factor of 1.57, and in order to maintain a particular  $SNR$  it is necessary to increase the integration time by a factor of approximately

---

2.5 (i.e.  $(1.57)^2$ ) compared to analogue correlation. Increasing the number of levels used only by a small amount leads to a significant reduction in the degradation factor and a further reduction is obtained by sampling faster than the Nyquist rate. For example, using three levels of quantisation with a sampling frequency four times the Nyquist rate yields a degradation factor of approximately 1.2.

In order to obtain a  $D$  value as low as possible, in the work presented here the sampling frequency was up to 25 times higher than Nyquist rate and 12 levels of quantisation were used.

Note that this is the upper limit for the proposed measurement system. Other factors degrading the SNR are presented in the next section.

## **4.5 NOISE IN THE SENSOR ELECTRONICS**

One of the most stringent requirements on a measurement system is the minimisation of the noise level. The signal-to-noise ratio is a function of several noise-generating mechanisms and the noise power depends upon contributions from the various individual noise sources as well as the design of the detector circuits. As discussed in Section 4.4, one of the noise sources is the correlator itself. The other major sources of noise in the system are thermal noise (Johnson noise) and shot noise.

### **4.5.1 *Thermal noise***

Thermal noise is defined as voltage fluctuations in the equivalent input resistor of the amplifier (required to elevate the detected signal level) and in the amplifier itself (Wolf, 1978). The thermal noise power for an equivalent load resistor  $R_L$  can be calculated from

$$i^2 = \frac{4kT}{R_L} \Delta f$$

$$P_{TN} = 4kT\Delta f, \quad (4.36)$$

where  $P_{TN}$  = thermal noise power (W)

$k$  = Boltzmann's constant

$T$  = temperature (K)

$\Delta f$  = electrical bandwidth of the receiver (Hz)

$R_L$  = detector load resistor ( $\Omega$ )

Note that the thermal noise spectrum has an essentially uniform infinite distribution (white noise), so that its influence on the correlation can be neglected. Moreover, the thermal noise was further minimised by using a transimpedance amplifier (Section 5.4.1) as the front end of the amplifier so that a much smaller equivalent load resistor (of the order of tens of ohms) of the photodetector was required to produce the same signal level.

#### 4.5.2 Shot noise

Shot (or quantum) noise is associated with the quantisation of charge and it is a consequence of the statistical nature of the process by which the incoming light generates electrical carriers in the detector. The shot noise power can be calculated from the expression

$$P_{SN} = 2e(i_s + I_D)R_L\Delta f, \quad (4.37)$$

where  $e$  = the electron charge (C)

$i_s$  = the average detector current (A)

$I_D$  = photodetector's dark current (A)

$R_L$  = detector load resistor ( $\Omega$ )

Like thermal noise, the shot noise spectrum also has a uniform power distribution over all frequencies and will therefore have little effect on the correlation function.

From these considerations it can be seen that both thermal and shot noise power are proportional to the bandwidth of the detector. As both thermal and shot, are in principle white noises they have no influence on cross-correlation.

### 4.5.3 Signal-to-noise ratio

For a photodetector having an incident optical power  $P$  and responsivity  $\rho$ , the photocurrent is given by

$$i_S = \rho P. \quad (4.38)$$

Thus, the average electrical signal power is given by

$$P_{ES} = i_S^2 R_L = (\rho P)^2 R_L. \quad (4.39)$$

Therefore the  $SNR$  of the detector is

$$SNR = \frac{P_{ES}}{P_{TN} + P_{SN}} = \frac{(\rho P)^2 R_L}{4kT\Delta f + 2e(\rho P + I_D)R_L\Delta f}. \quad (4.40)$$

For the low noise silicon PIN photodiode selected (Section 5.2), the typical values (from data sheet Optek Technology, 1990) are:

$\rho = 0.55 \text{ A/W}$ ,  $I_D = 0.1 \text{ nA}$ ,  $R_L = 50 \text{ k}\Omega$ ,  $T = 295 \text{ K}$  and  $\Delta f = 1500 \text{ kHz}$ .

Substituting these values in equation (4.40) the  $SNR$  expressed in dB becomes

---

$$SNR_{dB} = 10 \log_{10} SNR = 60 \text{ dB},$$

which is much higher than the  $SNR$  of the correlator itself (equation 4.34). Therefore, it is clear that the correlator is the dominant contributor to the noise in the system.

## 4.6 CONCLUSION

In this chapter, the theory of operation of the sensor using cross-correlation to measure velocity has been described. From the calculations presented it can be seen that the  $SNR$  for the cross correlator strongly depends on the measured speed of the moving surfaces (as the speed increases the  $SNR$  improves). In the case of the photodetector the situation is reversed. However, as the above calculations show, for the conditions applicable to this work, the  $SNR$  of the photodetector is much higher than that of the correlator and therefore the former does not limit the system performance.

Like thermal noise, the shot noise spectrum also has a uniform power distribution over all frequencies and will therefore have little effect on the correlation function.

From these considerations it can be seen that both thermal and shot noise power are proportional to the bandwidth of the detector. As both thermal and shot, are in principle white noises they have no influence on cross-correlation.

### 4.5.3 *Signal-to-noise ratio*

For a photodetector having an incident optical power  $P$  and responsivity  $\rho$ , the photocurrent is given by

$$i_S = \rho P. \quad (4.38)$$

Thus, the average electrical signal power is given by

$$P_{ES} = i_S^2 R_L = (\rho P)^2 R_L. \quad (4.39)$$

Therefore the  $SNR$  of the detector is

$$SNR = \frac{P_{ES}}{P_{TN} + P_{SN}} = \frac{(\rho P)^2 R_L}{4kT\Delta f + 2e(\rho P + I_D)R_L\Delta f}. \quad (4.40)$$

For the low noise silicon PIN photodiode selected (Section 5.2), the typical values (from data sheet Optek Technology, 1990) are:

$\rho = 0.55 \text{ A/W}$ ,  $I_D = 0.1 \text{ nA}$ ,  $R_L = 50 \text{ k}\Omega$ ,  $T = 295 \text{ K}$  and  $\Delta f = 1500 \text{ kHz}$ .

Substituting these values in equation (4.40) the  $SNR$  expressed in dB becomes

---

$$SNR_{dB} = 10 \log_{10} SNR = 60 \text{ dB},$$

which is much higher than the  $SNR$  of the correlator itself (equation 4.34). Therefore, it is clear that the correlator is the dominant contributor to the noise in the system.

#### **4.6 CONCLUSION**

In this chapter, the theory of operation of the sensor using cross-correlation to measure velocity has been described. From the calculations presented it can be seen that the  $SNR$  for the cross correlator strongly depends on the measured speed of the moving surfaces (as the speed increases the  $SNR$  improves). In the case of the photodetector the situation is reversed. However, as the above calculations show, for the conditions applicable to this work, the  $SNR$  of the photodetector is much higher than that of the correlator and therefore the former does not limit the system performance.

---

$$SNR_{dB} = 10 \log_{10} SNR = 60 \text{ dB},$$

which is much higher than the  $SNR$  of the correlator itself (equation 4.34). Therefore, it is clear that the correlator is the dominant contributor to the noise in the system.

## 4.6 CONCLUSION

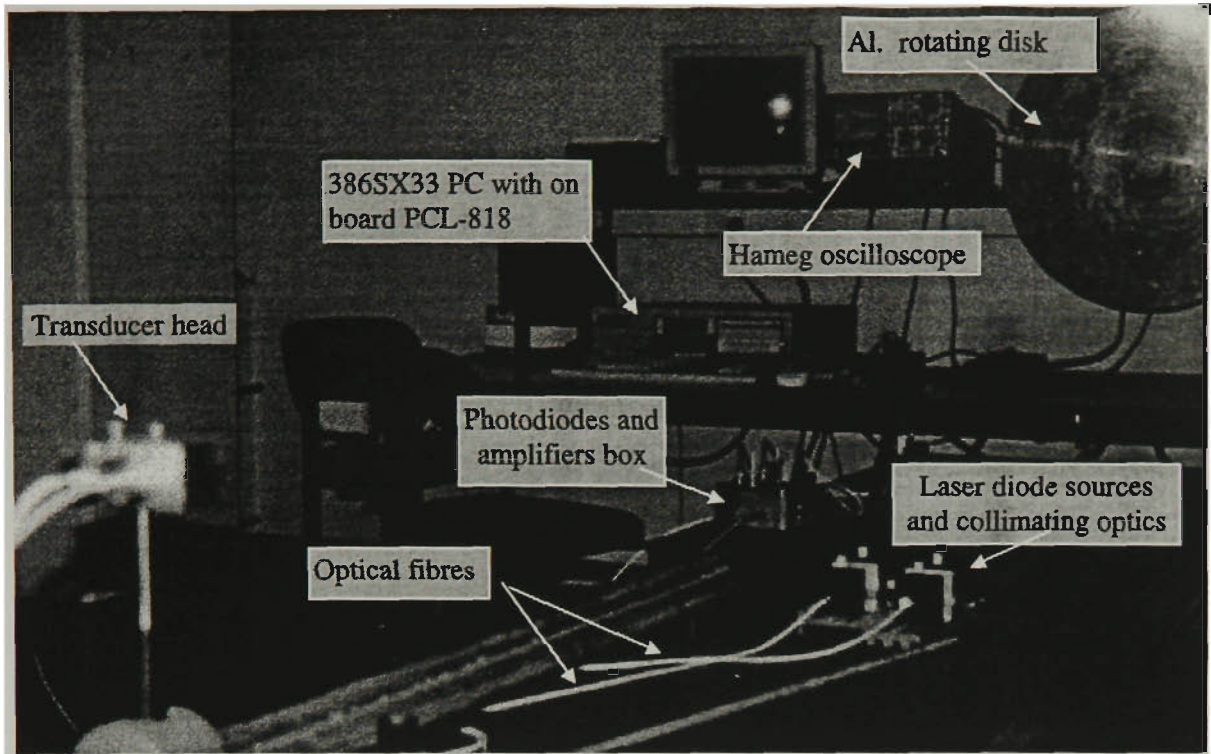
In this chapter, the theory of operation of the sensor using cross-correlation to measure velocity has been described. From the calculations presented it can be seen that the  $SNR$  for the cross correlator strongly depends on the measured speed of the moving surfaces (as the speed increases the  $SNR$  improves). In the case of the photodetector the situation is reversed. However, as the above calculations show, for the conditions applicable to this work, the  $SNR$  of the photodetector is much higher than that of the correlator and therefore the former does not limit the system performance.

---

## Chapter 5      APPARATUS AND ITS APPLICATIONS

### 5.1      INTRODUCTION

The basic configuration of the fibre optic speed measurement system is shown in Figure 5.1 and Photograph 1. With the aid of two low cost compact disk (CD) lenses, light from two laser diodes (Sharp-LT022PS) was injected into two multimode fibres. These fibres guide the light to the transducer head, where it is collimated by two short focal length lenses and launched as two separate beams onto the moving surface. Each of the two sensors built into the transducer head contains a second fibre which guides the light scattered from the moving surface onto the photodetectors (OPF480). The amplified electrical signals are fed into a PCL-818 card which comprises two analogue to digital converters interfaced to a computer. A Hameg oscilloscope was also used to continuously monitor the form and amplitude of the electrical signals before digitisation. The digitised signals were stored in two data arrays used by the (software) cross correlator (equation 4.14). By locating the global maximum of the cross-correlation function, the time delay can be found and hence the speed of the moving surface (equation 4.24). Data acquisition and the signal processing can be completed quickly (within half of second) so updated speed information can be displayed on the computer screen. If necessary, further post-processing can be used to average or smooth the displayed speed.



Photograph 1. Experimental arrangement for the fibre optic based continuous speed measurement system.

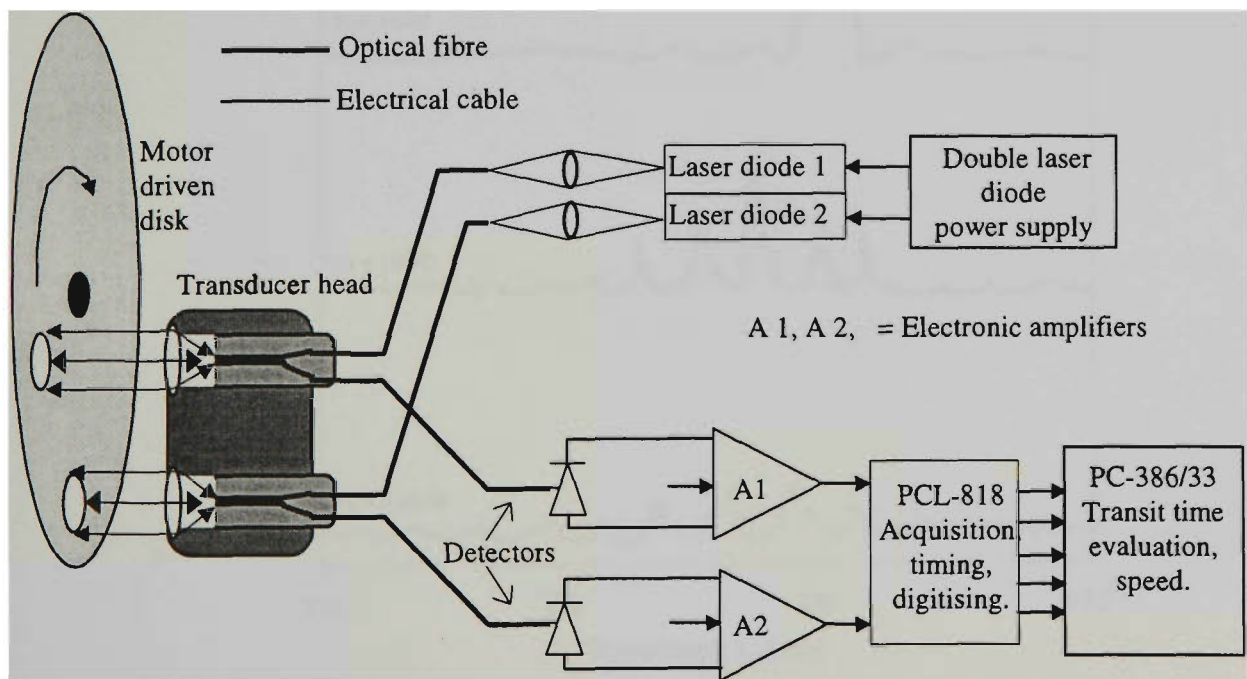


Figure 5.1. Schematic diagram for the fibre optic based speed measurement system.

## 5.2 LASER DIODE AND POWER SUPPLY

A multitude of optical sources are available (Section 2.2.1) and the appropriate laser diode selected for this work was the inexpensive (A\$10) GaAlAs Sharp LT022PS. This diode has a nominal power output of 3 mW (with a maximum of 5 mW). It is a compact low noise device with a SNR of about 60 dB (Sharp Laser Diodes, 1992). Figure 5.2 shows that the laser diode (at 3 mW) has a single longitudinal mode at 780 nm (22°C).

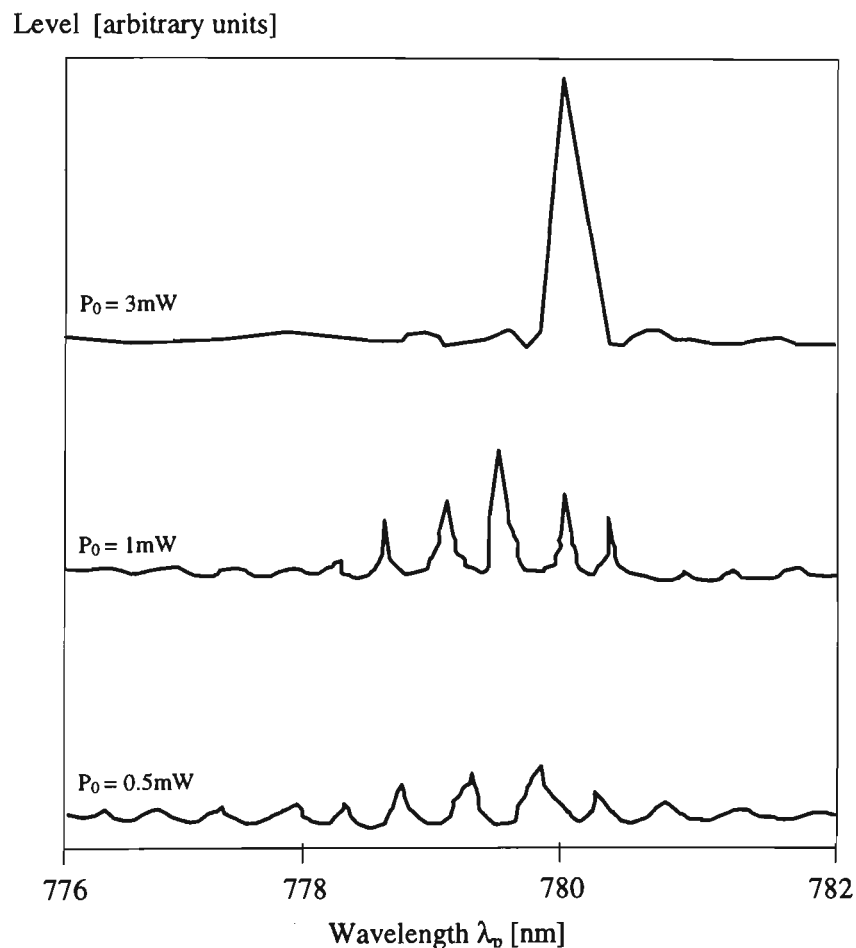


Figure 5.2. The dependence of optical power output on wavelength for the LT022PS laser diode.

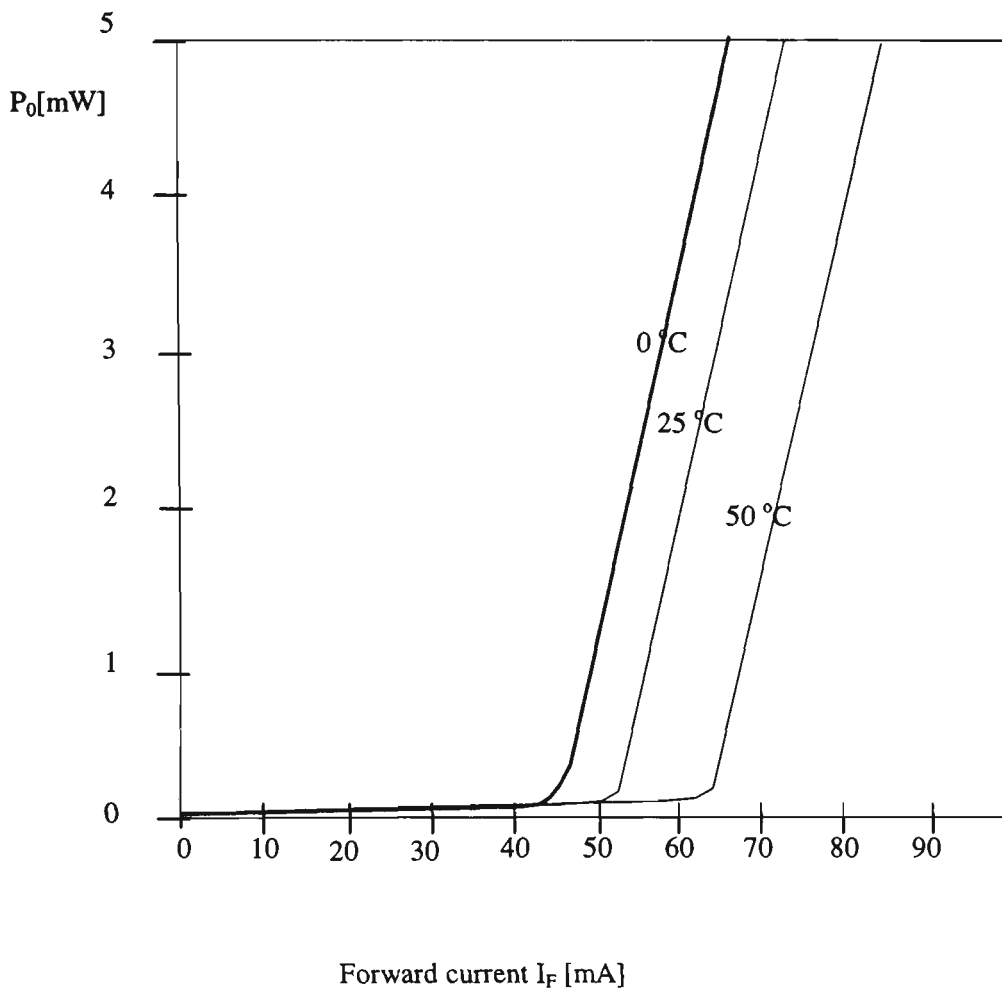


Figure 5.3. Optical power output as a function of forward current for the LT022PS laser diode.

The relationship between optical power and drive current is given in Figure 5.3 (Sharp Laser Diodes, 1992). The effect of temperature on the threshold current is also presented in Figure 5.3. In this work, the light is intensity modulated so wavelength stability is not restrictive and special measures are not required to keep the laser diodes at a constant temperature. The forward current for both laser diodes was set to 76 mA which corresponds to 3 mW optical power at about 32 °C. Although it would have been preferable to use the maximum power available from



---

The core of the double laser diode power supply is the integrated circuit IR3C07 which not only provides the automatic power control function but also features a slow start characteristic in order to eliminate power surges.

The 5 V DC from the integrated voltage regulator LM3407T5 is distributed to the laser diodes via switches  $K_1$  and  $K_2$ . The 560 k $\Omega$  trimmer in series with the 560 k $\Omega$  resistor (for current protection) were used to adjust the output of the laser diodes to 3 mW of optical power.

### 5.3 PHOTODETECTORS

The photodetectors selected for this project were OPF480. The OPF480 is a low noise silicon PIN photodiode mounted in a low cost package for fibre optic applications. It offers fast response at low bias and is compatible with LED and laser diode sources working in the 750–900 nm wavelength region. Low capacitance provides improved signal-to-noise performance and large bandwidth making this photodetector especially useful for optical sensing systems (Opteck Technology, 1992). In Figures 5.5 and 5.6 the basic characteristics of the diode are plotted. From the curve representing the normalised responsivity versus wavelength (Figure 5.6) it can be seen that at a wavelength of 780 nm the responsivity is about 97% of the maximum that delivers a current of 0.55 amperes per watt. Since the output is coupled to a transimpedance amplifier the reverse voltage across the photodetector is 5V yielding a dark leakage current under 0.1 nA (Figure 5.5). An additional advantage of this arrangement is that a high *SNR* value is provided for the cross correlator.

The photodetectors were mounted directly onto the circuit board of the

---

sensor electronics. By mounting them in optical connector adapters a good light transfer from the FC terminated optical fibre was achieved.

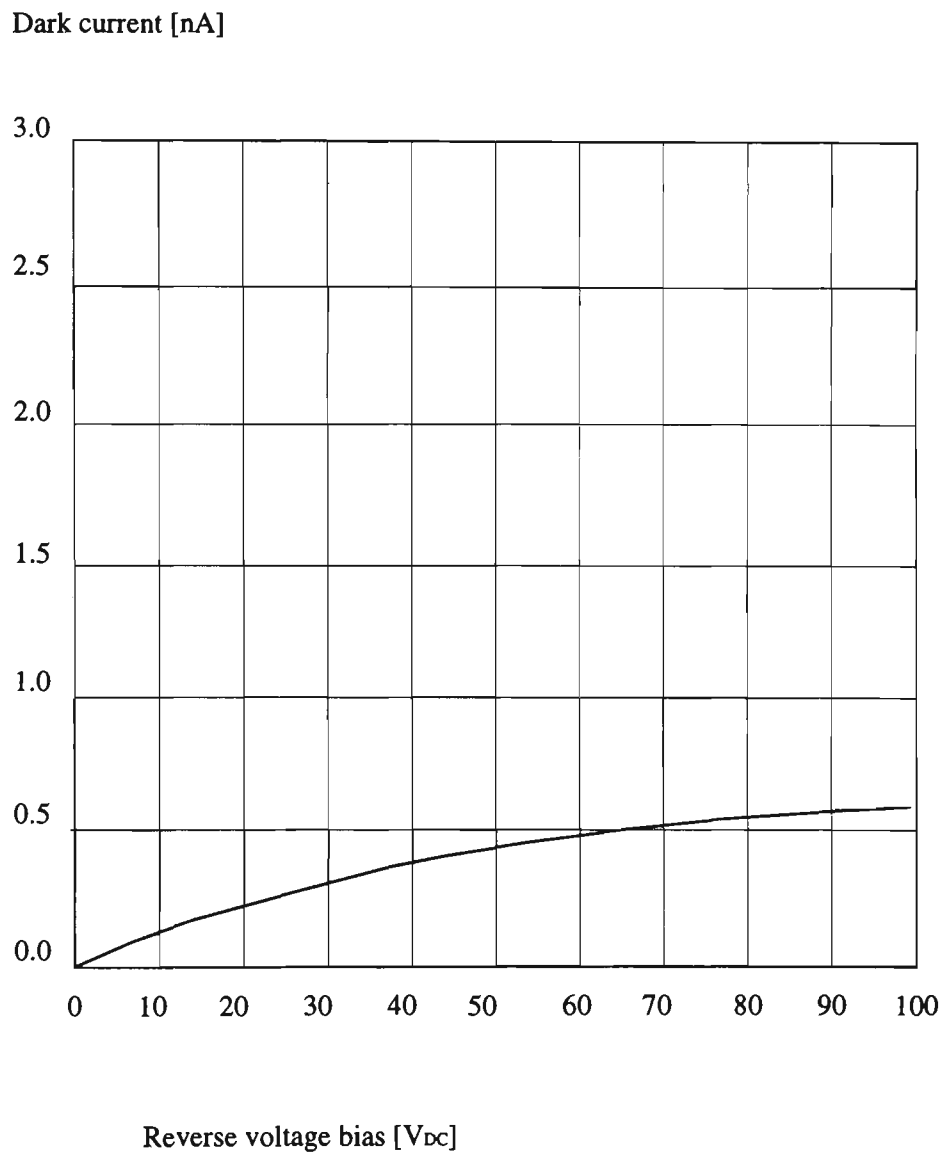


Figure 5.5. Dark leakage current versus reverse voltage for the LT022PS laser diode.

---

Normalised responsivity

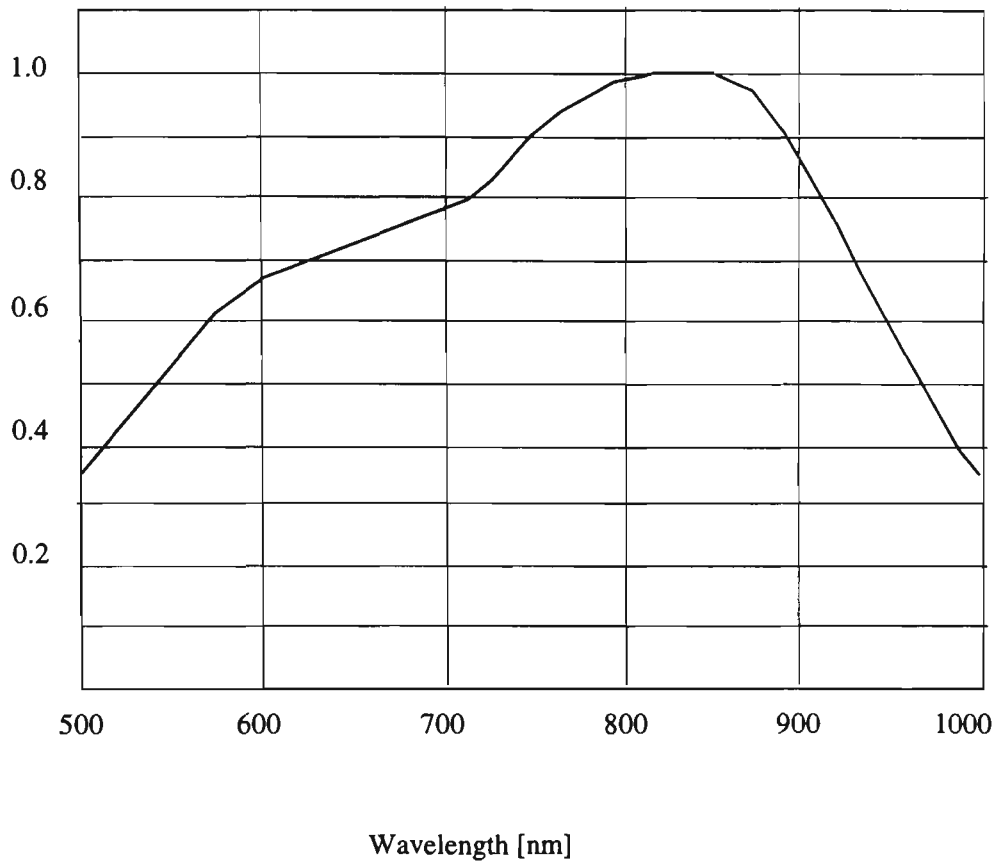


Figure 5.6. Normalised responsivity versus wavelength for the silicon photodiode.

## 5.4 SENSOR ELECTRONICS

The sensor electronics were comprised of the transimpedance (Section 5.4.1) and voltage amplifiers (Section 5.4.2), employed to provide sufficient voltage gain for digitisation of the signal by the A/D converter of the PCL-818 Laboratory Card (Section 5.7).

### 5.4.1 Transimpedance amplifier

Since the photodiode is essentially a current output device, it usually is operated with a current-to-voltage converter-type amplifier. Figure 5.7 shows such an arrangement (Kuecken, 1987).

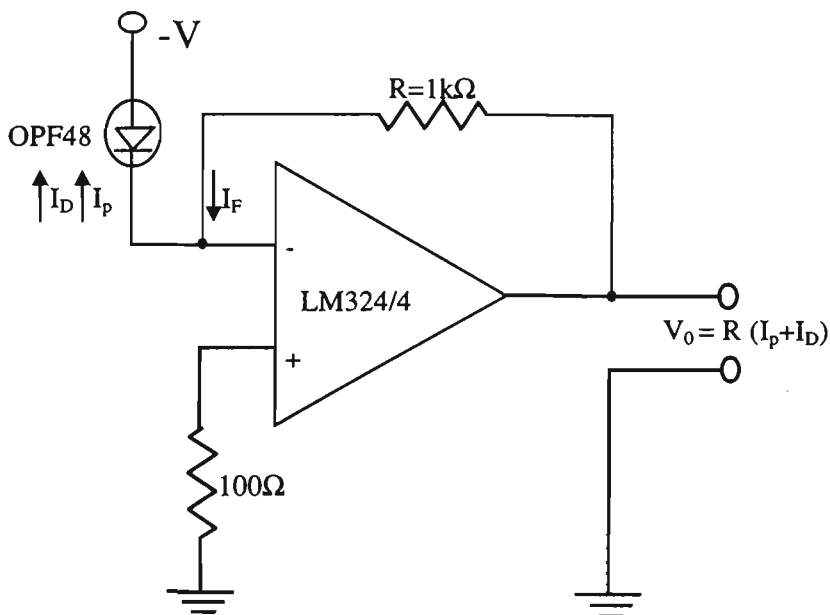


Figure 5.7. The transimpedance amplifier (Kuecken, 1987).  $I_p$  and  $I_D$  are the photocurrent and dark current of the photodetector, respectively.

---

The expression for the output voltage  $V_D$  from the transimpedance amplifier is given by

$$V_D = R(I_p + I_D). \quad (5.1)$$

This provides the photodiode with a small effective load resistance, and consequently with a very high signal to noise ratio (equation 4.40).

Note that this diode has a very low internal capacitance and therefore a relatively low noise level.

#### **5.4.2     *The voltage amplifier***

As depicted in Figure 5.8, the voltage amplifier comprises four individual differential amplifiers on one LM324 IC powered from the same source (National Semiconductor, 1990). The gain of the individual op-amps was kept low to obtain 100 kHz gain-bandwidth product (the typical unity gain of the LM324 is 1 MHz).

Using the components shown in Figure 5.8, the frequency response of the amplifier is flat in the frequency range of 10 Hz to 50 kHz.

The first op-amp,  $O_1$ , has a gain of 10, and an input impedance of 47 k $\Omega$  assuring a good power transfer from the transimpedance amplifier.  $O_2$  also has a gain of 10, while the third op-amp,  $O_3$  has a variable gain in the range 1 to 4.7 so that for the total gain of the amplifier can be varied linearly from 100 to 470 using the potentiometer  $R_8$ . The final op-amp,  $O_4$  has a gain of unity (voltage follower) assuring a low output impedance (1 k $\Omega$ ) as required by the input to the analogue to digital converters of the PCL-818 Laboratory Card (Section 5.7).

The measured signal to noise ratio for the entire sensor electronics comprising transimpedance amplifier and voltage amplifier was about 22 dB providing a suitable input signal for the cross-correlator. In order to obtain meaningful measurement of the SNR of the sensor electronics,

the frequencies of input signals (a few hundred of Hertz), were kept well below the cut off frequency of the measuring equipment.

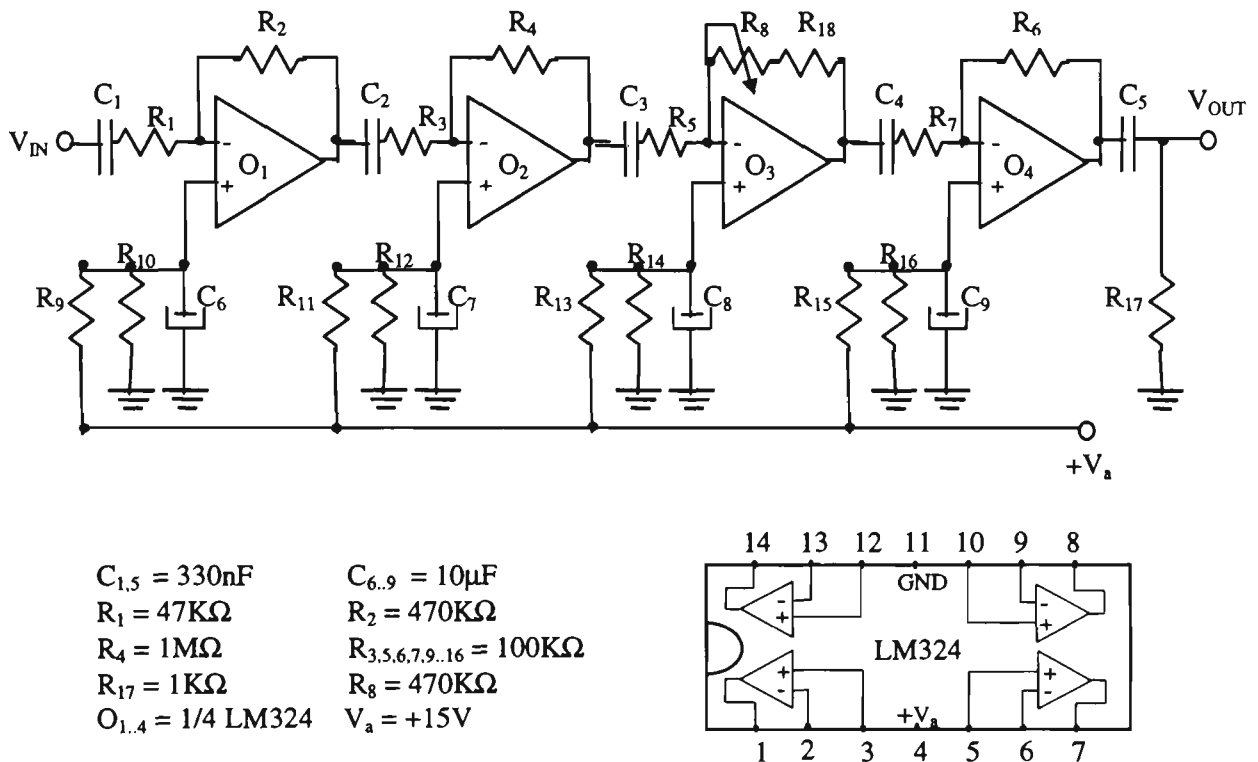


Figure 5.8. The schematic diagram of the voltage amplifier.

## 5.5 OPTICAL FIBRES AND COMPONENTS

During the experimental work two types of multimode step index optical fibres were used, namely 50/125 $\mu\text{m}$  (50  $\mu\text{m}$  core and 125  $\mu\text{m}$  cladding) and 100/140  $\mu\text{m}$ . With the 50/125  $\mu\text{m}$  fibre a  $-5.6 \text{ dBm}$  light level could be launched (276  $\mu\text{W}$ ) into the fibres, and with the 100/140  $\mu\text{m}$ , a level of  $-0.1 \text{ dBm}$  (970  $\mu\text{W}$ ) was used. Although the difference between the numerical aperture of the fibres was small, 0.22 for 50/125 $\mu\text{m}$  and 0.27 for the 100/140  $\mu\text{m}$  (experimentally measured), use of the larger core fibres enabled the maximum distance of measurement (between the

---

transducer head and the moving surface) to be extended from 0.4 m to 5 m (Figure 5.9).

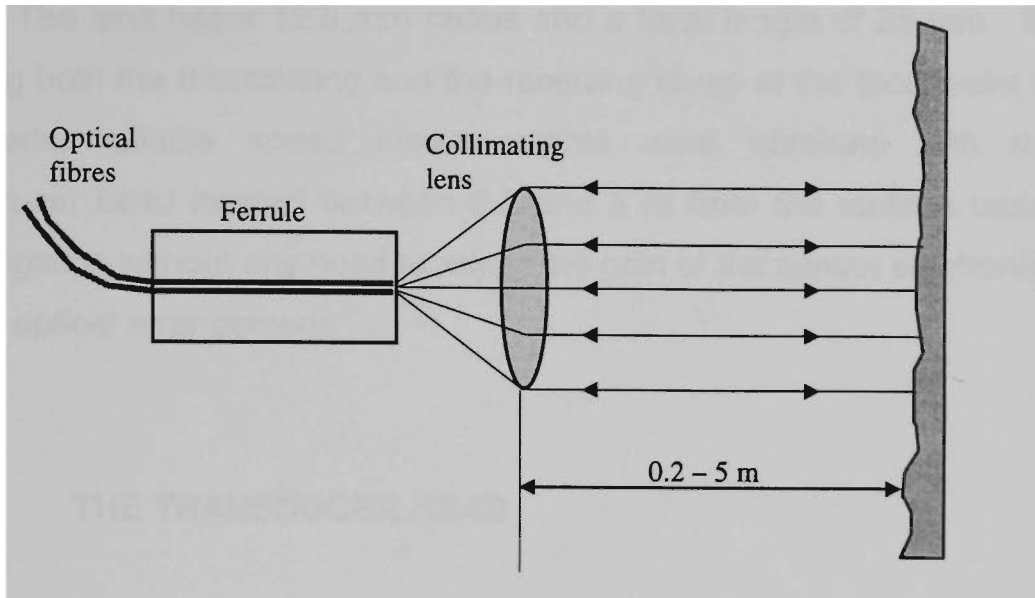


Figure 5.9. The optical path of the transmitted and scattered light.

In order to construct the fibre optic sensor, four sections of optical fibre were prepared as follows:

Two receiving fibres were pigtailed with FC connectors and by mounting the photodetectors in matching FC connector adapters a low loss transfer was obtained. The remaining ends were carefully prepared for insertion into the ferrule of the transducer head (Figures 5.10 and 5.11).

In the case of the two transmitting fibres, one end of each fibre was inserted into separate ferrules of the transducer head and the other ends were coupled to the laser diode sources. All the fibres were jacketed ensuring good mechanical rigidity and stability for the whole optical system.

---

The light was launched into each fibre with the aid of a low cost CD lens, which is known to have a very low power loss ( $\cong 0.3$  dB) at 780 nm wavelength. A convergent lens was selected to collimate this light toward the moving surface and focus the scattered light into the receiving fibre. The lens has a 12.5 mm radius and a focal length of 25 mm. By placing both the transmitting and the receiving fibres at the focal point of the lens, reliable speed measurements were obtained with the transducer head located between 0.2 and 5 m from the surface under investigation without any need to adjust the gain of the sensor electronics or the optical arrangement.

## 5.6 THE TRANSDUCER HEAD

The initial configuration transducer head (mark 1) is depicted in Figure 5.10 and Photograph 2. This version of the transducer head employing 50/125  $\mu\text{m}$  multimode optical fibres was used to conduct the initial trials (Section 6.2). From the figure it can be seen that two pairs of jacketed optical fibres (1) are introduced into the ferrules (8). The ferrule is a metallic cylinder that can move horizontally inside a larger cylindrical aluminium holder (3). The ferrule is set so that the end of the fibres are at the focal point of the convergent lens (5). After the stripped fibres (2) ends were inserted into a small hole in the ferrule, a special polymer epoxy (7) was used to glue the fibres in place. The tips of the fibres were then polished.

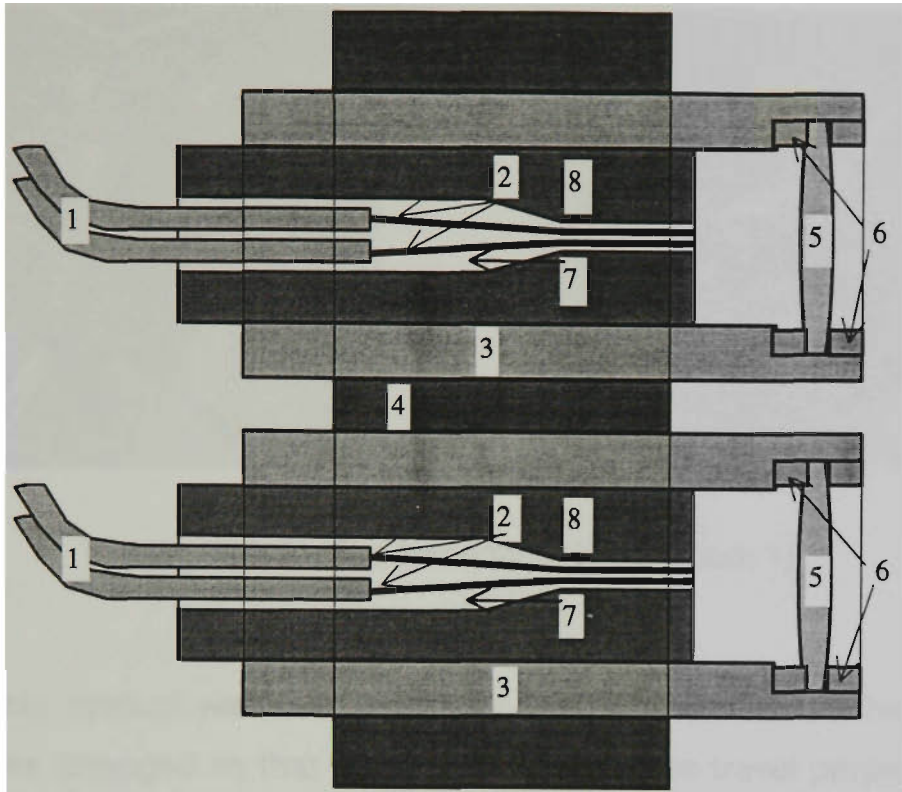


Figure 5.10 Mark 1 version of the transducer head (see text for details).

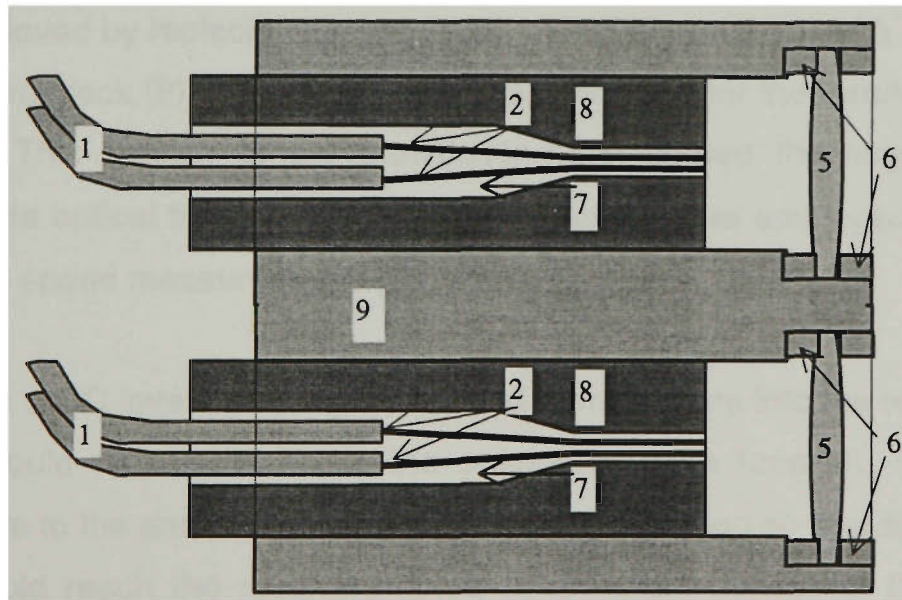
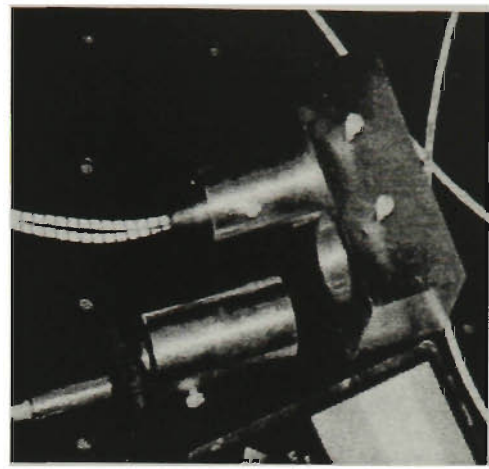
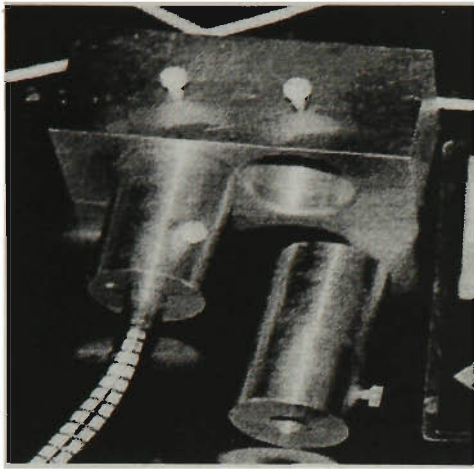


Figure 5.11. The mark 2 version of the transducer head (see text for details).



Photograph 2. The transducer head (mark 1).

The whole system was made rigid by the outer aluminium holder (4) which was arranged so that the light from the fibres travel perpendicular to the moving surface. The lenses were held in place by the Teflon rings (6).

A second version of the transducer head depicted in Figure 5.11 was designed to ensure a better parallelism between the light paths. This was achieved by replacing the two holders (3 in Figure 5.10) with a single aluminium block (9) in which precision parallel holes for the ferrules were made. This version of the transducer head utilised the larger core multimode optical fibres (100/140  $\mu\text{m}$ ) and later it was employed for the real time speed measurements (Section 6.4).

Although a DC level due to light reflected from the lens into the receiving fibres would not contribute to the cross-correlation function, it would contribute to the shot noise. The housing was designed so that any stray light would reach the receiving fibres at an angle outside of the fibre acceptance cone.

---

## 5.7 PCL-818 LABORATORY CARD

The PCL-818 (Advantech Co., Ltd., 1993) is a high speed, multi-function data acquisition card with programmable gain for the IBM PC. The specifications for this card and the software make it ideal for a wide range of applications in industrial and laboratory environments, in particular data acquisition, process control, automatic testing and automation. It has 12 analogue to digital converters and software support for a number of programming languages. Software control of the input gain of the card (from 0.5 to 4.0) extends its applicability, although for the work presented in this thesis the software gain was kept to unity and the amplifier gain in the detector circuit was adjusted as necessary. Depending on the hardware configuration (Advantech Co., Ltd., 1993) the card supports three different modes for performing data transfer:

- Software data transfer,
- Interrupt data transfer,
- Direct Memory Access (DMA) data transfer.

A brief description of each follows.

**Software data transfer.** This is the simplest method for analogue to digital (A/D) conversion. The function performs a predefined number (N) of A/D conversions of the analogue signal. In order to keep a constant time interval between conversions, the driver can utilise an on board internal clock (pacer) as a timing signal. The driver triggers an A/D conversion and waits for the next clock pulse before performing the next conversion. The process continues until the N<sup>th</sup> conversion is performed and then the driver returns control to the application.

**Interrupt data transfer.** The driver returns control to the application immediately. The A/D conversions are processed in the background and as soon as one conversion is completed, the application is interrupted

---

and saves the converted data. This process is continued until the  $N^{\text{th}}$  conversion is completed.

**Direct Memory Access (DMA) data transfer.** In this case the driver returns control to the application immediately. The A/D conversions are processed (in the background) and when one conversion is complete the driver activates the DMA to transfer the data. This process is continued until the  $N^{\text{th}}$  conversion is completed.

Depending on the data acquisition frequency (Section 4.3.1), and the programming language used to drive the card, any of these modes may be implemented. However, due to the operational time restriction of the software, the data acquisition frequency was limited to about 50 kHz, and accordingly the sensor electronics were designed to match this frequency limitation (Section 5.4).

In the experimental work presented here, software data transfer and Direct Memory Access data transfer processes were extensively used (Section 5.8). Software data transfer was used whenever data flow control was required while DMA was used for the real time measurements in order to minimise the total time of data acquisition.

## 5.8 SOFTWARE DRIVERS

In order to drive the PCL-818 Laboratory Card, compute the cross-correlation function and determine the speed, a number of programs (in different programming languages) were written and tested. Irrespective of the programming language used, each program was required to accomplish the following tasks:

- drive the data acquisition,
- select the data acquisition frequency,
- select the number of  $x(t)$  and  $y(t)$  points,

- 
- generate arrays of data ( $x[i]$  and  $y[j]$  ),
  - compute a low resolution cross-correlation  $R_{xy}(\tau)$  (equation 4.22),
  - generate an array  $R_{xy}(\tau)$  and estimate the maximum  $R_{xy}(\tau)$ ,
  - perform a second pass to obtain higher resolution of the cross-correlation function near the estimated maximum of  $R_{xy}(\tau)$ ,
  - apply the parabola apex approximation (equation 4.19),
  - compute the average speed (equation 4.24).

These functions are reflected in the structure of the programs listed in Appendices 2, 3 and 4. Although programs written in assembler run faster, the time required for digitising and acquisition of data is dominant, so in this case there is virtually no advantage in using a low level language. The execution time difference between the programmes written in assembler and Pascal for this application was so small that the latter was preferred. Moreover, compared to assembler, Pascal possesses the advantages of a high level language, allowing easy and straight forward editing, debugging and programme maintenance. This, of course, speeds up the software development and optimisation time of the program.

## 5.9 HAMEG DIGITAL STORAGE OSCILLOSCOPE

A Hameg digitising oscilloscope was extensively used for monitoring the analogue signals at the input to the digitiser of the PCL-818 card. Although the oscilloscope was not used for processing the signals it was useful during the visual alignment of the optics and for verifying the digitised data displayed on the computer screen. This was in fact the method employed to experimentally determine the degradation factor  $D$  (Section 4.4).

---

Note that during the initial experiments, a Tektronix DS602 digitising oscilloscope was used (Section 6.2) for data acquisition. This oscilloscope can be connected to a remote PC via a General Purpose Interface Bus (GPIB), through which data acquisition can be controlled. Later, the role of the Tektronix digitising oscilloscope was fulfilled by the PCL-818 card.

## **5.10 CATEYE INTEGRATED VELOCIMETER**

The Cateye integrated velocimeter was extensively used during the experimental work presented in this thesis to enable the continuous comparisons of speed values. The Cateye comprises a magnetic sensor and electronics that count the magnetic induction coming from a magnet fixed to a rotating surface of known radius. The linear speed is computed by averaging the time between pulses over several revolutions. The disadvantages of this device are that it can only measure the speed of the rotating surfaces, the radius has to be known in advance and the magnet must be mounted on the moving surface in order to measure the linear velocity.

The accuracy of the Cateye velocimeter is about 1% for a constant speed (Cateye Co. Ltd., 1993). In order to obtain reliable performance characteristics for the optical sensor, repeated measurements of constant speed were made, the results averaged and then compared to the Cateye.

---

## Chapter 6      EXPERIMENTAL RESULTS

### 6.1      INTRODUCTION

In this chapter the experimental results obtained using the fibre optic sensor described in the previous chapter are presented. The specially constructed transducer head was employed to obtain the analogue signal from the moving surface. The Tektronix oscilloscope was used for data acquisition until a dedicated system based on a relatively inexpensive PCL-818 Laboratory Card (Section 5.7) was assembled. Then the cross-correlation technique was demonstrated to be suitable for the fibre optic speed measurement sensor (Section 6.2).

In order to drive the card and compute the speed of the moving surface, a number of computer programmes were developed. Since direct cross-correlation uses multiplication operations extensively, one of the major problems encountered in designing a practical system was the excessive time spend on numerical computation. To overcome this problem, a double pass cross-correlation technique was developed. With this technique it was possible to reduce the total time of computation without affecting the precision of time delay estimation (Section 6.5).

### 6.2      INITIAL TRIALS

The experimental set-up for the initial trials is shown in Figure 6.1. At this stage, a 0.10 m radius aluminium disc driven by an electric motor was used to simulate a moving surface. The first version of the transducer head (described in Section 5.6) using 50/125  $\mu\text{m}$  multimode optical fibres allowed about 290  $\mu\text{W}$  of optical power to be directed at the moving surface. Reversed biased silicon photodiodes (Figure 6.1) with

---

their 1 M $\Omega$  load resistors (required to obtain sufficient signal level), were AC coupled to the digitising oscilloscope through 0.1  $\mu$ F capacitors to remove the DC offset, thereby ensuring zero mean signals required by the cross-correlation principle (Chapter 4). Note that no external amplifiers were used at this stage. A maximum range of 0.40 m between the transducer head and the aluminium disc was achievable with this arrangement. The amplitude of the output signal from the photodetectors was between 20 mV and 50 mV. A Tektronix digitising oscilloscope was interfaced via a GPIB to a Vectra (Hewlett Packard) computer that was also used for the cross-correlation calculations.

In order to compute a smooth cross-correlation function, 4096 data points were acquired. A computer programme was written to store the acquired values sequentially in two data arrays  $x(kt)$  and  $y(kt)$  and then compute and store the cross-correlation function  $R_{xy}(\tau)$  in a third array. Typical signals and their cross-correlation function are displayed in Figure 6.2. It can be seen that the time delay between the two signals equals the abscissa of the maximum of the cross-correlation function.

The digitised signals were noisy ( $SNR = 6.8$  dB) in these initial trials due to the high value of the load resistor in the circuit of the detector and electromagnetic interference due to poor shielding. These problems were addressed in the final design of the system (Section 5.4). Even in these conditions a smooth cross-correlation function was obtained (Figure 6.2), demonstrating the suitability of this technique for the measurement of speed.

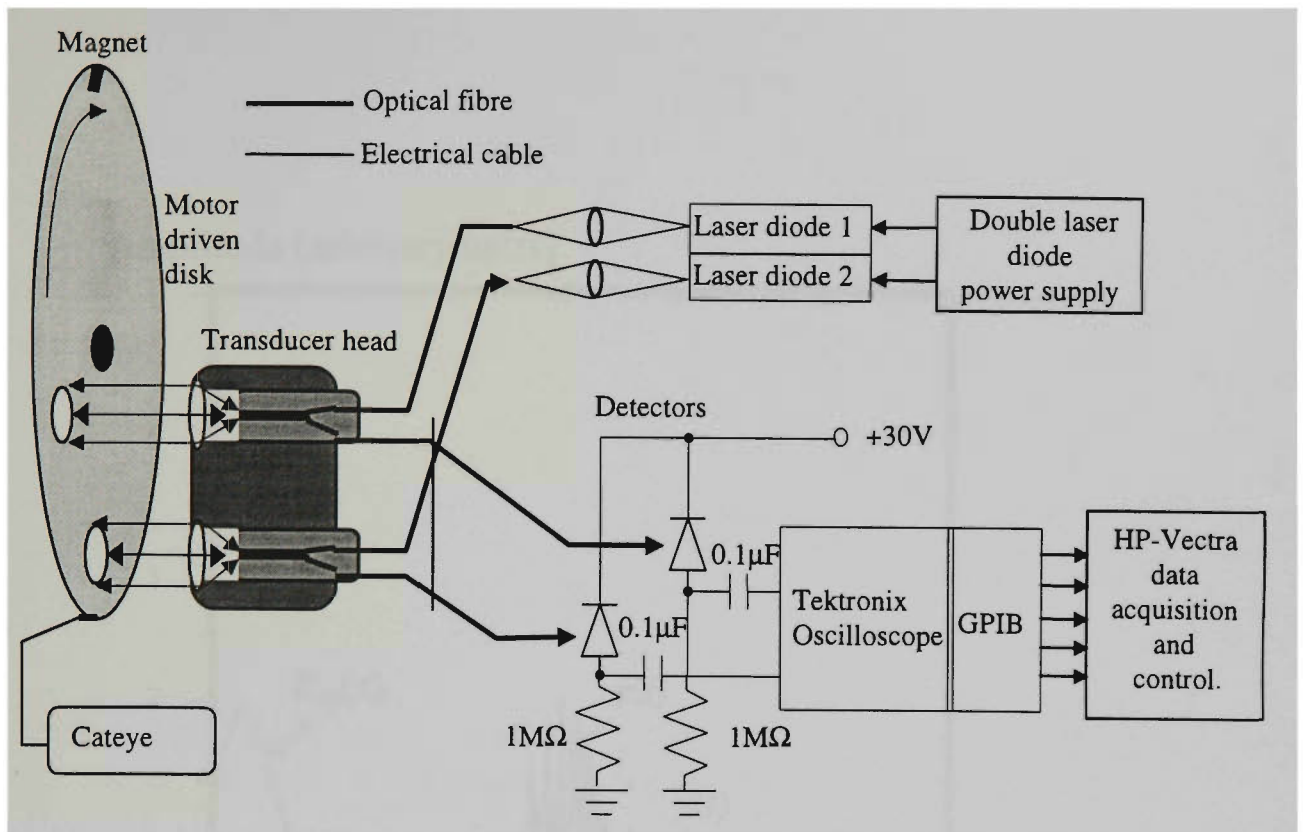


Figure 6.1. Experimental arrangement for the initial trials. The sensors within the transducer head are 30 mm apart.

However, the poor signal-to-noise ratio degrades the results obtained with this measurement configuration. In Figure 6.3 the speed measured with the Cateye integrated velocimeter is plotted against the speed determined using the optical fibre system. Taking the Cateye as reference for speed comparison, the relative error in speed measurement ( $\epsilon$ ) for an aluminium surface was  $5 \pm 2\%$ .

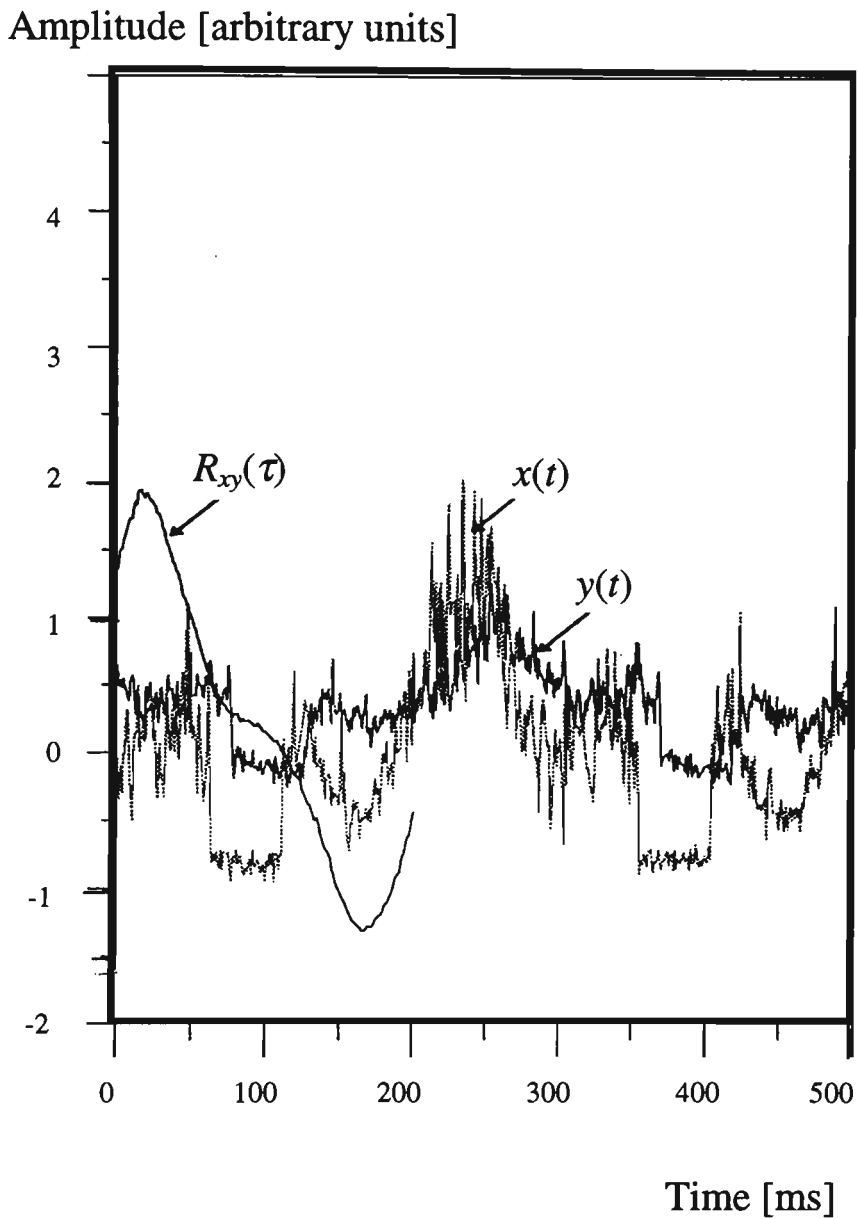


Figure 6.2. Digitised signals and their cross-correlation function.  
 $x(t)$  = reference signal,  $y(t)$  = delayed signal and  
 $R_{xy}(\tau)$  = cross-correlation function.

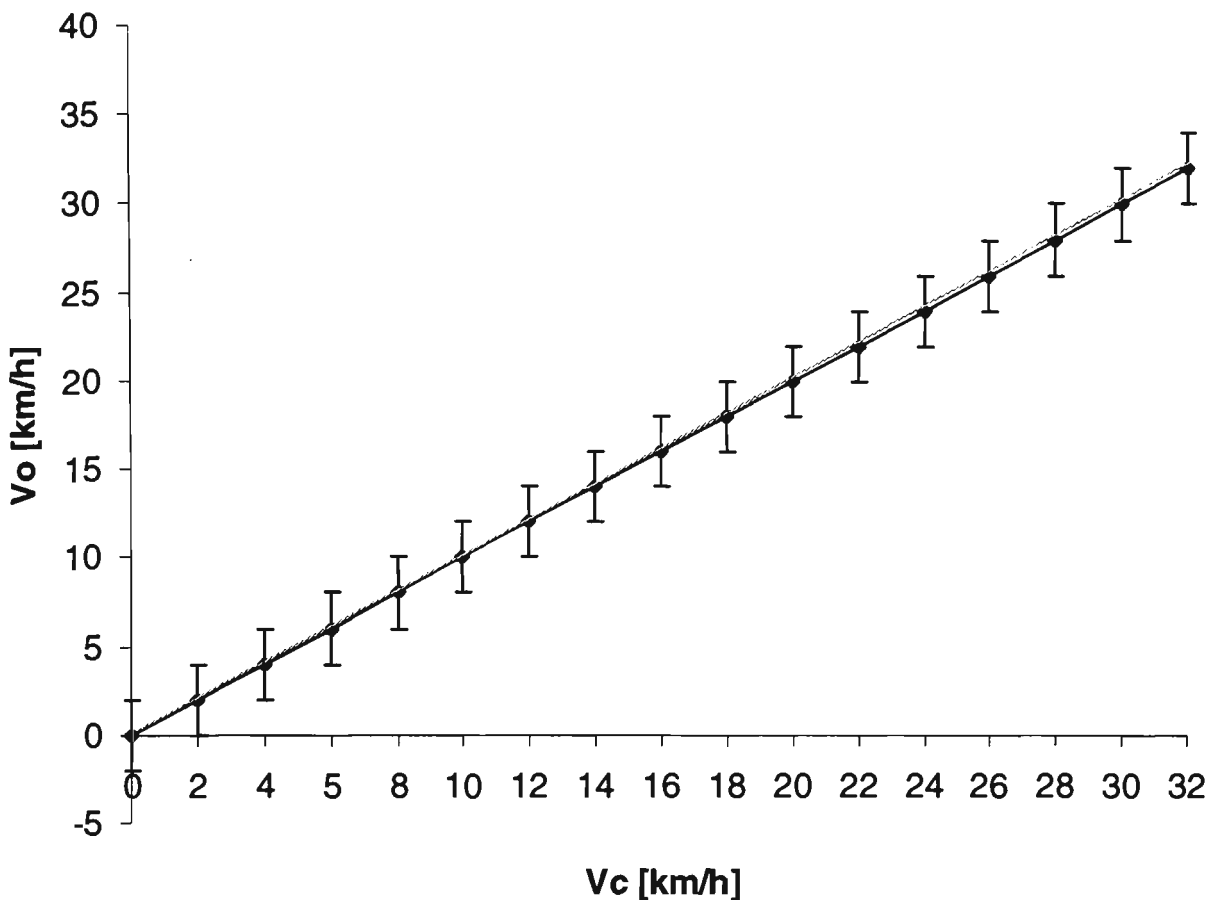


Figure 6.3. Comparison between Cateye integrated velocimeter ( $x$ -axis) and optical sensor system ( $y$ -axis). The dotted line represents a 1:1 speed ratio. The error bars on the Cateye trace are too small to display on this diagram.

### 6.2.1 *Discussion of the results from the initial trials*

The initial trials showed that the  $SNR$  of the signal used to compute the cross-correlation function was unsatisfactory. During those trials it became obvious that the total time required for obtaining the final speed was unacceptable for a practical speed measurement device.

The data acquisition was accomplished with the Tektronix digitising oscilloscope with the digitised information being transferred and stored

---

on a PC. The cross-correlation was computed using a Pascal programme listed in Appendix 1. In order to create a practical speed-measuring device, a dedicated system was designed and built (Figure 5.1).

The multimode optical fibres were changed from 50/125  $\mu\text{m}$  to a larger core size, namely 100/140  $\mu\text{m}$ . Thus, a higher optical power was injected into the fibres and consequently the working distance between the transducer head and the moving surface was increased by a factor of ten. The new configuration increased the signal-to-noise ratio of the sensor system from 6.8 dB to 22 dB. Furthermore, by using the PCL-818 card and the programme listed in Appendix 3, the total time needed to acquire the value of speed was reduced from 42 min to 72 s. Further developments in the cross-correlation computing technique (Section 6.5) have subsequently decreased the total measurement time to just 1.8 s.

### **6.3 SELECTION OF SURFACES FOR REAL TIME MEASUREMENTS**

In order to investigate the applicability of the optical sensor in diverse conditions, a number of surfaces were selected and tested. In Figure 6.4 the frequencies corresponding to the maximum power spectrum are plotted along with signal amplitude for different surfaces at a constant gain of 100 and distance of 0.40 m between the transducer head and the moving surface. These settings were selected for these trials because it was found experimentally that reliable measurements were obtained for the variety of surfaces chosen without a need to alter the optical alignment.

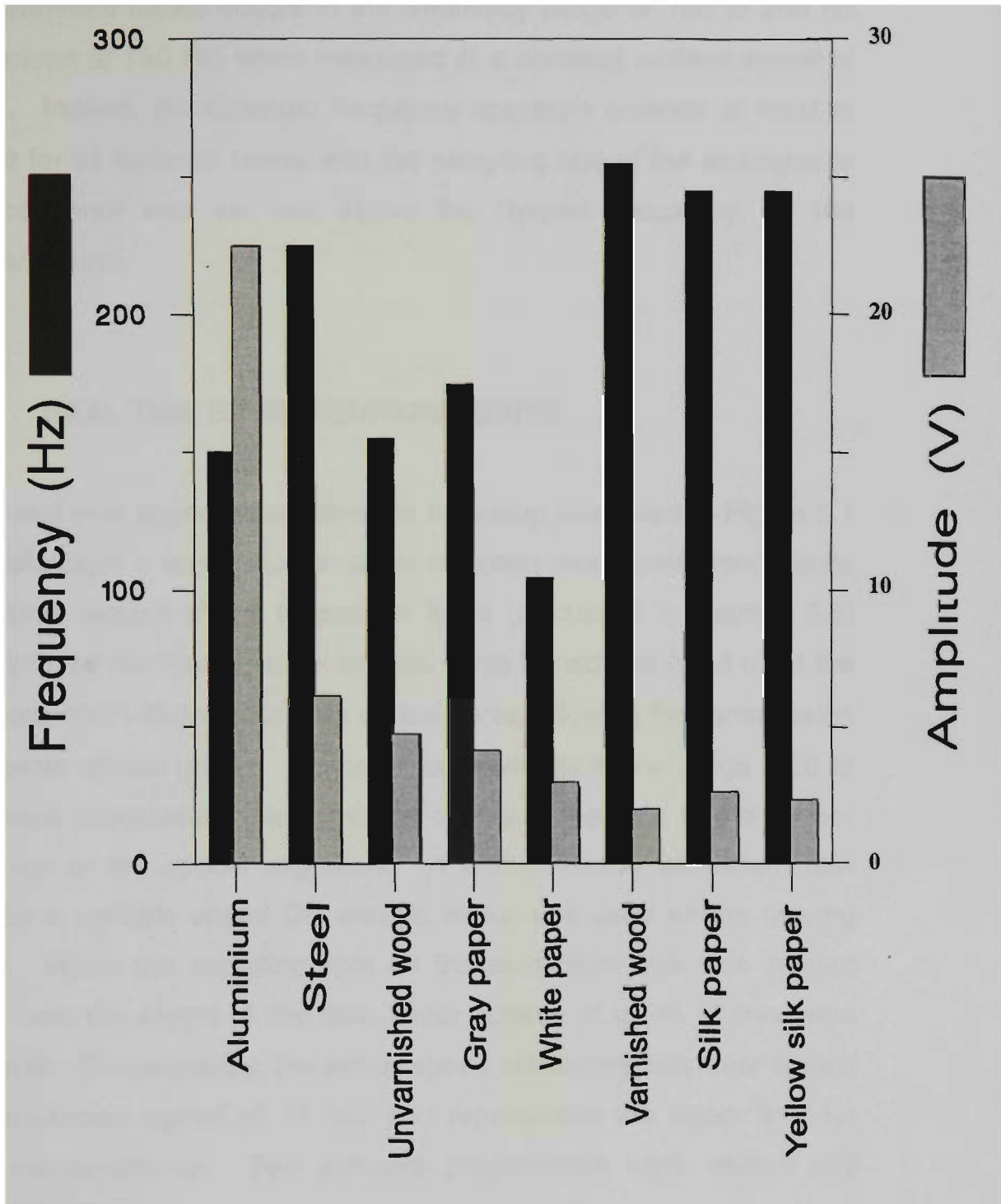


Figure 6.4. The frequencies and signal amplitudes corresponding to the maximum power spectrum at a constant speed of 1.6 m/s. Frequency values are proportional to the speed, whereas the amplitude indicates the surface reflectivity in each case. (Higher frequencies indicate surfaces that will produce better correlation).

---

Figure 6.4 shows that the maximum of the power spectrum of the signal for the surfaces tested occurs in the frequency range of 100 to 250 Hz (with a mean at 190 Hz) when measured at a constant surface speed of 1.6 m/s. Indeed, the detected frequency spectrum extends at least to 3500 Hz for all surfaces tested and the sampling rate of the analogue to digital converter was set well above the Nyquist frequency, at 104 samples/second.

## **6.4 REAL TIME SPEED MEASUREMENTS**

For the real time speed measurements the setup presented in Figure 5.1 and Photograph 1 was used. In order to obtain more consistent results the second version of the transducer head (discussed in Section 5.6) was employed for these measurements. This transducer head used the larger core 100/140 $\mu$ m multimode optical fibres, allowing for transmission of a greater optical power. Hence, measurements in the range 0.20 to 5.0 m were successfully made without changing the gain of the sensor electronics or the optical alignment. A 0.30 m radius aluminium disk driven by a variable speed DC electric motor was used as the moving surface. When the sampling spot on the aluminium disk was located 0.28 m from the centre of the disk, linear speeds of up to 17 m/s were achievable. Consequently, the actual speed measurements were limited to the maximum speed of 17 m/s and represented the upper limit for speed measurements. Two software programmes were written and extensively used for process control. One provided a continuous speed measurement with the numerical results displayed on the monitor screen (Appendix 3) and the other (Appendix 2) was used to demonstrate the relationship between the two input signals and the resulting cross-correlation function. Both programmes made use of the PCL-818 card drivers for data acquisition and DMA data transfer to computer memory (Section 5.7). The programmes were tested for a range of sampling rates and various record lengths. In Figures 6.5, 6.6, 6.7 and 6.8 the

---

results for a surface moving at different speeds are presented. Each graph shows the reference signal  $x(kt)$ , the delayed signal  $y(kt)$  and the cross-correlation function  $R_{xy}(\tau)$ . In addition, the number of points in the arrays (record length), the index of the maximum of the cross-correlation function ( $N_{\max}$ ), the sampling rate ( $f$ ) and the calculated speeds are shown. The horizontal axis represents the array index of time ( $k$ ) for input signals  $x(kt)$  and  $y(kt)$ . The time delay corresponding to the maximum of the cross-correlation function can be computed from  $\tau = k\Delta t$ . Note also that both signals have a mean amplitude of zero required by the cross-correlation function (Section 4.2). However, for clarity, one of the signals was shifted vertically.

The signals depicted in Figures 6.5 and 6.6 were acquired under similar conditions. The sensor head receives the reflected light from the same circular track on the moving surface and, apart from a slightly different scale, the signals in the two figures are similar. A careful examination of reference and delayed signal show individual differences due to the presence of a slight offset between the two light spots on the moving surface. In fact, the size of the light beam used in these measurements is a trade-off between transverse offset error and the frequency of the signal. A large light beam will reduce the tracking error due to transverse offset but decrease the signal frequency and therefore the accuracy of the speed measurement. Fortunately, the offset is small and the correlation function is well defined with a sharp peak representing the maximum and therefore allowing accurate speed determination. It can be seen that the maximum of the cross-correlation function in the first figure (Figure 6.5) corresponds to  $N_{\max}$  of 26 while in the second figure it corresponds to 33 (note diagrams are not drawn to scale), yielding surface speeds of 1.86 and 1.48 m/s respectively.

The results presented in the next two figures (Figure 6.7 and 6.8) were acquired with the transducer head in the same position relative to the

---

moving surface as discussed in the previous paragraph. This time, the frequency of data acquisition was increased from 1666 Hz to 2500 Hz. As expected, the signal pattern is similar to the previous figures. The correlation function shows little discernible difference because no improvement in the sharpness of the cross-correlation function is achievable as long as the frequency of data acquisition is much higher than the Nyquist frequency of the input signals. By using a higher sampling rate the total time of measurement can be dramatically reduced. In this case, by increasing the frequency of data acquisition from 1666 to 2500 Hz, the total time of measurement was decreased by about 50%.

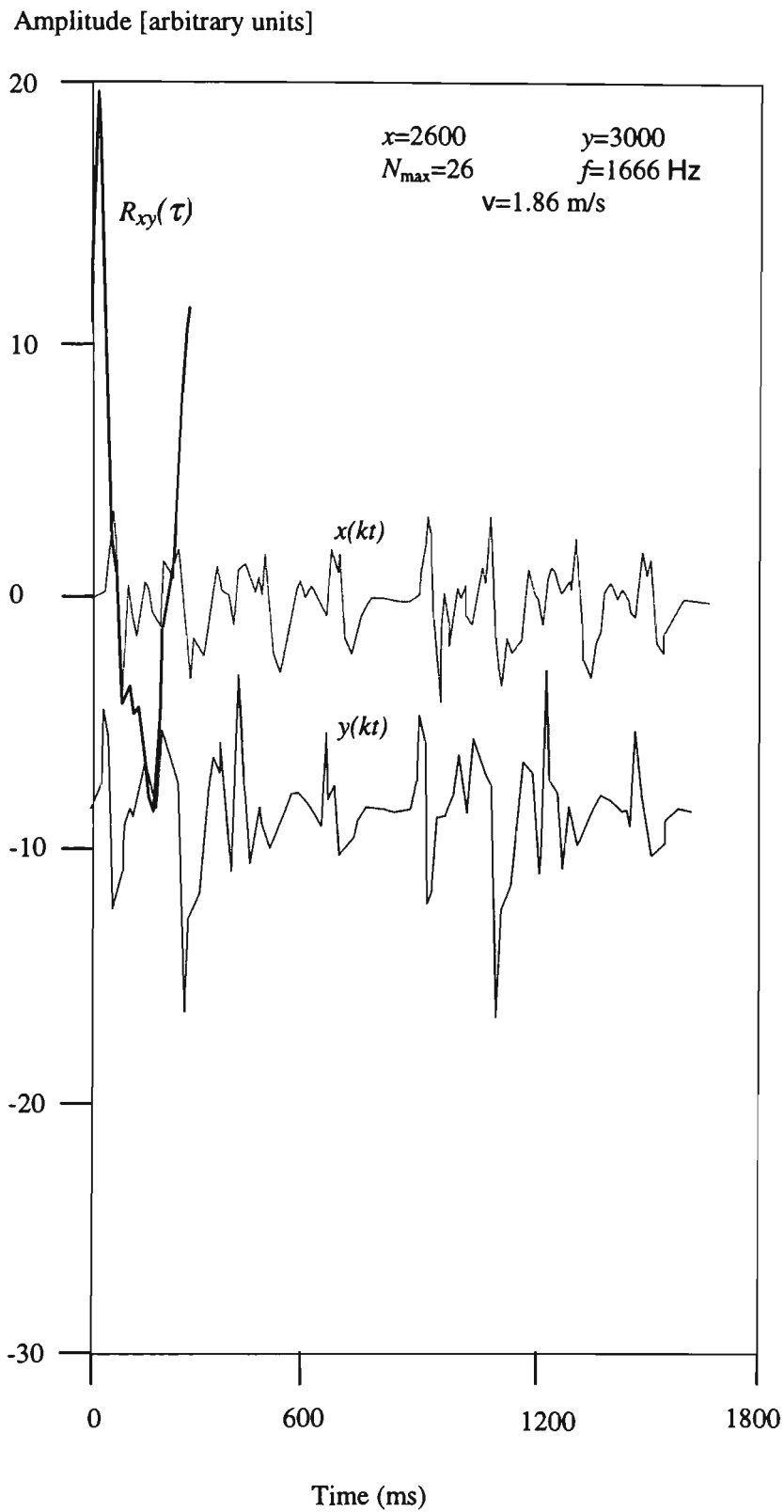


Figure 6.5. Input signals and their cross-correlation function.

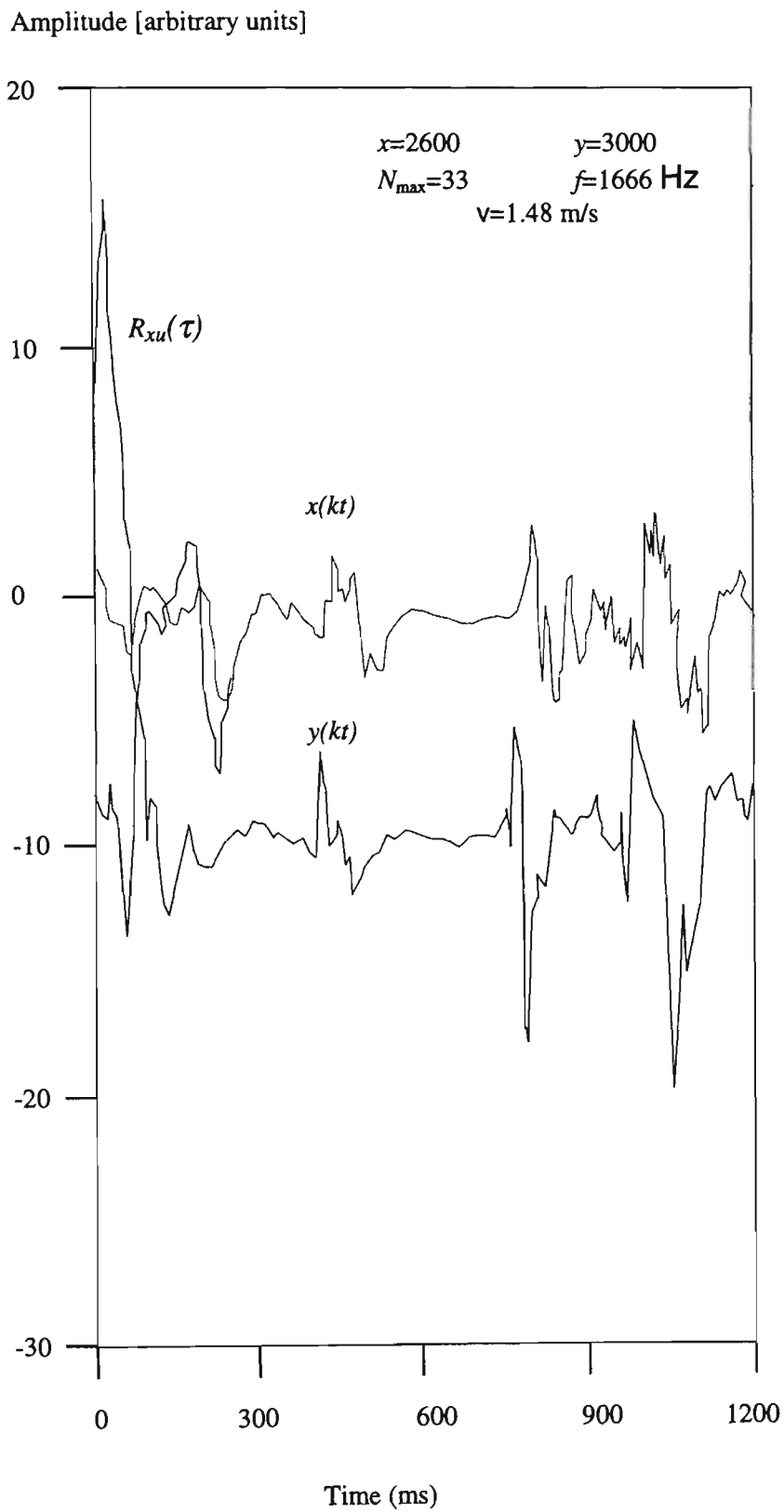


Figure 6.6. Input signals and their cross-correlation function.

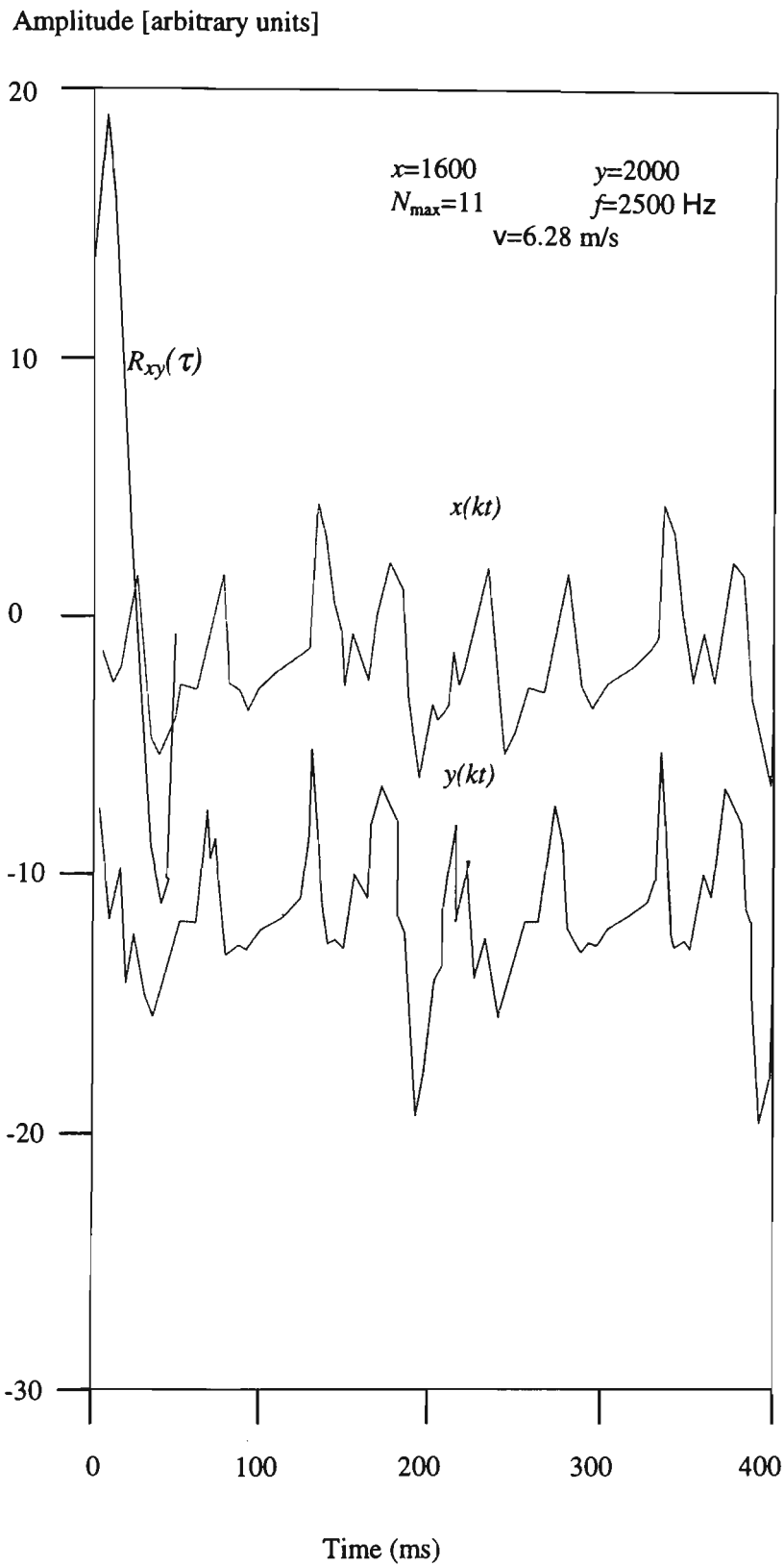


Figure 6.7. Input signals and their cross-correlation function.

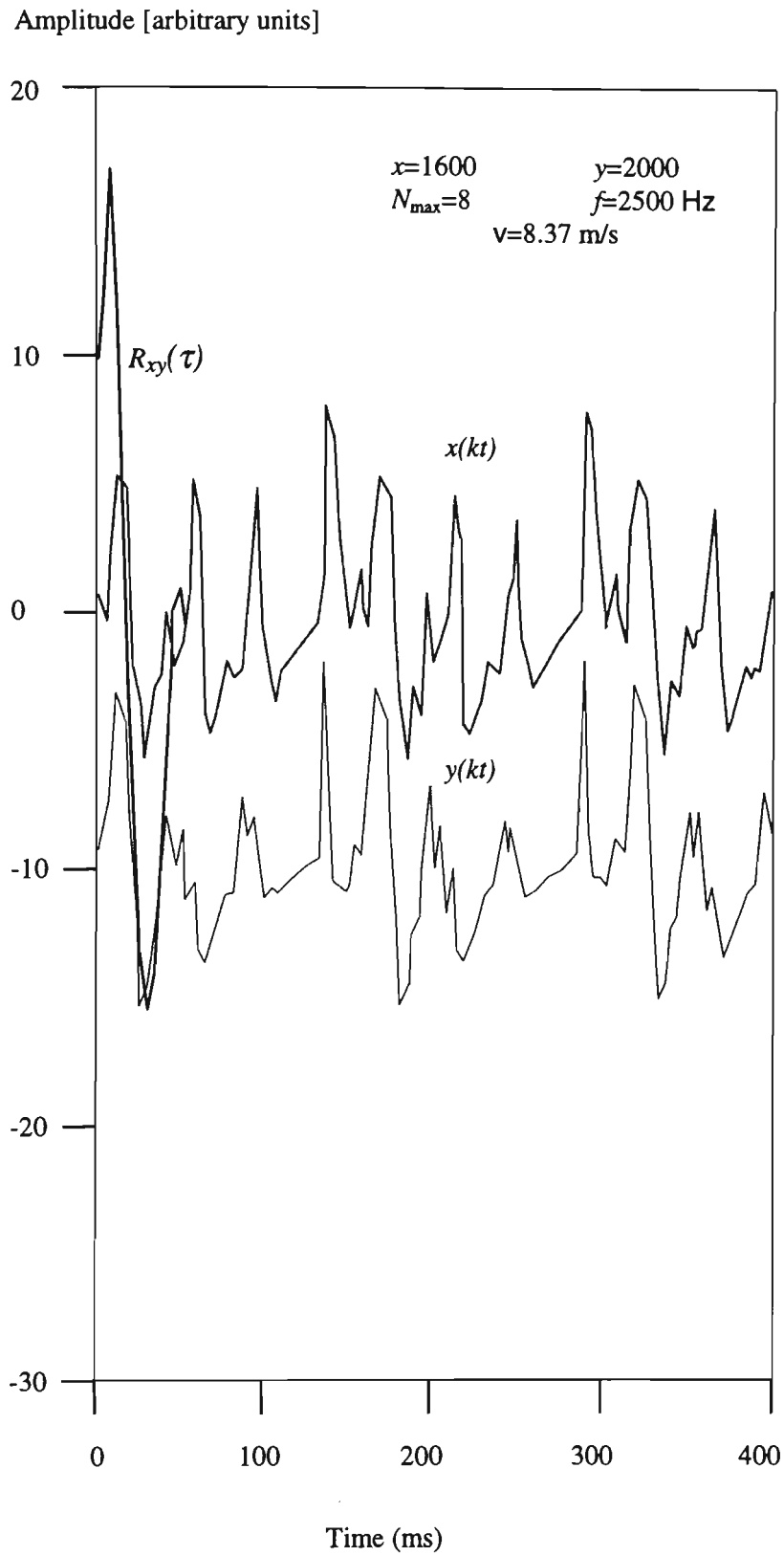


Figure 6.8. Input signals and their cross-correlation function.

---

## 6.5 CUSTOMISATION OF PROCESSING TECHNIQUE TO IMPROVE SENSOR TIME RESPONSE

The optical fibre sensor and the associated electronics, discussed in Sections 6.2 to 6.4, allowed reliable measurements for the range of surfaces tested, although the total time required to obtain the speed was unacceptably long for a practical device. Therefore, the next objective was to optimise the system in order to reduce the measurement time. Section 4.2 provides the background theory for the evaluation of the time delay  $\tau$  using cross-correlation by implementing the equation

$$R_{xy}(\tau) = \frac{1}{N} \sum_{k=1}^N x(kt) y(kt + \tau)$$

and the time delay is estimated by

$$\tilde{D} = \arg [\max R_{xy}(\tau)].$$

To illustrate the advantages of using the double pass cross-correlation a specific example is used. Assuming the computer has to store two arrays of data, 2600 points as  $x$  and 2400 points representing signal  $y$ . Since the number of cross-correlation points here is 200 (i.e. 2600 – 2400), then  $2400 \times 2600 \times 200 = 1.248 \times 10^9$  integer multiplications must be performed before the maximum of the function can be determined. In this particular case, an IBM PC based on 33MHz 80386 Intel chip can compute the cross-correlation in 74 seconds. In order to reduce computation time the double evaluation cross-correlation method was developed and implemented. In this method, the same arrays were used but the cross-correlation function was computed twice. First, using every tenth point in the arrays, an approximate correlation function was computed and its maximum located. Then, knowing the maximum of this correlation function a second correlation function was computed using all

---

the available points in the array within a narrow range centred at the approximate maximum. It was sufficient to use only 10 points on either side of the initial delay estimate. By following this procedure, the same resolution as in a full calculation was obtained but the number of integer multiplications was dramatically reduced. For the above example, it means  $1.248 \times 10^7$  multiplications for the first evaluation and  $1.248 \times 10^8$  multiplications for the second evaluation which gives a total of  $1.378 \times 10^8$ . That is almost an order of magnitude faster than the full calculation, which in turn translates to a computing time of 8.6 seconds instead of the original 74 seconds. Note that depending on the application, shorter array lengths could be used (for example 1000 and 1200 points) and hence the total measurement time can be further reduced (1.8 seconds). Examples of typical signals and their cross-correlation functions obtained with the double evaluation (or double pass) method are shown in Figures 6.9 and 6.10. The waveforms and their cross-correlation functions are plotted on the same graph.  $R_{xy}(\tau)$  represents the first and  $R'_{xy}(\tau)$  the second pass cross-correlation function respectively. Again, for clarity, the traces are offset vertically.

The cross-correlation function is band limited and it displays a symmetric peak around its maximum (Section 4.2.2). Therefore it can be approximated with a convex parabola in the neighbourhood of its maximum and the continuous time estimate can be found by locating the apex of the parabola (equation 4.20) using three points about the maximum of the correlation. Using this method, finer (subsample) estimates can be obtained (equation 4.21).

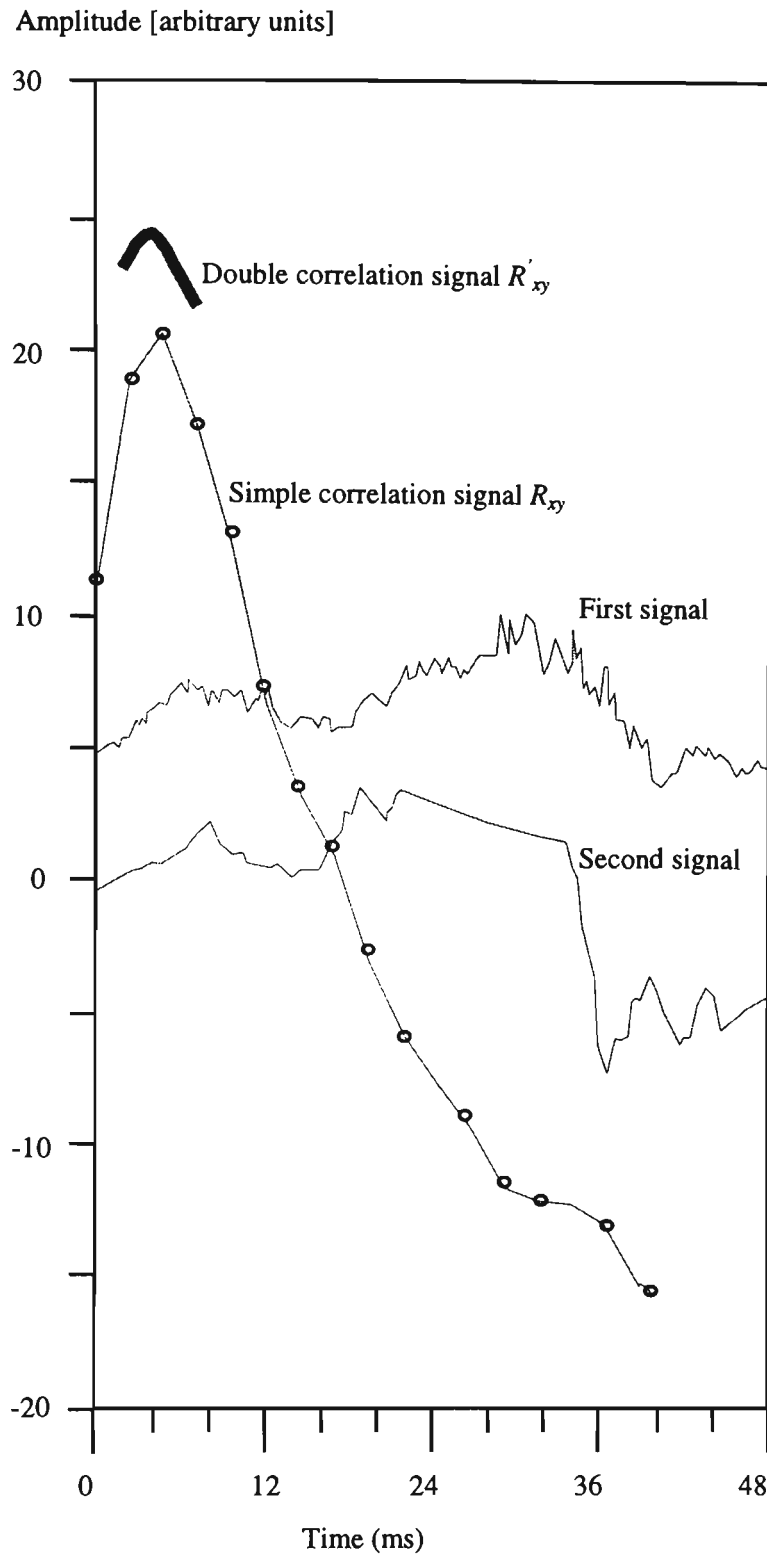


Figure 6.9. Two signals and the resulting approximate (simple) and double cross-correlation functions for a moving surface. (The difference in appearance of the two signals is due a slight misalignment between the transmitting and receiving fibres in the first sensor).

Amplitude [arbitrary units]

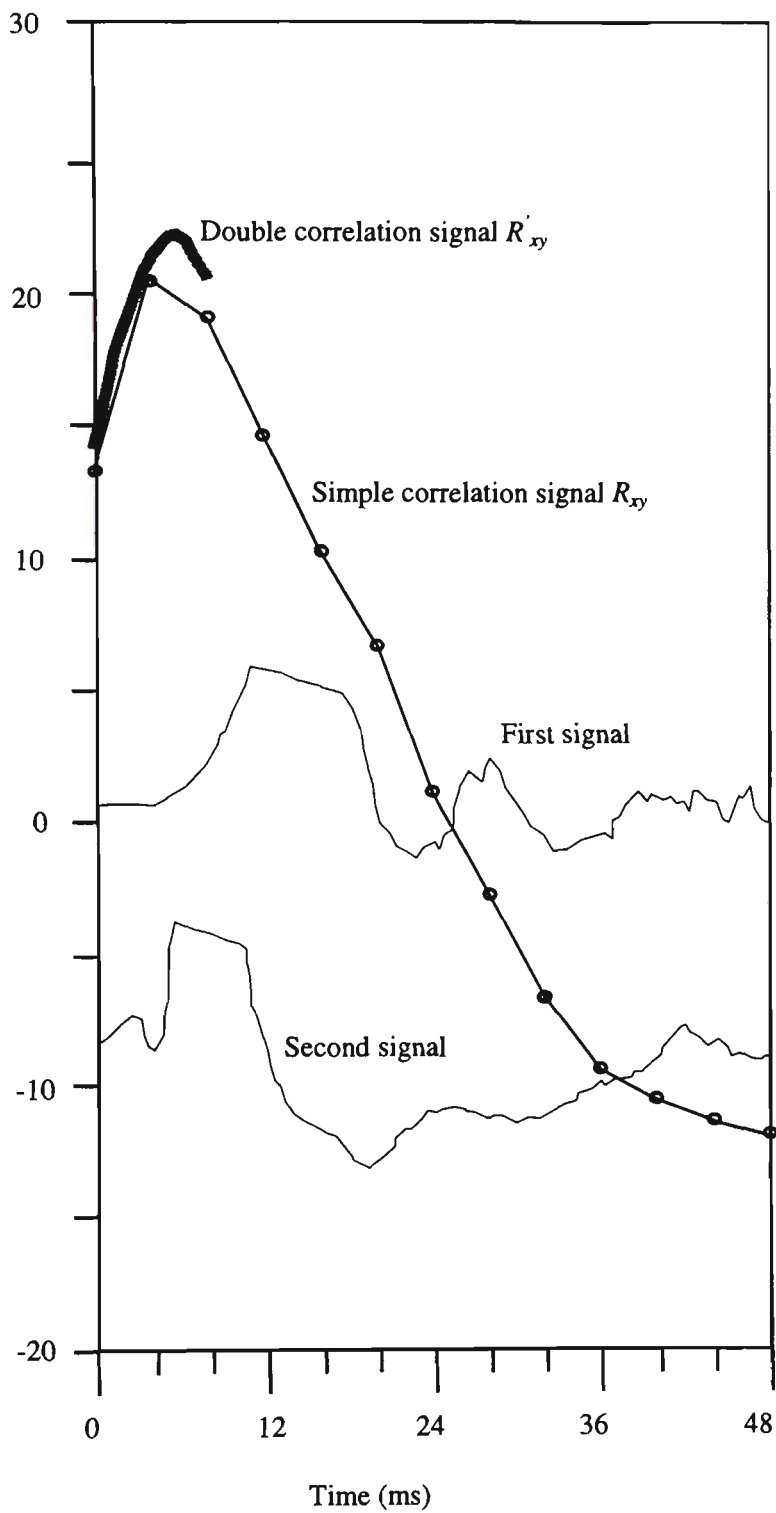


Figure 6.10. Another example showing signals and the resulting simple and double cross-correlation functions.

---

## 6.6 PRACTICAL SPEED LIMITS AND UNCERTAINTIES

In Section 4.4, it was shown that the correlator has an excellent signal-to-noise ratio. Therefore, in theory, the uncertainty of the speed measurement depends on the sampling rate and record length of the digitiser. That is, given sufficient record length for signal correlation, the speed uncertainty is directly related to the time interval between the two successive data points. In practice, Nyquist frequency and more importantly the beam waist governs the accuracy of time interval determination and hence the speed measurement. The uncertainty for speed determination is given by

$$\frac{\Delta v}{v} = \frac{\Delta L}{L} + \frac{\Delta t}{t} + O(\text{correlator}) \quad 6.1$$

where  $O(\text{correlator})$  is very small and can be neglected.

The two pairs of fibre sensors within the transducer head are 30 mm apart creating uncertainty ( $\Delta L = 0.2$  mm at the moving surface). This contribution to the total uncertainty depends on the machining precision (location and parallelism) of the transducer head and our ability to determine the separation of fibres—relative error of about 0.7%. Any angular deviation of sensing fibres and/or tilt of the moving surface will affect beam waste uncertainty by creating an elliptical spot at the surface of the target as well as altering real separation of the beams.

In Section 6.3 it was shown that the power spectrum of the signal for the surfaces tested extends to at least 3500 Hz for all surfaces tested. This upper frequency limit is speed dependent and it is attributed to the “low pass” filtering nature of the collimating optics (beam waist). That is each probe beam has a significant waist leading to integration of surface characteristics preventing the interpolation of higher frequencies. In the

---

worst case this would produce uncertainty in the absolute speed reading of about 9% for a surface moving at 30 km/h (at a frequency of data acquisition of 400 Hz). However, by increasing the sampling frequency the uncertainties could be reduced to a few percent.

The bandwidth of the electronics affects only the lower limit for speed measurement, as upper frequencies of the order of GHz may be easily achieved. On the other hand the AC coupling necessary for the operation of the correlator impose a low frequency limit. For the current speed sensor configuration the lower cut-off is at 5 Hz and hence it is not practical to measure speeds lower than 0.2 km/h.

## 6.7 RESULTS

Real time measurements were carried out using the arrangement shown in Figure 5.1. In order to assess the capabilities of the speed measurement system, a number of experiments were carried out under different conditions and the results are presented graphically in Figures 6.11 to 6.13.

The speed of the aluminium surface was measured simultaneously using the commercial Cateye instrument (Section 5.10) and the optical fibre sensor system. The speed measured with the optical system is plotted in Figure 6.11 as a function of the speed determined by the Cateye. Note that the dotted line represents a 1:1 speed ratio. The relative error ( $\epsilon_r$ ) for surface speeds ranging from 0.27 to 7.78 m/s was between 0.1% and 2.4% with mean value of 1.2%. This is a considerable improvement compared to the 5% mean relative error in the initial trials, implying that the system presented in this thesis is competitive with other speedometers.

---

In practice, the distance between the transducer head and the moving surface may need to be changed and, therefore, a number of experiments were conducted to assess the effect of distance on the accuracy of this instrument. Using a simple geometrical argument it can be shown that the apparent speed is directly proportional to the transducer head distance from the moving surface. The experimental results are presented in Figure 6.12. In these measurements the speed of the surface was kept constant (1.6 m/s) and  $v$  represents the apparent speed measured by the sensor at different distances from the moving surface. The gradient in Figure 6.12 represents the sensitivity of the sensor with distance of the transducer head from the moving surface and is given by

$$m = \Delta v / \Delta L = 0.68 \text{ (m/s)m}^{-1}$$

This linear dependence of the speed on the distance between the transducer head and the moving surface is attributed to the change in the separation between the two sampling points on the moving surface with respect to the nominal value of 30 mm within the transducer head. This is a consequence of the small misalignment (nonparallelism) between the two transmitting optical fibres. The variation of the speed with the distance between transducer head and moving surface may be used as an efficient experimental method for aligning the two ferrules.

It was pointed out in Section 3.3 that one of the most difficult problems encountered when using optical systems for speed measurement was the angular alignment of sensors. In order to determine the sensitivity of the system on angular misalignment, another set of experiments was carried out to determine the apparent speed as a function of alignment angle. The alignment angle is the angle between the transducer head axis and the normal to the moving surface (note that in this case the alignment angle represents the angle of a cone so alignment in both the  $x$  and  $y$  axes is considered). Simple geometrical arguments can be used

to show that the measured velocity will vary cosinusoidally with the alignment angle (between the incident beam and the normal to the surface) as confirmed by qualitatively in Figure 6.13. The experimental results demonstrate a speed deviation of only 0.2% for a misalignment of  $\pm 4^\circ$ .

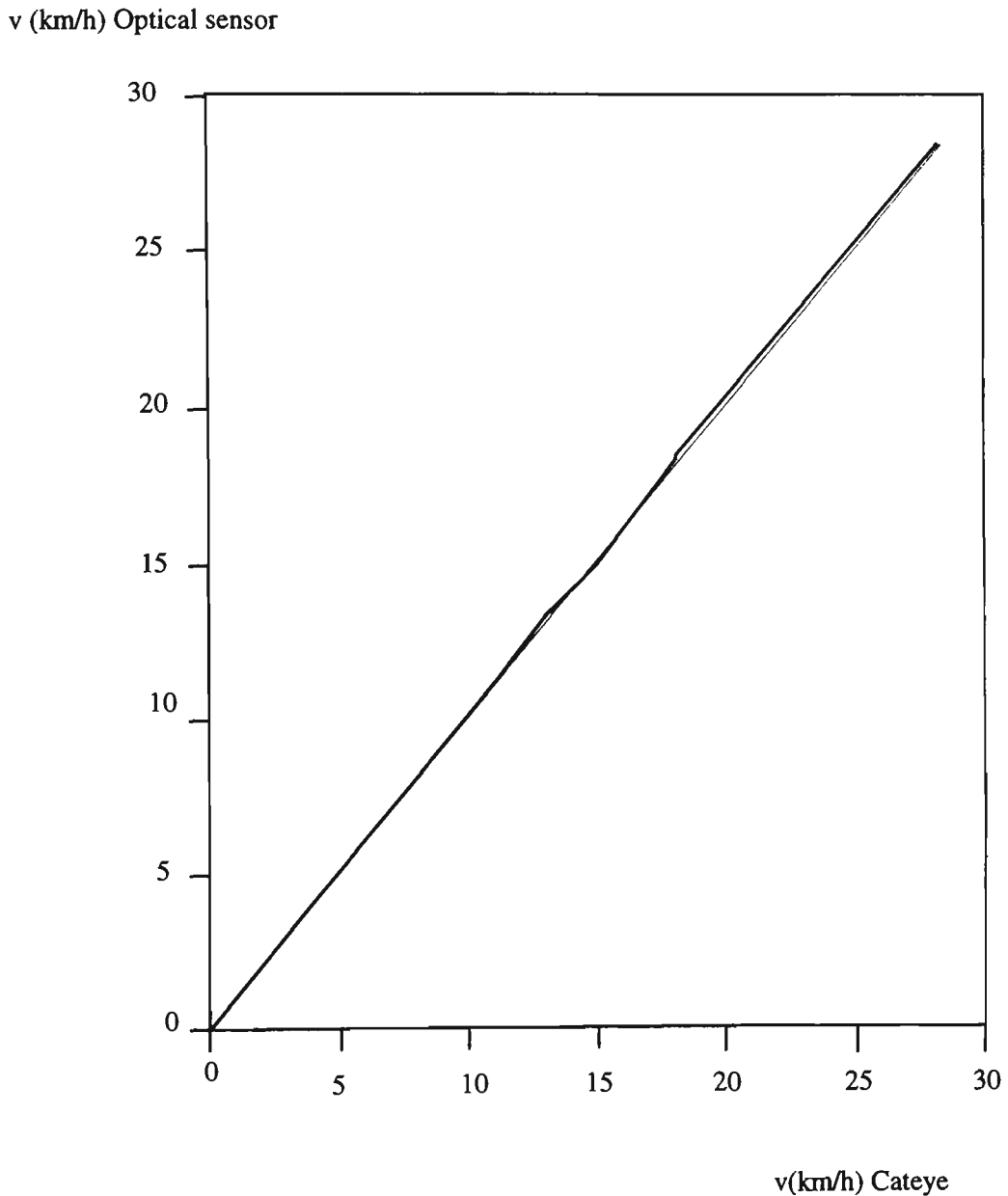


Figure 6.11. Comparison between the speed measured by the optical fibre sensor and the Cateye, commercial sensor. The dotted line represents a 1:1 speed ratio.

v (km/h)

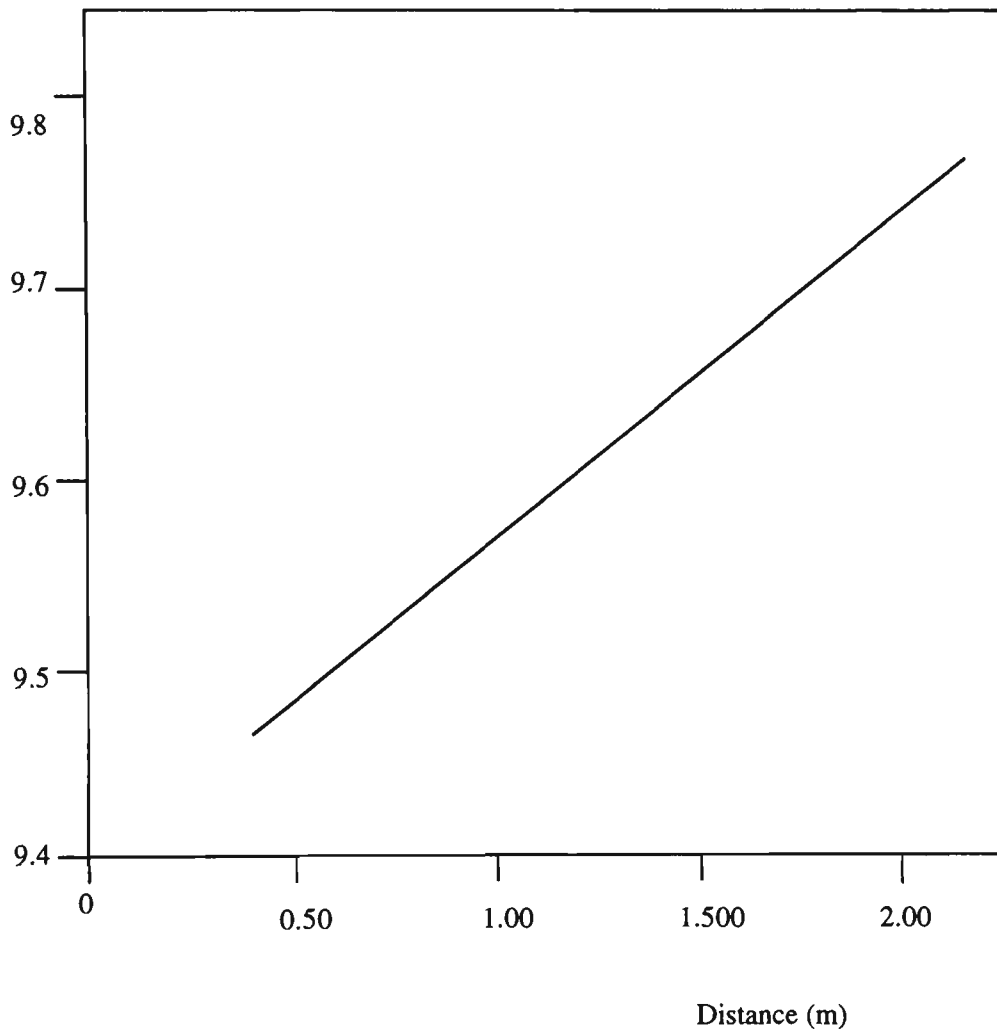


Figure 6.12. Apparent speed of a moving surface plotted as a function of the distance between the transducer head and moving surface.

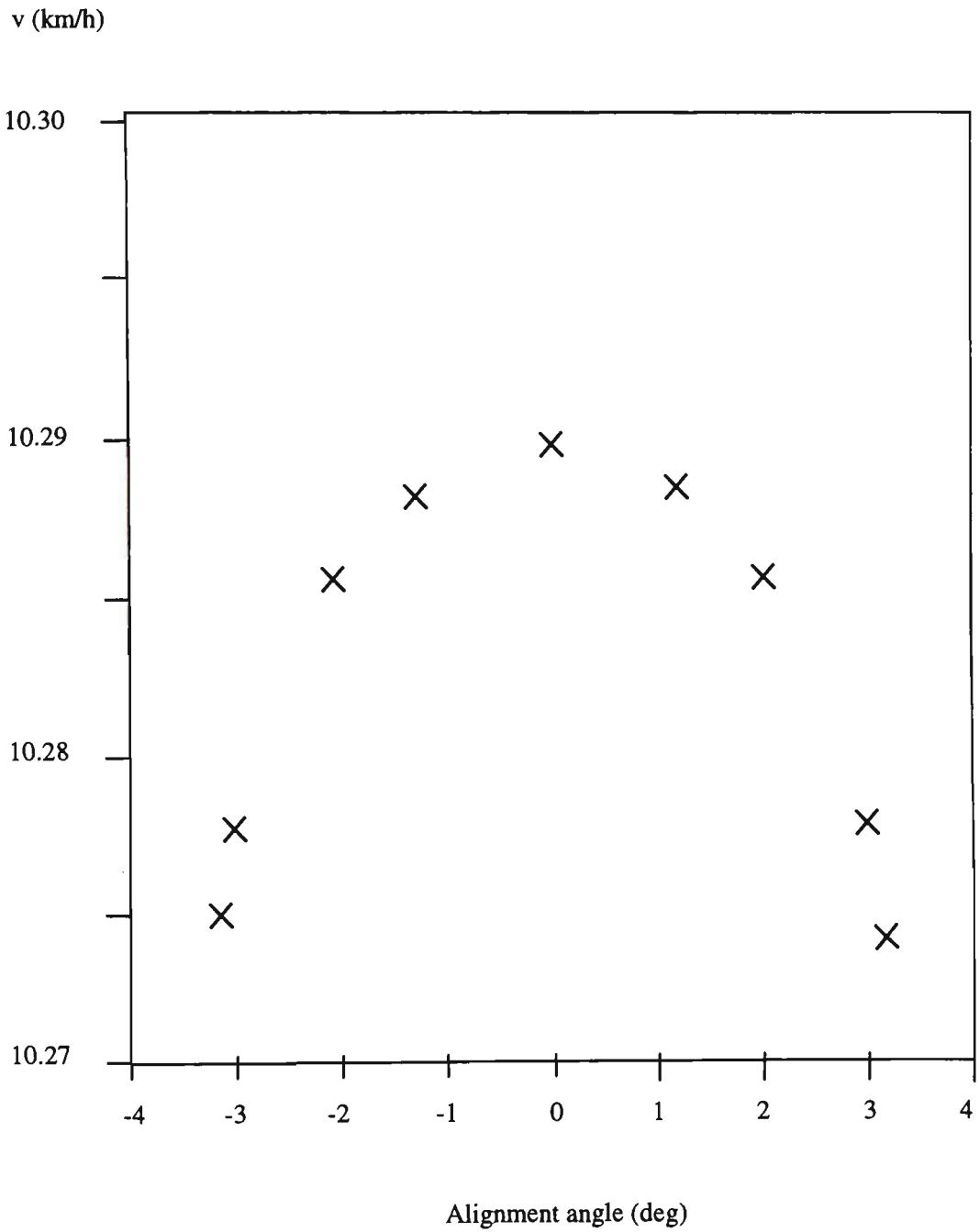


Figure 6.13. Apparent speed of the moving surface plotted as a function of the alignment angle.

---

## 6.8 CONCLUSIONS

In this chapter the methodology and results of the experiments are presented. The initial trials had demonstrated that the cross-correlation technique can be successfully used for the speed measurement of surfaces moving with non-deterministic motion.

The mark 1 version of the transducer head had a parallelism problem resulting in substantial uncertainties in speed measurement. The problem was addressed and rectified in the mark 2 version of the sensor by constructing the transducer head from a single aluminium block. The design allowed for linear adjustment of the optical fibre holders (ferrules) to focus the light on the target surface. By changing the optical fibres to a larger core diameter, the intensity delivered to the surface dramatically increased (by about a factor of five) and consequently the sensor was capable of reliable measurements at transducer-target separations of up to four metres. In addition, a new processing technique was developed (double cross-correlation) allowing more efficient use of the computing time and hence, faster display updates.

The experiments carried out under various conditions and on different surfaces have demonstrated the wide scope for practical applications of this optical sensor system.

Although the current sensor is capable of measuring speeds up to 30 km/h, the range can be easily extended to match industrial tachometers.

---

## Chapter 7      CONCLUSIONS

### 7.1      FINAL CONCLUSION

An optical fibre based speed measurement sensor using a cross-correlation technique for time delay estimation has been developed. In spite of the simple design and the use of low cost components compared with other more sophisticated and rather expensive speed measurement systems, the sensor presented in this thesis is accurate and competitive. Without any optical realignment or adjustment of the sensor electronics, even at a range of 4 metres no significant loss in accuracy was observed. Being non-intrusive, this system can be used to measure the speed of moving surfaces for which the process of measurement itself could affect the state of motion as well as for surfaces which are continuously in motion. In addition this optical fibre sensor for speed measurement is a safe and reliable device for performing measurements in hazardous as well as electromagnetically noisy environments.

The absolute uncertainty of up to 10% at 30 km/h for this sensor is not a serious limitation of the technique as a smaller cross-section light beam with fast analogue to digital card would decrease the errors. Of course, care must be taken to ensure that the two beams would view the same area to provide sensible data for the correlator. Ultimately, the maximum speed determination is limited by the roughness of the surface.

The resolution of the system is governed by the speed of the moving surface and the sampling rate. At higher speeds the beam waist (i.e. the average frequency of the power spectrum of the surface) becomes the dominant source of uncertainties and thus limits the resolution. At lower speeds the beam waist has progressively smaller effect on resolution as long as the sampling rate of the digitiser is kept constant.

---

The zero mean signal input required by the correlator imposes a low frequency limit on electronics. For the current speed sensor, the lower cut-off is at 5 Hz and hence measuring speeds lower than 0.055 m/s is not practical.

## **7.2 FUTURE WORK**

In order to enhance the reliability of the system presented in this thesis the optical fibre speed measurement system will be built as a practical, self contained, easy to operate and portable device. An embedded system based on a Motorola 68HC11 microcontroller will be designed and built. Dedicated "on chip" software will be developed for automatic gain control and smart data acquisition. These features will enable the system to automatically adapt itself to the prevailing conditions.

---

## REFERENCES

Advantech Co. Ltd, "PCL-818 High Performance Data Acquisition Card with Programmable Gain, User's Manual", 1993.

Beck, M. S., "Adaptive control: fundamental control and application", Proceedings of first Annual Advanced Control Conference, Purdue University, IN, USA, 1974, pp. 1-25.

Beck, M. S., "Correlation in Instruments: cross correlation flowmeters", Instrument Science and Technology, Vol. 2, Chapter 8, Adam Hilger, 1984.

Bendat, S. J. and Piersol, G. A., "Measurement and Analysis of Random Data", Wiley, 1967.

Bendat, S. J. and Piersol, G. A., "Engineering Applications of Correlation and Spectral Analysis", Wiley-Interscience Publication, New York, 1980.

Bentley, J. P., "Principles of Measurement Systems", Longman Scientific and Technical, 2nd edition, New York, 1992.

Boiarski, A. A. and Kingsley, S. A., "Differential Doppler Velocimetry Using Polarisation Preserving Fibres", Proc. IEEE Vol. 71, pp. 214-216, 1983.

Boucher, R. E. and Hassab, J. C., "Analysis of discrete implementation of generalised cross-correlator", IEEE Transactions on Acoustic Speech and Signal Processing", Vol ASSP-29, No 3, pp. 609-611, June 1981.

Bowers, F. K. and Klingler, R. J., "Quantisation Noise of Correlation Spectrometers", Astronomy and Astrophysics Supplement, Vol. 15, pp. 373-380, 1974.

---

Cateye Co. Ltd., Kuwazu, Higashi-ku, Osaka, Japan, 1993.

Champeney D. C, "Fourier Transforms in Physics", Adam Hilger, Bristol, UK, 1985.

Colella, G. M. and Neti, S., "Development of a Fibre Optic Laser Doppler Anemometer for Bubbly Two Phase Flow", Proceedings of ASME-Engineering, pp. 137-143, Phoenix, Arizona, USA, 1982.

Cussani, R., "Performance of Fast Time Delay Estimators", IEEE Transactions on Acoustics, Speech and Signal Processing, Vol 37, No. 5, May 1989, pp. 757-759.

Dakin J. and Culshaw B. "Optical Fibre Sensors", Volumes 1 & 2, Artech House, Boston, USA, 1988.

Danel, F., "Fiber Optic and Endoscopic LDA Systems", Proceedings of the LDA Symposium, Copenhagen, Denmark, pp. 490-496, 1975.

Durst, F., Melling, A. and Whitelaw, J. H., "Principles and Practice of Laser-Doppler Anemometry", Academic Press Inc., Great Britain, 1976.

Dyott, R. B., "The Fiber-Optic Doppler Anemometer", Microwave Optics and Acoustics, Vol 2, pp.13-18, 1978.

Edmund Scientific Co., Annual Reference Catalog for Optics, Science and Education, #19N1, Edmund Scientific Co., Barrington USA, 1989.

Fortney L. R., Principles of Electronics: Analog and Digital Harcourt Brace Jovanovich, Orlando USA, 1987.

---

Gogoasa I., Murphy M. and Szajman J., "An Extrinsic Cross Correlation Based Optical Fibre Sensor Speed Sensor". Paper accepted for publication in Meas. Sci and Technol., 1996.

Gusmeroli, V. and Martinelli, M., "Distributed laser Doppler velocimeter", Optics Letters, Vol 16, pp. 1358-1360, September 1991.

Hewlett Packard, Fibre Optic Handbook (Hewlett Packard, Germany 1988.

Jacovitti, G. and Scarano, G., "Discrete Time Techniques for Time Delay Estimation", IEEE Transactions on Signal Processing, Vol 41, No. 2, pp. 525-534, February 1993.

Jacovitti, G., Neri, A. and Cusani, R., "On a Fast Digital Method of Estimating the Autocorrelation of a Gaussian Stationary Process", IEEE Transactions on Acoustic Speech and Signal Processing, Vol ASSP-32, No. 5, pp. 968-976, Oct. 1984.

Jordan, J. R., "Correlation Algorithms, Circuits and Measurement Applications", IEEE Proceedings Vol 133, Pt G, pp. 58-72, February 1986.

Keck, D. B., "Fundamentals of Optical Fibre Communication, 2nd edition, Academic Press, 1981.

Krohn, D. A., "Fibre Optic Sensors, Fundamentals and Applications", Instrument Society of America, 1988.

Kuecken, A. J., "Fiber Optics – a Revolution in Communications", TAB Profesional and Reference Books, USA, 1987.

---

Kyuma, K., Tai, S., Hamanaka, K. and Nunoshita, M., "Laser Doppler Velocimeter with a Novel Optical Fiber Probe" Applied Optics, Vol 20, pp. 2424-2427, 1981.

Mansfield, P., H., "Electrical Transducers for Industrial Measurement", Butterworths, London, 1973.

Melchior, H., "Demodulation and photodetection techniques", North-Holland Publishing, Amsterdam, 1972.

Moddemaijer, R., "On the Determination of the Position Extrema of Sampled Correlators", IEEE Transactions on Signal Processing , Vol 39, No. 1, pp. 216-218, January 1991.

Murphy, M., Gogoasa, and I., Szajman, J., "Optical Fibre Speed Sensor Using Cross Correlation", 18 th ACOFT Proceedings, Wollongong, NSW, pp. 141-144, Australia, 1993.

National Semiconductor Corporation, Analog Devices, Data Book, 1990.

Optek Technology Inc., "Optical Devices and Laser Diode Instrumentation", Product Bulletin, Texas, September 1990.

Papoulis, A., "Probability, Random Variables and Stochastic processes", McGraw-Hill, 1967.

Ross, D. A., Dhatwal, H. S. and Dyot, R. B., "The Determination of the Standard Deviation of the Size Distribution of a Coloidal Suspension of Submicron Particles Using the Fiber Optic Doppler Anemometer, FODA" Journal of Colloid and Interface Science, Vol 64, pp.533-542, 1978.

PCL-818 Laboratory Card, Reference Book, Advantech, 1993.

---

Ruth, B., "Velocity Measurement by the Laser Speckle Method Using Optical Fibers", Optics and Laser Technology, Vol 19, No. 2, pp. 83-90, April, 1987.

Sasaki, O. and Watanabe, T., "Dual Single-Beam Laser Doppler Velocimeter", Applied Optics, Vol. 20, pp. 3990-3991, 1980.

Sasaki, O., Sato, T., Abe, T., Mizuguchi, T. and Niwaiama, M., "Follow-Up-Type Laser Doppler Velocimeter Using Singlemode Optical Fibers", Applied Optics, Vol 19, pp.1306-1308, 1980.

Seastar Optics Inc., Optical devices and laser diode instrumentation, Product Catalog, Canada, 1993.

Sharp Laser Diodes, Diodes User's Manual, March 1992.

Sullivan, M. C., "Efficient Autocorrelation Estimation Using Relative Magnitudes", IEEE Transactions on Acoustics, Speech, and Signal Processing, Vol 37, No. 3, pp. 445-447, March 1989.

Usher, M. J., "Sensors and transducers", Macmillan Publishers Ltd., London, 1985

Watkins, D. and Holloway, G. A., "An Instrument to Measure Cutaneous Blood Flow Using the Doppler Shift of Laser Light", IEEE Transactions on Biomedical Engineering, BME-25 pp. 28-33, 1978.

Wolf, H. F., "Handbook of Fiber Optics : Theory and Applications", Garland Publishing, 1978.

Yeh, C., Handbook of Fiber Optics : Theory and Applications, Academic Press, USA, 1993.

---

Yeh, Y. and Cummins, H. Z., "Localised Flow Measurements with an He-Ne Laser Spectrometer", Applied Physics Letters, Vol 4, pp. 176-182, 1964.

---

# Appendices

---

# Appendix 1

```
{*****
* Program : Compute
* Description : DEMONSTRATIV PROGRAM for cross correlation.
* It uses two files where data from the Tektronix digitiser were stored
* as input of x[i] and y[j], computes cross correlation function and
* stores it in another file for further processing using graphing programmes.
*****
program compute;
uses crt;
const n1 = 3000;
      n2 = 4000;
      n3 = n2-n1+1;

type   a = array [1..n1] of real;
       b = array [1..n2] of real;
       c = array [1..n3] of real;
       d = string[12];
       e = array [1..5] of d;

var    f,n,r,i,j,k : integer;
          x : a;
          y : b;
          z : c;
          g : e;
          t,max,p,sum : real;
outfile1,outfile2,infile,outfile : text;
          q,w : char;

begin
  writeln ('Infile name, and path ?');
  readln (g[1]);
  assign (infile,g[1]);
  reset (infile);
  writeln ('Outfile name and path ?');
  readln (g[2]);
  assign (outfile,g[2]);
  rewrite (outfile);
  writeln ('Outfile1 name and path ?');
  readln (g[2]);
  assign (outfile1,g[2]);
  rewrite (outfile1);
  writeln ('Outfile2 name and path ?');
  readln (g[2]);
  assign (outfile2,g[2]);
  rewrite (outfile2);
  { writeln ('Time-base ?');
  readln (p);
```

```

for i := 1 to n1 do
  begin
    readln(infile,y[i]);
    writeln(outfile1,y[i]:4:4);
  end;

  reset(infile);
  for i:= 1 to 5120 do begin
    readln (infile,q);
  end;

  for j:=1 to n2 do begin
    readln(infile,x[j]);
    writeln(outfile2,x[j]:4:4);
  end;
sound(1000);
delay(400);
nosound;
  for j:= 1 to n3 do
    begin
      sum:=0;
      for i:= 1 to n1 do
        begin
          sum:=(x[j-1+i]*y[i]+sum);
        end;
      sum:=sum/(n1*1e6);
      z[j]:=sum;
      writeln(outfile,z[j]:4:4);
    end;

sound(800);
delay(100);
nosound;
    max:=z[1];
    r:=1;
    for j:=1 to n3 do
      begin
        if z[j] > max then
          begin
            max:=z[j];
            r:=j;
          end;
      end;
    writeln(outfile,r,'*****');
    writeln(outfile 'v='4096/(r*t);
    close (infile);
    close (outfile);
    close (outfile1);
    close (outfile2);
  end.

```

## Appendix 2

```
{ *****
* Program   : CARD.DEM                               *
* Description : DEMONSTRATIVE PROGRAM for PCL-818   *
* pacer trigger A/D conversion with DMA data transfer. *
*****
}
program card;
uses crt;

CONST n1 = 3000;
      n2 = 2600;
      n3 = n1-n2+1;
      nd = 10;

VAR
  param : array[0..60] of word; { If two boards installed, need to
                                declare the second parameter array }
  dat   : array[1..2*n1] of integer; { Conversion data buffer }
  func  : integer;

{$L 818TPF}
{$F+}

procedure pcl818(func:integer;var param:word);external;
TYPE
  a = array [1..n1] of real;

VAR
  ri,ndi,g,f,n,r,i,j,k : integer;
  x,y : a;
  Z,data,l,DataBuf,v,t,max,p,sum : real;
  q,w : char;
  file1,file2,file3 : text;

BEGIN
  param[0] := 0;      { Board number }
  param[1] := $300;  { Base I/O address }
  param[2] := 3;     { Buffer A DMA channel }
  param[4] := 2;     { IRQ level : IRQ2 }
  param[5] := 100;   { Pacer Rate = 1M / (10 * 100) = 1 kHz }
  param[6] := 10;
  param[7] := 0;     { Trigger mode, 0 : pacer trigger }
  param[8] := 0;     { Non-cyclic }
```

```

param[10] := ofs(dat[1]); { Offset of A/D data buffer A      }
param[11] := seg(dat[1]); { Segment of A/D data buffer A      }
param[12] := 0;          { Data buffer B address, if not used,  }
param[13] := 0;          { must set to 0.                    }
param[14] := (2*n1);     { A/D conversion number             }
param[15] := 1;          { A/D conversion start channel      }
param[16] := 2;          { A/D conversion stop channel      }
param[17] := 8;          { Overall gain code, 0 : 10V       }
{ param[45] : Error code
param[46] : Return value 0
param[47] : Return value 1 }

```

```
clrscr;
```

```

assign(file1,'a:\y');
assign(file2,'a:\x');
assign(file3,'a:\z');
rewrite(file1);
rewrite(file2);
rewrite(file3);

```

```

sound(400);
delay(40);
nosound;

```

```

func := 3;
pcl818(func, param[0]); { Func 3 : Hardware initialization  }
if (param[45] <> 0)
then
  BEGIN
    writeln(' DRIVER INITIALIZATION FAILED !');
    exit;
  END;

```

```

func := 4;
pcl818(func, param[0]); { Func 4 : A/D initialization      }
if (param[45] <> 0)
then
  BEGIN
    writeln(' A/D INITIALIZATION FAILED !');
    exit;
  END;

```

```

func := 6;
pcl818(func, param[0]); { Func 6: Pacer trigger A/D conversion  }
if (param[45] <> 0)     {      with DMA data transfer      }
}
then
  BEGIN

```

```

        writeln('A/D DMA DATA TRANSFER FAILED !');
        exit;
    END;

repeat
    func := 7;
    pcl818(func, param[0]);      { Func 7: Check DMA status      }
until((param[46] AND 1) = 0); { 0 : not active, 1 : active      }

sound(600);
delay(40);
nosound;

for i := 1 to (n2) do
    BEGIN
        y[i] := dat[2*i] shr 4 ;
        y[i] :=20* y[i] /4096-10 ;
        writeln(file1,y[i]:2:2);
    end;
    writeln;
    writeln('*****');

    for j := 1 to (n1) do                { assign data to x
    }
    BEGIN
        x[j] := dat[2*j-1] shr 4 ;
        x[j] :=20* x[j] / 4096-10 ;

        writeln(file2,x[j]:2:2) ;
    end;

    sound(800);
    delay(40);
    nosound;

{***** ==CROSS CORRELATION== ***** }

t:= param[5]*param[6]/1E6 ; {sec}
l:=0.301416 {meter};
r:=0;
max:=0;
j:=1;

while j<= n3 do
    BEGIN
        sum:=0;
        i:=1;
        while i<= n2 do
            begin

```

```

sum:=(x[j-1+i]*y[i]+sum);
i:=i+nd;
end;

Z:=SUM*10/N2;
writeln(file3,Z:4:2);
IF Z>MAX THEN
  BEGIN
    MAX:=Z;
    R:=J;
  END;
j:=j+1;
END;

writeln(file3);
writeln(file3,r);
v:= l/((r+1)* t);
  writeln ( file3,v:4:6,' m/s = ',(v*3.6):4:6,' km/h');

sound(1000);
delay(40);
nosound;
  close(file1);
  close(file2);
  close(file3);

END. (program)

```

## Appendix 3

```

{ *****
*Program: CARD Description :      CONTINUOUS VELOCITY      *
*                               MEASUREMENT PROGRAM      *
* for PCL-818 pacer trigger, A/D conversion with DMA data transfer *
*****
}
program card;
uses crt,dos;

CONST n1 = 2600;
      n2 = 2400;
      n3 = n1-n2+1;
      nd = 10;

```

---

VAR

param : array[0..60] of word; { If two boards installed, need to declare  
the second parameter array }  
dat : array[1..(n1+n2)] of integer; { Conversion data buffer }  
func : integer;

{ \$L 818TPF }

{ \$F+ }

procedure pcl818(func:integer;var param:word);external;

TYPE

a = array [1..n1] of real;  
b = array [1..n2] of real;

VAR

ri,ndi,r,i,j : integer;  
x : a;  
y : b;  
z,data,l,DataBuf,v,t,max,p,sum : real;  
m,n,o,q,me,ne,oe,qe:word;

BEGIN

param[0] := 0; { Board number }  
param[1] := \$300; { Base I/O address }  
param[2] := 3; { Buffer A DMA channel }  
param[4] := 2; { IRQ level : IRQ2 }  
param[5] := 10; { Pacer Rate = 1M / (10 \* 100) }  
param[6] := 100;  
param[7] := 0; { Trigger mode, 0 : pacer trigger }  
param[8] := 0; { Non-cyclic }  
param[10] := ofs(dat[1]); { Offset of A/D data buffer A }  
param[11] := seg(dat[1]); { Segment of A/D data buffer A }  
param[12] := 0; { Data buffer B address, if not, }  
param[13] := 0; { used must set to 0. }  
param[14] := (n1+n2); { A/D conversion number }  
param[15] := 1; { A/D conversion start channel }  
param[16] := 2; { A/D conversion stop channel }  
param[17] := 8; { Overall gain code, 0 : 10V }  
{ param[45] : Error code  
param[46] : Return value 0  
param[47] : Return value 1 }

REPEAT

sound(400);  
delay(20);  
nosound;

```

func := 3;
pcl818(func, param[0]); { Func 3 : Hardware initialization      }
if (param[45] <> 0)
then
  BEGIN
    writeln(' DRIVER INITIALIZATION FAILED !');
    exit;
  END;

```

```

func := 4;
pcl818(func, param[0]); { Func 4 : A/D initialization          }
if (param[45] <> 0)
then
  BEGIN
    writeln(' A/D INITIALIZATION FAILED !');
    exit;
  END;

```

```

gettime(m,n,o,q);
{writeln(m,'*',n,'*',o,'*',q);}

```

```

func := 6;
pcl818(func, param[0]); { Func 6: Pacer trigger A/D conversion }
if (param[45] <> 0)      {      with DMA data transfer      }
then
  BEGIN
    writeln('A/D DMA DATA TRANSFER FAILED !');
    exit;
  END;

```

```

gettime(m,n,o,q);
{writeln(m,'*',n,'*',o,'*',q);}

```

```

repeat
  func := 7;
  pcl818(func, param[0]); { Func 7: Check DMA status          }
  until((param[46] AND 1) = 0); { 0 : not active, 1 : active }
gettime(me,ne,oe,qe);

```

```

{writeln(me,'*',ne,'*',oe,'*',qe);}
sound(1000);
delay(40);
nosound;

```

```

for i := 1 to (n2)
  BEGIN
    y[i] := dat[2*i-1] shr 4 ;
    y[i] :=20* y[i] /4096-10 ;
  end;

```

```

for j := 1 to (n1) do used
BEGIN
    x[j] := dat[2*j] shr 4 ;
    x[j] :=20* x[j] / 4096-10 ;
end;

sound(2000);
delay(100);
nosound;

{***** ==CROSS CORRELATION== *****}

t:=((100*(oe-o)+(qe-q))/100)+((n1+n2)*10e-6);
{writeln(t:4:4);    }
t:= 2*t/(n1+n2);
{writeln(t:4:4);}
l:=0.0301416 {meter};
r:=1;
max:=0;
j:=1;

{First approximation}

while j<= n3 do
BEGIN
    sum:=0;
    i:=1;
    while i<= n2 do
    begin
        sum:=(x[j-1+i]*y[i]+sum);
        i:=i+nd;
    end;
    Z:=SUM*10/N2;
    IF Z>MAX THEN
        BEGIN
            MAX:=Z;
            R:=J;
        END;
    j:=j+nd;
END;
{writeln(r);

v:= 1/((r+1)* t);
    writeln (v:4:6,' m/s =',(v*3.6):4:6,' km/h');
until keypressed;
end. {program}

```

---

## Appendix 4

```
{
*****
* Program   : ADTRIG.PAS
* Description : program for PCL-818 pacer trigger A/D
*             conversion with software data transfer.
*****
}
program card;
uses crt,dos;

CONST      n1 = 1600;
           n2 = 1400;
           n3 = n1-n2+1;
           nd = 10;

var
  param : array[0..60] of word; { If two boards installed, need to
                                declare the second parameter array }
  dat   : array[1..(2*n1)] of integer; { Conversion data buffer }
  func  : integer;
{$L 818TPF}
{$F+}
procedure pcl818(func:integer;var param:word);external;

TYPE
  a = array [1..n1] of real;
  b = array [1..n2] of real;
  f = string[12] ;
  e = array [1..5] of f;
VAR   ri,ndi,r,i,j : integer;
      x : a ;
      z,y : b ;
      g : e ;
u,W,D,data,l,DataBuf,v1,v2,t,max,sum,t2: real;
p,m,s,q,p1,m1,s1,q1:word;

BEGIN
clrscr;

  param[0] := 0;          { Board number }
  param[1] := $300;      { Base I/O address }
```

```

param[5] := 100;          { Pacer Rate = 1M / (50 * 100) = 200 Hz }
param[6] := 15;
param[7] := 0;          { 0: Pacer trigger          }
param[8] := 0;
param[10] := ofs(dat[1]); { Offset of A/D data buffer A      }
param[11] := seg(dat[1]); { Segment of A/D data buffer A    }
param[12] := 0;          { Data buffer B address, if not used, }
param[13] := 0;          { must set to 0.                  }
param[14] := (2*n1);     { A/D conversion number           }
param[15] := 1;          { A/D conversion start channel    }
param[16] := 2;          { A/D conversion stop channel     }
param[17] := 8;          { Overall gain code, 0 : +/- 5V   }
{ param[45] : Error code
  param[46] : Return value 0
  param[47] : Return value 1 }

  sound(400);
  delay(20);
  nosound;

D:=0;
gettime(p,m,q,s);

Repeat
  func := 3;
  pcl818(func, param[0]); { Func 3 : Hardware initialization }
  if (param[45] <> 0)
  then
    BEGIN
      writeln(' DRIVER INITIALIZATION FAILED !');
      exit;
    END;

  func := 4;
  pcl818(func, param[0]); { Func 4 : A/D initialization      }
  if (param[45] <> 0)
  then
    BEGIN
      writeln(' A/D INITIALIZATION FAILED !');
      exit;
    END;

  func := 5;
  pcl818(func, param[0]); { Func 5 : "N" times of A/D trigger }
  if (param[45] <> 0)
  then
    BEGIN
      writeln(' A/D SOFTWARE DATA TRANSFER FAILED !');
      exit;
    END;

```

```

sound(1000);
delay(40);
nosound;

for i := 1 to (n1) do          { assign data to x          }
  BEGIN
    y[i] := dat[2*i-1] and $FFF ;
    y[i] :=20* y[i] /4096-10 ;
  end;
for i:=1 to n2
  do begin
    u:= y[i+n3];
    y[i]:=u;
  end;

  for j := 1 to (n1) do      { assign data to x          }
    BEGIN
      x[j] := dat[2*j] and $FFF ;
      x[j] :=20* x[j] / 4096-10 ;
    end;

```

```
{***** ==CROSS CORRELATION== *****}
```

```

t:=2*param[5]*param[6]/10e6;
l:=0.0301416 {meter};
assign(outfile3,g[3]);
rewrite(outfile3);
r:=1;
max:=0;
j:=1;
while j<= n3 do
  BEGIN
    sum:=0;
    i:=1;
    while i<= n2 do
      begin
        sum:=(x[j-1+i]*y[i]+sum);
        i:=i+nd;
      end;
      Z[j]:=SUM*10/N2;
      writeln(outfile3,z[j]:2:2);
      IF Z[j]>MAX THEN
        BEGIN
          MAX:=Z[j];
          R:=J;
        END;
    j:=j+nd;
  END;
                                     {end of the first evaluation      }

```

```

if r<=nd then begin
  r:=nd;
end;
if r>=(n3-nd) then begin
  r:=(n3-nd)
end;
ndi:=nd;
ri:=1;
max:=0;
  for j:= (r-ndi) to (r+ndi) do
    BEGIN
      sum:=0;
      for i:=1 to n2 do
        begin
          sum :=(x[j-1+i]*y[i]+sum);
        end;
        z[j]:=sum/(n2-10);
        Writeln(outfile3,z[j]:2:2);
        if z[j]>max then
          begin
            max:=z[j];
            ri:=j;
          end;
      END;
      {end pf the second evaluation      }
ri:=ri-n3 ;

writeln(outfile3,ri);
v1:= l/((ri-1)* t);
  writeln ( outfile3,v1:2:2,' m/s = ',(v1*3.6):2:2,' km/h');
  writeln(v1:2:2,'m/s =',(v1*3.6):2:2,'km/h');

*****{ parabola apex }*****
t2:=(-t/2*(z[ri+1]-z[ri-1]))/(z[ri+1]-2*z[ri]+z[ri-1])+(t*ri);

v2:=4*l/t2;
writeln(v2:2:2,'km/h');

sound(600);
delay(20);
nosound;

  until keypressed
end.

```

---

## Appendix 5

```
{
*****
* Program   :FASTFUR.PAS
* Description: program for determining the Fast Fourier Transforms
*for the signals corresponding to surfaces under observation
*****
}

uses crt;

const   nn = 1024;
        nn2 = 2*nn;
        isign=1;

type    a = array [1..nn2] of real;
var     outfile3,infile:text;
        i,j:integer;
        data:a;
procedure fft(VAR data:a; nn,isign:integer);

var
    ii,jj,n,mmax,m,j,istep,i : integer;
    wtemp,wr,wpr,wpi,wi,theta : double;
    tempr,tempi,wrs,wis      : real;
begin
    n := 2*nn;
    j := 1;
    FOR ii := 1 to nn do begin
        i:=2*ii-1;
        IF j > i then begin
            tempr := data[j];
            temp_i := data[j+1];
            data[j] := data[i];
            data[j+1] := data[i+1];
            data[i] := tempr;
            data[i+1] := temp_i;
        END;
        m:= n div 2;
        WHILE (m >= 2) AND (j > m) do begin
            j := j-m;
            m := m div 2;
        END;
        j := j+m;
```

```

    END;
mmax := 2;
WHILE (n>mmax) do begin
    istep := 2*mmax;
    theta := 6.28318530717959/(isign*mmax);
    wpr := -2.0 *sqr(sin(0.5*theta));
    wpi := sin(theta);
    wr := 1.0;
    wi := 0.0;

    FOR ii:=1 to (mmax div 2) do begin
        m := 2*ii - 1;
        wrs := wr;
        wis := wi;
        FOR jj := 0 to (n-m) div istep do begin
            i := m +jj*istep;
            j := i+mmax;
            tempr := wrs * data[j]-wis*data[j+1];
            tempi := wrs*data[j+1]+wis*data[j];
            data[j] := data[i]-tempr;
            data[j+1] := data[i+1]-tempi;

            data[i] := data[i]+tempr;
            data[i+1] := data[i+1]+tempi;
        END;

        wtemp := wr;
        wr := wr*wpr-wi*wpi+wr;
        wi := wi*wpr+wtemp*wpi+wi;
    END;
mmax := istep;
END;
end;

begin

    { assign (infile,'d:\e_ibm.dat');
      reset (infile); }
    assign (outfile3,'d:\fft1');
    rewrite (outfile3);

    for j:=1 to nn2 do begin
        data[j]:=0;
    end;

    for j:=1 to nn do begin

        data[j]:=10*sin(6.28318530717959*j/100)+10*sin(6.28318530717959*j/50);
    end;

```

---

```
sound(1000);
delay(400);
nosound;
fft(data,nn,1);

for i:=1 to nn div 2 do begin
j:=2*i-1;
data[i]:=sqrt(sqr(data[j])+sqr(data[j+1]));
writeln( outfile3,data[i]:4:2);
end;
      { close (infile); }
      close (outfile3);
end. {program}
```

---

## *Publications*

The paper “An extrinsic cross correlation based optical fibre speed sensor” was published in Meas. Sci. and Technol 7 1996.

The paper “Optical fibre speed sensor using cross correlation” was published in Proceedings of the 18th Australian Conference on Optical Fibre Technology (ACOFT-18 '93).

# An extrinsic optical fibre speed sensor based on cross correlation

I Gogoasa†, M Murphy‡ and J Szajman

Optical Technology Research Laboratory, Department of Applied Physics,  
Victoria University of Technology, PO Box 14428, MCMC, Melbourne, Victoria  
8001, Australia

Received 5 January 1996, in final form 23 April 1996, accepted for publication  
8 May 1996

**Abstract.** An extrinsic non-contact optical fibre speed sensor based on cross correlation is reported. The sensor launches and receives reflected light from a moving surface which has a random reflection profile. The reflected optical signals are processed using cross correlation which enables determination of speed. The advantage of this arrangement is its non-contact and non-invasive operation. The current version of this sensor can measure the translation speeds of up to  $30 \text{ km h}^{-1}$ .

## 1. Introduction

Using conventional (non-optical) sensing methods, the operational environment may affect the transducer's performance and result in an incorrect measurement [1]. In the case of optical-fibre-based sensor systems, these effects are reduced because fibres have well-documented stability and immunity [2] to external interference. A large number of such sensors have evolved, including those for the measurement of speed in machines undergoing deterministic motion [2], although these sensors usually rely upon periodic optical modulation from a surface marker [3]. In terms of cost and implementation, such simple sensors are potentially attractive but would only be of use if the monitored surface underwent a rotation or known motion.

There are, of course, surface movements which would result in non-deterministic signals, a good example of which would be the optical reflection from a sealed road surface. Since road surfaces are naturally rough and graded to improve highway safety, it would be difficult to generate a deterministic optical signal unless the road were deliberately marked (conventional road speed measurement relies upon a periodic signal from a gear box or road wheel which may be mechanical or electrical in form [4]).

The subtle manipulation of such a non-deterministic signal would be useful in motion measurement for vehicles in general and for measurements in environments where (although the motion may be periodic) neither mechanical contact nor surface marking would be practical. An example of such an industrial scenario would be in the power generation sector, where any rotating surface of generating plant could be addressed optically with no need

to shut the system down. The optical fibre sensor would be immune from electrical noise from machinery and, since no contact with moving plant is required, it would be safe and simple in operation.

This paper reports upon such an optical-fibre-based speed sensor which uses the signal processing technique known as cross correlation [1]. The sensing system correlates two 'identical' but non-deterministic signals, one of which has been deliberately delayed in time with respect to the other. Although motion-generated noise or pseudo-random patterns monitored at two points has been widely used for flow measurement [3,5], application of this technique to solid moving surfaces is of considerable interest. Cross correlation is known to offer signal-to-noise ratio (SNR) advantages [6] and its use in the work presented in this paper is a more detailed extension of that reported earlier [7].

## 2. Theoretical considerations and sensor design

A randomly varying signal may be processed using cross correlation, the resultant function being useful for signal filtering or sensing instrumentation applications [1]. For use in time-delay estimation, the same signal must be detected at two spatially different positions (in the case of speed, acceleration, distance and so on). The two signals (received by the two separate sensors) are out of phase in time and by varying this phase delay correlation between them is possible.

A schematic diagram of a simple cross-correlation-based sensing system is given in figure 1. Here the signal is detected by each sensor, multiplied and averaged. The mathematics describing this process is straightforward and the complete process may be described through the integral [1]

† Present address: CSIRO Division of Atmospheric Research, Aspendale, Melbourne, Victoria, Australia.

‡ Present address: GEC-Marconi Research Centre, West Hanningfield Road, Great Baddow, Chelmsford, Essex CM2 8HN, UK.

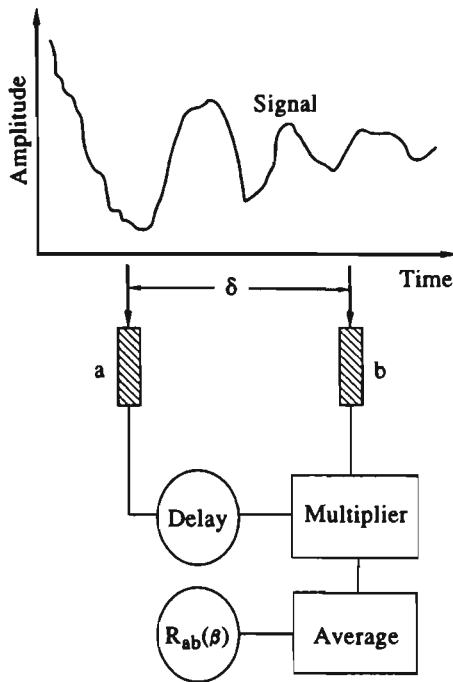


**Figure 1.** A simple correlator.  $\delta$  is the spatial separation between the transducers 'a' and 'b'.

$$R_{ab}(\beta) = \frac{1}{T} \int_0^T a(t - \beta)b(t) dt. \quad (1)$$

Note that  $T$  is the observation period for a continuous signal and  $\beta$  is an induced time delay at sensor 'a'. Since the signals are 'random' (white noise over a bandwidth limited by the nature of the surface under investigation) their resultant Fourier spectrum will have a constant amplitude  $A$ , up to a cut-off frequency  $f_c = \omega_c/(2\pi)$ . In this case, equation (1) simplifies to a Fourier transform of the power spectral density [6] and mathematically reduces to

$$R_{ab}(\beta) = A \frac{\sin[\omega_c(\beta - \tau)]}{\beta - \tau}. \quad (2)$$

Equation (2) has a maximum when  $\beta$  equals the transit time  $\tau$  between the two transducers 'a' and 'b'.

These expressions refer to a continuous signal, whereas for the digitized signal in a computer-based measurement system such data will be characterized by a set of  $N$  samples for each channel. Each data set will be available only at discrete time intervals  $\Delta T$  so the time difference between signals received by sensors will be  $m\Delta T$  with  $m = 0, 1, 2, 3, \dots, N - 1$ . Thus, the correlation function of the signal is found by evaluating the set of  $R_{ab}(m\Delta T)$  terms. That is,

$$R_{ab}(m\Delta T) = \frac{1}{N} \sum_{i=1}^N a_{i-m} b_i \quad (3)$$

where  $b_i$  is the sample value at the time  $i\Delta T$  and  $b_{i-m}$  is that at the time  $(i - m)\Delta T$ ,  $m$  sampling intervals earlier.

For the practical implementation of cross correlation, the form of optical sensor design adopted is given in figure 2. It comprises twin collimating optical fibres and a lens arrangement. Each spatial sensor is made up of an optical fibre launch/receive pair integrated into the optical transducer head. The collimating optics

were designed to allow range-independent measurements to be made during optical signal sampling, thereby allowing remote measurements without compromising the system's SNR. The signals were sampled current-converted voltages from two PIN photodetectors. Figure 3 shows these photodetectors coupled to the two optical fibres scanning the monitored surface. The optical fibres used were 100/140  $\mu\text{m}$  multimode and their pairing allowed simultaneous optical illumination and addressing of the surfaces. Optical illumination was effected from a pair of low-cost, compact disc (CD) 780 nm, 3 mW laser diodes, coupled into the fibres using a CD lens arrangement. After photodetection, each electrical signal was digitized and the mean of the product evaluated to generate a cross correlation function. When  $m\Delta T = \tau$  for any point on the moving surface (between the optical sensors), then  $R_{ab}(m\Delta T)$  is a maximum (equation (2)) and, since both  $\delta$  (the spatial separation between 'a' and 'b') and  $\tau$  are now known, the speed ( $v = \delta/\tau$ ) could be determined.

Signal voltages were limited to  $\pm 5$  V and analogue-to-digital conversion was facilitated by using a Laboratory PCL-818 card. Data acquisition and correlation processing were performed using programmes written in assembler language. The second signal 'b' was progressively correlated with the first signal 'a' until the software detected a maximum in  $R_{ab}(m\Delta T)$ . Once the maximum in  $R_{ab}(m\Delta T)$  was resolved then the calculation of the surface speed was possible.

### 3. Results

To simulate the moving surface, a low-reflectivity duralium disc was initially selected which had been contaminated by the natural corrosion processes in a non-uniform manner. Each optical fibre pair was arranged in the transducer so that the launch/receive efficiency of this coupling arrangement was maximized to around 2%. The optical fibre transducer was placed approximately 1 m (distance  $x$  in figure 2) from the moving surface. Typical signals for each channel, are shown in figure 4. These were correlated in time and the resulting  $R_{ab}(m\Delta T)$  (also in figure 4), is shown to have the characteristic form [1], where the abscissa of its maximum equals the transit time for any point on the moving surface. For the example presented in figure 4,  $\tau$  was 5.9 ms, yielding a surface speed of 5.1  $\text{m s}^{-1}$ . Figure 5 shows a comparison between the optical fibre correlation sensor and a 'Cateye' [8] commercial speed sensor. The Cateye comprises a magnet fixed to a rotating surface of known radius. A microprocessor counts the pulses generated by a stationary magnetic probe (placed near the moving surface) and computes the average linear speed for one complete revolution. For the range of speeds shown, it was found that there was a difference of only a few per cent between the two systems for each measurement.

### 4. Discussion

The duralium surface generated a non-deterministic signal up to the point at which the period of revolution for this surface was completed. The electrical signal

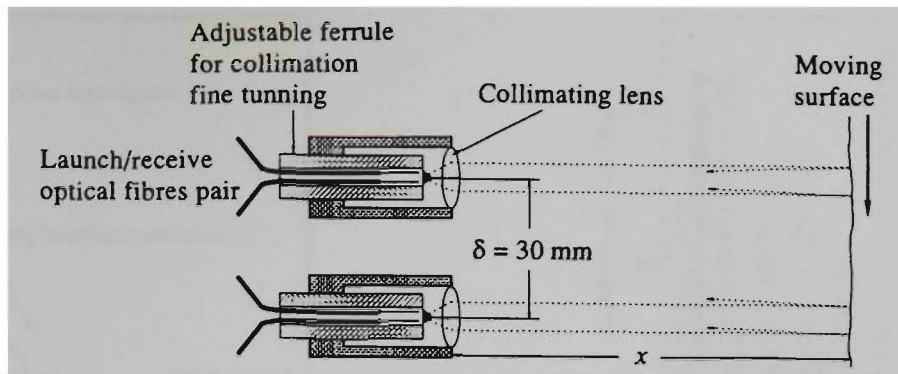


**Figure 2.** The transducer head for the optical-fibre-based speed sensor. Two sensors are separated by  $\delta = 30$  mm. The transducer was normally located at distance of  $x \approx 1$  m from the moving surface.

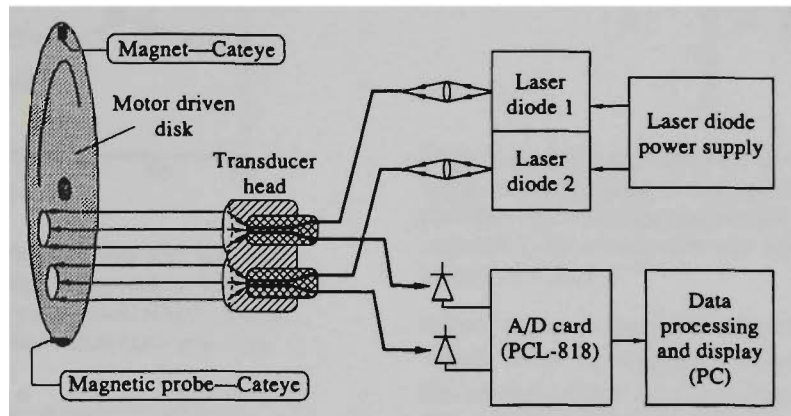


**Figure 3.** A schematic diagram of the experimental arrangement. Note that the Cateye's magnet is shown attached to the top of the disc (moving surface) and the sensor coil is depicted at the bottom of the drawing.

from the photodetection circuit was resolved into its frequency components using a DSA602 Tektronix digitizing oscilloscope.

Since surface characteristics would affect the Fourier spectrum of a scattered signal, a range of surfaces were examined to establish whether the sampling rate for our system would depend upon the surface addressed. Figure 6 shows that the maximum of the power spectrum of the signal for the surfaces tested occurs in the frequency range of 120–250 Hz (with a mean at 200 Hz) when measured at a constant surface speed of  $1.6 \text{ m s}^{-1}$ . Indeed, the detected frequency spectrum extends at least to 3500 Hz for all surfaces tested and the sampling rate of the analogue-to-digital converter was set well above the Nyquist frequency, at  $10^4 \text{ samples s}^{-1}$ . This upper frequency limit [5] is speed-dependent and it is attributed to the 'low-pass' filtering nature of the collimating optics. That is, each probe beam has a significant waist, leading to integration of surface characteristics, preventing the interpolation of higher frequencies. In the worst case, this would produce uncertainty in the absolute speed reading of about 9% for a surface moving at  $30 \text{ km h}^{-1}$ . A light beam of smaller cross section would decrease this uncertainty; however, care would have to be taken to ensure that the two beams would view the same area to provide meaningful data for the correlator.

To address the issue of the information update to a user of such a system, the authors have employed a 'two-pass correlation' technique, which is based upon selective

use of data. The theory described and the experimental data presented so far are based upon basic cross correlation principles. In reality, since we are operating with digitized discrete points, a large volume of data (contained in two arrays) must be shifted (in the time domain) and processed using equation (3). This requires a considerable amount of computing time and not only reduces the ability for quick information updates, but also increases the measurement error for  $dv/dt \neq 0$ .

'Simple correlation' uses every tenth data point to generate a rough cross correlation function. After a global maximum had been found, a more precise calculation was performed near this maximum. The second pass re-iterates the calculation using a limited span of data points on either side of the simple correlation maximum, but this time all the points in the range are used. Two-pass correlation reduces processing time by a factor of 20.

Experimentally, the signal scattered from the monitored surface would vary in amplitude depending upon the level of contamination and particle grade. A number of trials were conducted on the scattering surfaces to examine their performance. Figure 6 shows how the signal amplitude and the bandwidth are affected by different surfaces. In all cases, the amplitude was well above the noise floor for the system. Road speed trials have yet to be conducted.

Since the transducer was designed to be range-independent, experiments were carried out to measure the surface speeds over distances in the range 0.2–5 m. It was felt by the authors that this measurement range represented

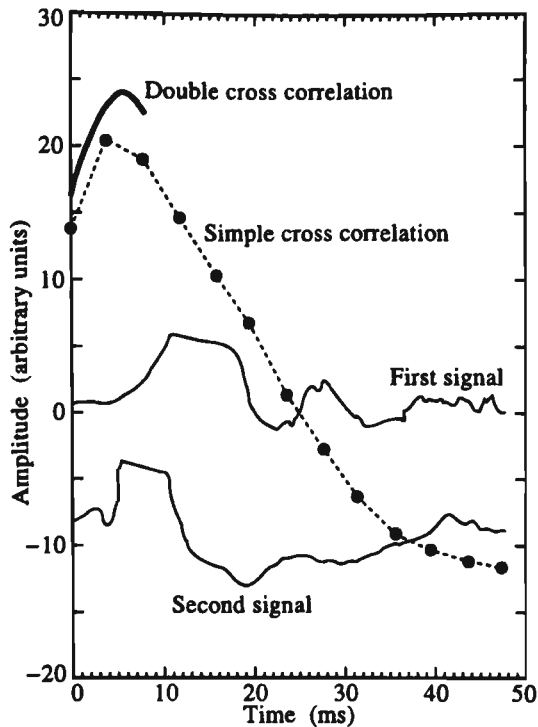


Figure 4. Experimental data showing the first and the delayed second signal. The simple correlation (first pass) and the more accurate second pass performed over a limited data range near the global maximum are also plotted (see text).

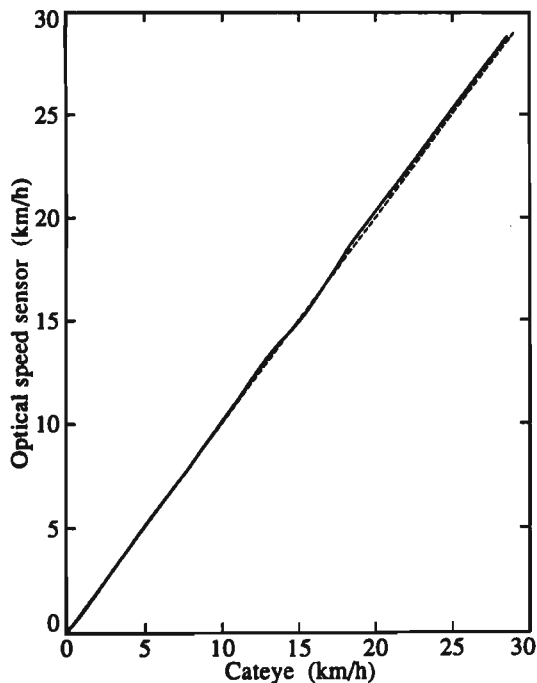


Figure 5. A comparison of the performance of the optical sensor and the commercial Cateye speedometer. The dotted line represents the 1:1 speed ratio.

practical isolation from a moving surface. For these range trials, there was no measurable deterioration in the system's performance.

## 5. Conclusions

An optical fibre sensor for the measurement of surface speed has been constructed with a performance comparable to that of a commercial sensor. The commercial sensor

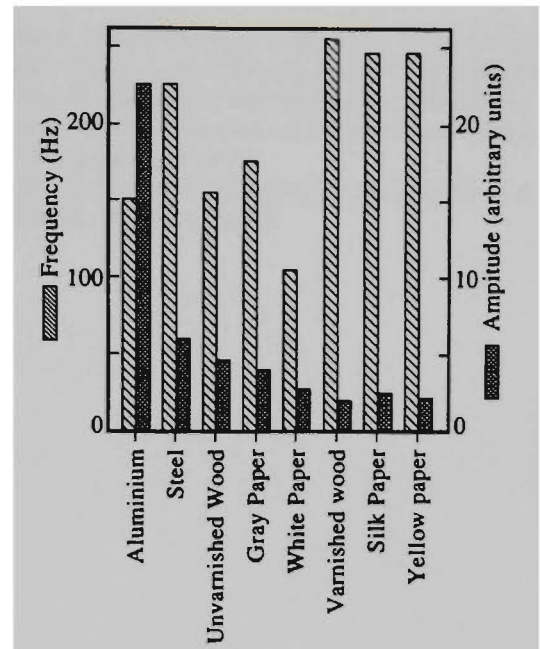


Figure 6. Optical properties of selected surfaces. In each case, the amplitude of the reflected signal at the detector and the approximate bandwidth for the material are indicated. All measurements were performed at a constant speed of  $1.6 \text{ m s}^{-1}$ .

relied upon a periodic electrical pulse from a magnet which must be attached to the moving surface, whereas the optical sensor is of non-contact type and suitable for an electromagnetically hostile environment. The advantages with this optical fibre sensor are that it is of non-contact operation and requires no invasive procedures. Measurements are effectively continuous, whereas for the Cateye sensor the velocity read-out is only updated once every revolution, thereby yielding an average value.

The design of transducer head still requires consideration of a number of issues, including its performance with a greater range of surfaces and angular dependence (tilt of head with respect to the moving surface) of the speed measurement. An additional uncertainty of around 1% for a misalignment of  $\pm 4^\circ$  would be tolerable when dealing with an efficient reflective surface. The absolute uncertainty of 9% at  $30 \text{ km h}^{-1}$  is not a serious limitation of the technique because a light beam of smaller cross section with a fast analogue-to-digital card would increase the accuracy of the sensor. Ultimately, the maximum speed is limited by the roughness of the surface. Applications for this sensor would be in a wide range of speed and distance measurements. We believe that this sensing system has practical potential if microprocessor-based.

## Acknowledgment

The authors thank The Victoria University of Technology for the award of a 1993 seeding grant, which enabled equipment procurement for this initial study.

## References

- [1] Bentley J P 1992 *Principles of Measurement Systems* 2nd edn (New York: Longman)
- [2] Culshaw B and Dakin J (ed) 1989 *Optical Fibre Sensors: Systems and Applications* (Boston: Artech House)

- [3] Krohn D A 1988 *Fibre Optic Sensors, Fundamental and Applications* (Research Triangle Park, NC: Instrument Society of America)
- [4] Usher M J 1985 *Sensors and Transducers* (London: Macmillan)
- [5] Beck M S 1984 *Correlation in Instruments: Cross Correlation Flowmeters* (Bristol: Hilger)
- [6] Cusani R 1989 Performance of fast time delay estimators *IEEE Trans. Acoust. Speech Signal Processing* **37** 757-9
- [7] Murphy M, Gogoasa I and Szajman J 1993 Optical fibre speed sensor using cross correlation *Proc. 18th ACOFT (Wollongong)* pp 141-4
- [8] Cateye Co Ltd 1993 *Operating Instructions* (2-8-25 Kuwazu, Higashi, Osaka)

# Optical Fibre Speed Sensor Using Cross Correlation

M M Murphy

I Gogoasa

J Szajman

*Optical Technology Research Laboratory, Department of Applied Physics  
Victoria University of Technology, Melbourne Vic*

The preliminary results for an optical fibre speed sensor are reported. This sensor scans optical signals reflected from a moving surface which are processed using the cross correlation method. Since the sensor makes two spatial measurements determination of surface speed was possible.

## 1. INTRODUCTION

Electronic sensors often require consideration of the environment, which may affect their performance [1]. With optical fibre based sensors, these effects are less significant, due to their general immunity, which is well documented [2]. A range of sensors have evolved [2], including those for the measurement of speed, in the case of rotating surfaces [3]. For these, a periodic optical reflection from the surface is detected and the time between successive signals allows speed to be evaluated.

These simple sensors may be applicable for monitoring surfaces undergoing a rotation or periodic displacement, however, there may be a need for speed monitoring of a random surface such as a road or non-deterministic motion in a machine. By using cross correlation, the monitoring of such surfaces is possible by correlating the "randomness" from two separate detectors. This method has been used previously for flow rate monitoring [4], and has been adopted in the work reported in this paper for optical fibre based speed sensing.

## 2. EXPERIMENTAL

The mathematics describing cross correlation is reported elsewhere [1], and requires here that a signal is detected by two spatially separated sensors. In this work, these signals are sampled voltages ( $x(t)$  and  $y(t)$  ( $t$  is time)) from two photodetectors. These photodetectors are coupled to two horizontally displaced (" $\delta$ " in Figure 1) optical fibres scanning an illuminated rough surface. The optical fibre arrangement (Figure 1) was constructed to form a transducer head which incorporated two optical fibre (50/125  $\mu\text{m}$ ) pairs providing illumination of the surfaces to be monitored. Illumination was effected by using a pair of low cost compact disc (CD) 780 nm, 3 mW laser diodes, coupled using a CD lens arrangement. The transducer signal was digitised and the mean of the product  $x(t+\beta)\cdot y(t)$  evaluated to generate a cross correlation function  $R_{xy}(\beta)$  ( $\beta$  being an induced time shift). When  $\beta$  equalled the transit time ( $\tau$ ) for any point on the moving surface, between each optical fibre pair, then  $R_{xy}(\beta)$  was a maximum and speed ( $\delta/\tau$ ) was determined.

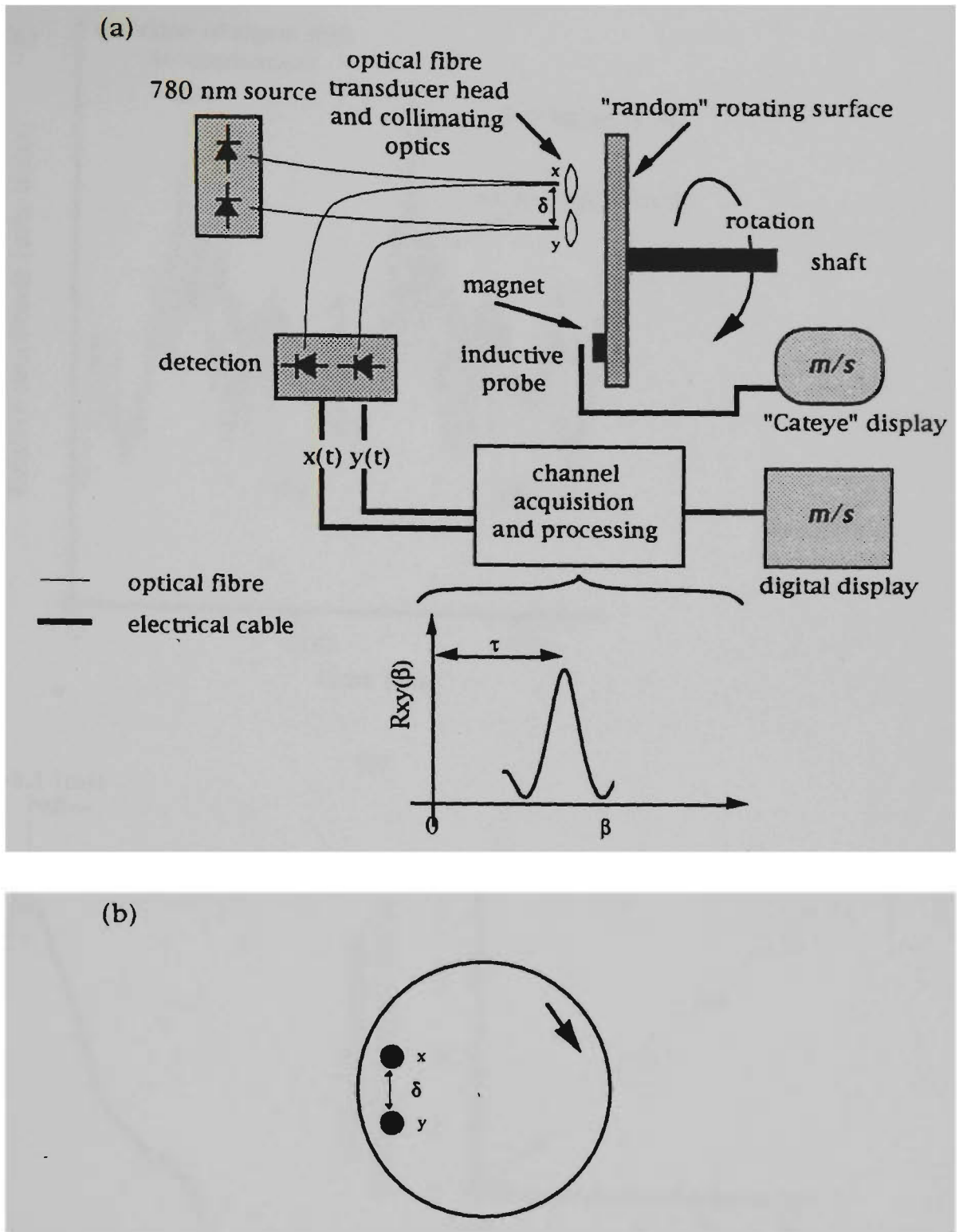


**Figure 1** Experimental arrangement, showing (a) a schematic of the optical fibre cross correlation and electronic "Cateye" speed sensors and (b) the physical position of the two sensing points with respect to the rotating surface.

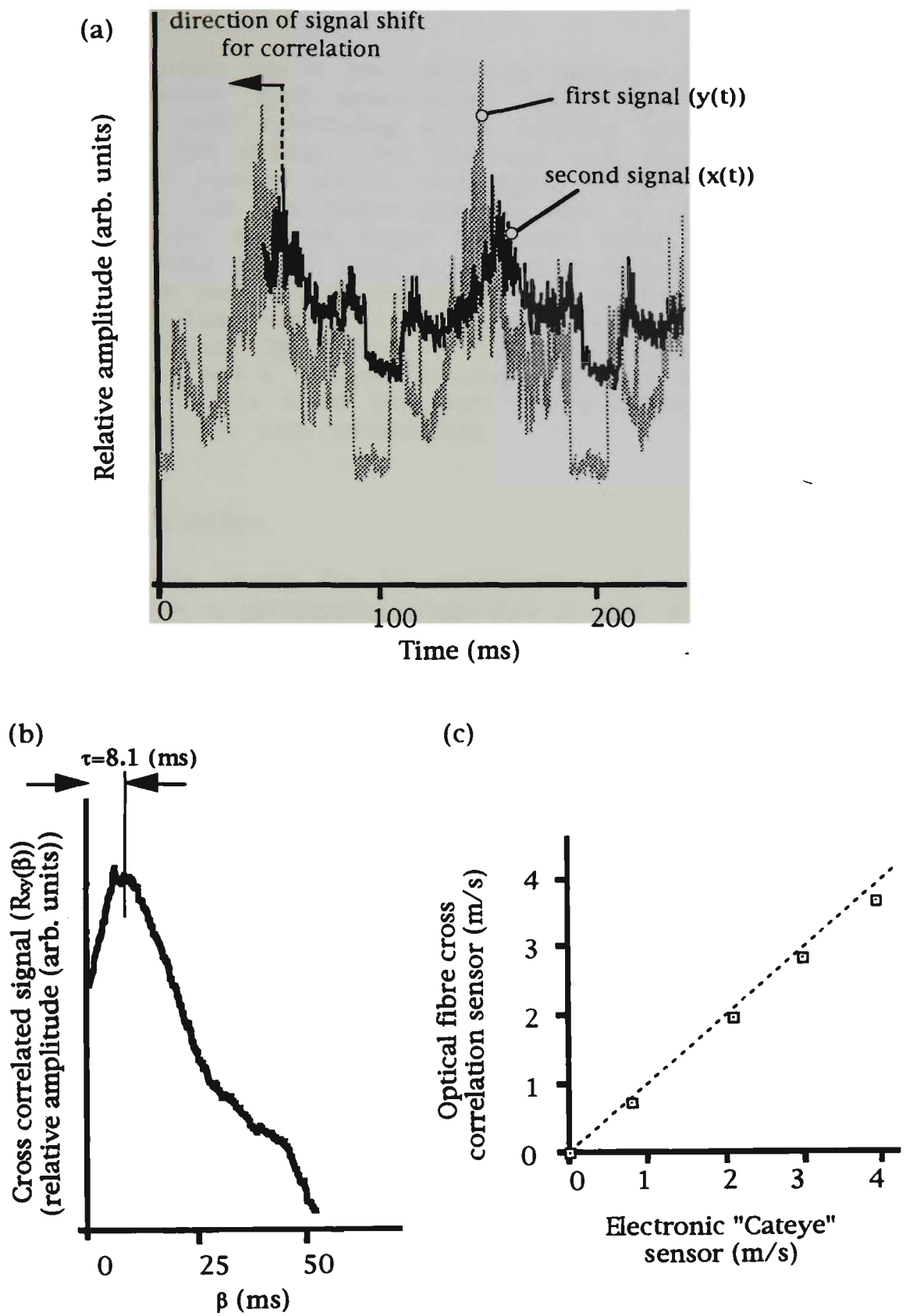


**Figure 2** (a) Relative detected signal amplitudes for each channel, (b) the relative cross correlated signal and (c) a comparison between the optical fibre cross correlated sensor and the electronic Cateye sensor in measuring speed (m/s), where the dotted line represents a 1:1 speed ratio

### 3. RESULTS

The moving surface was a low reflectivity duralium disc, contaminated in a non-uniform manner. Each launch/receive optical fibre pair was arranged in the transducer with collimating lenses enabling almost range independent measurements. The optical fibre transducer was placed approximately one metre from the moving surface, and typical signals for each channel, are given in Figure 2(a). The shorter signal is made up of 800 samples and was correlated in time with the longer (reference) signal of 1000 samples. The resulting correlation (Figure 2(b)), is shown to have a distinct peak, and the abscissa (of the peak) equals the transit time ( $\tau$ ) for a point on the moving surface. For the data presented,  $\tau$  was 8.1 ms, yielding a surface speed of 3.7 m/s ( $\delta=30$  mm). Figure 2(c) shows a comparison between the optical fibre correlation sensor and a "Cateye" [5] commercial speed sensor. For the range of speeds shown, it was found that there was a difference of a few percent between systems for each measurement.

### 4. CONCLUSIONS

An optical fibre sensor for the measurement of surface speed has been constructed, with a performance comparable to that of a commercial sensor. The commercial sensor relied upon a periodic electrical pulse from a magnet which must be attached to the moving surface, whereas the optical sensor is non-contact and suitable for an electromagnetically noisy environment.

### 5. ACKNOWLEDGMENTS

The authors thank Victoria University of Technology for the award of a 1993 Seeding Grant, which enabled equipment procurement for this initial study.

### 6. REFERENCES

1. Bentley, J. P., Principles of Measurement Systems, Longman Scientific and Technical, 2nd Edition, New York, 1992.
2. Culshaw, B. and Dakin, J., Optical Fibre Sensors: Systems and Applications, Artech House, Norwood MA, 1988.
3. Krohn, D.A., Fiber Optic Sensors, Fundamentals and Applications, Instrument Society of America, 1988.
4. Beck, M. S., Correlation in Instruments: cross correlation flow-meters, Instrument Science and Technology, vol. 2, Chapter 8, Adam Hilger, 1984.
5. Cateye Co. Ltd., 2-8-25, Kuwazu, Higashi-ku, Osaka, Japan, 1993.